DESIGN, CONSTRUCTION, AND EVALUATION OF A WEDGE-SHAPED MATRIX SOLAR COLLECTOR FOR DRYING PEANUTS

By

RONNIE GLEN MORGAN

Bachelor of Science

Oklahoma State University

Stillwater, Oklahoma

1975

Submitted to the Faculty of the Graduate College
of the Oklahoma State University
in partial fulfillment of the requirements
for the Degree of
MASTER OF SCIENCE
December, 1976

DESIGN, CONSTRUCTION, AND EVALUATION OF A

WEDGE-SHAPED MATRIX SOLAR COLLECTOR

FOR DRYING PEANUTS

Thesis Approved:

Bobby L. Clary

Thesis Adviser

Gerald W. Parker

Charles E. Price

Norman N. Durham

Dean of Graduate College

ACKNOWLEDGMENTS

The author wishes to express that he is extremely grateful to his major adviser, Dr. Bobby L. Clary, for his never-ending patience and guidance as a professional and personal friend. I am very thankful for Dr. Clary's excellent assistance throughout the duration of this study.

Special appreciation is directed toward the other advisery members, Dr. Charles E. Rice of the Agricultural Engineering Department and Dr. Jerald D. Parker of the Mechanical and Aerospace Engineering Department. Their patience, criticism, and technical assistance are greatfully appreciated.

I wish to express my gratitude to Professor Jay Porterfield and Dr. Bobby Clary for obtaining funds to support this project. Appreciation is extended to the Agricultural Engineering Department for financial assistance through a half-time assistantship during this research. I also would like to recognize Professor Jay Porterfield for his patience, guidance and criticism as an administrative superior.

I extend my thanks to Mr. Jack Fryrear for his excellent assistance in the photography and preparation of figures. I am grateful to Terry Rice, Carol Cassel and Gary Steinkogler for their student assistance in laboratory and data analysis.

A very special appreciation is extended to Mrs. Donna Steinkogler for her laboring efforts in typing the rough and final drafts of this thesis.

I am grateful to Mr. Clyde Skoch and Mr. Norvil Cole for their assistance in laboratory preparation and construction.

For their many sacrifices and never-ending faith throughout this study I dedicate this thesis to my lovely wife Sharon and my parents, Glen Dale and Helen Morgan.

TABLE OF CONTENTS

Chapter Page

LIST OF TABLES

LIST OF FIGURES

NOMENCLATURE

A_L = Heat transfer area in air chamber and plenum, subject to conduction, per unit of collector absorber area, m^2/m^2

β = Average extinction coefficient of matrix, m^{-1}

C_p = Specific heat at constant pressure of air, w-hr/(Kg-K)

D_f = Mean diameter of matrix filament, m

e_b = Spectral emissitivity of matrix bed

e_c = Spectral emissitivity of collector cover

e_g = Radiant interchange factor between two parallel plates

E_{gx} = Radiant interchange factor between point x in matrix and collector cover, m^{-1}

f = Fanning friction factor, $2r_h\ (-dp/dz)/\rho_a\ u^2$

g_a = Acceleration of gravity, m/sec^2

G = Mass flow rate per unit area, $Kg/(hr\text{-}m^2)$

h_{va} = Average volumetric heat transfer coefficient, $w/(m^3\text{-}K)$

h_{vx} = Volumetric heat transfer coefficient at point x, $w/(m^3\text{-}K)$

Δh = Velocity head, m

I_o = Direct solar radiation normal to collector surface, w/m^2

k = Thermal conductivity of air, w-hr/(m-K)

m_b = Mass of the matrix sample, g

P = Static pressure, Pa

Pr = Prandtl number, $\mu c_p/k$

Q = Volumetric flow rate per unit area, $m^3/(min\text{-}m^2)$

r_h = Hydraulic radius of matrix, $D_f\lambda/4\ (1-\lambda)$

Re = Reynolds number, $4r_h\rho_a u/\mu$

St = Stanton number (modified), $h_{vx}\ (4\ r_h)/C_p\ G$

T_{ba} = Average matrix bed temperature, K

T_{bx} = Matrix bed temperature at point x, K

T_{ba}^* = Dimensionless average bed temperature, T_{ba}/T_{fo}

T_c = Temperature of collector cover, K

T_c^* = Dimensionless cover temperature, T_c/T_{fo}

T_f = Fluid temperature, K

T_{fa} = Average fluid temperature, K

T_{fa}^* = Dimensionless average fluid temperature, T_{fa}/T_{fo}

T_{fe} = Fluid temperature at collector outlet, K

T_{fe}^* = Dimensionless fluid temperature at collector outlet, T_{fe}/T_{fo}

T_{fl} = Fluid temperature at x = L, K

T_{fl}^* = Dimensionless fluid temperature at x = L, T_{fl}/T_{fo}

T_{fo} = Fluid temperature entering matrix (x=0), K

T_{fo}^* = Dimensionless fluid temperature at x=0, $T_{fo}/T_{fo}=1$

T_{fx} = Fluid temperature at point x in the matrix, K

u = Fluid velocity through matrix voids, m/sec

U_L = Overall heat transfer coefficient for collector walls and back plate, $w/(m^2-K)$

v = Fluid velocity, m/sec

v_∞ = Centerline fluid velocity, m/sec

V_i = Matrix sample bulk volume, cm^3

V_w = Volume of displaced water, cm^3

x = Distance traveled through matrix from its top surface, m

Y = Vertical distance from arbitrary datum, m

ρ = Fluid density, Kg/m^3

ρ_a = Density of air, Kg/m^3

ρ_b = Apparent (bulk) density of matrix, g/cm^3

ρ_f = Density of manometer fluid, Kg/m^3

ρ_s = Specific density of matrix solid, g/cm^3

dp/dz = Pressure loss through matrix per unit depth, Pa/m

τ_c = Effective transmittance of collector cover

σ = Stefan-Boltzmann constant, $w/(m^2-K^4)$

μ = Fluid dynamic viscosity, Kg/(m-sec)

η_b = Thermal efficiency of matrix bed, %

η_c = Thermal efficiency of matrix solar collector, %

ϕ = Dimensionless heat loss coefficient, $A_L\ U_L\ T_{fo}/\sigma\ T_{fo}^4$

ψ = Dimensionless direct solar radiation, $I_o/\sigma\ T_{fo}^4$

Γ = Dimensionless mass flow rate, $G\ C_p\ T_{fo}/\sigma\ T_{fo}^4$

θ = Dimensionless volumetric heat transfer coefficient, $h_{va}\ T_{fo}/\beta\ \sigma\ T_{fo}^4$

τ = Matrix optical depth, βx

λ = Matrix porosity, dimensionless

CHAPTER I

INTRODUCTION

The Problem

Abuse of hydrocarbon energy resources has created an energy shortage throughout the world. During winter and spring of 1974 there were definite uncertainties concerning availability of conventional fuel sources for agricultural harvesting and drying of crops. Although uncertainty of obtaining hydrocarbon fuels has created various problems for many farmers, another detriment is the continual increase in cost of these fuels. Projections on future hydrocarbon energy resources and fuel prices indicate that even more critical shortages are lurking in the future and other sources of energy must be sought. It is imperative that scientists associated with energy and agriculture engage in a combined effort in search for new and more efficient energy resources.

Previous researchers have indicated that solar energy has a definite potential for supplying a portion of our present and future energy needs. Low temperature agricultural crop drying offers potential for efficient utilization of solar energy.

Many collectors being promoted for their high efficiencies are either complex in construction and/or have moderate to high initial costs. Therefore, it is desirable to design a simple low-cost

efficient solar collector that may be easily constructed. Since this collector is to be used for crop drying, it is desirable that air be used as a cheap and abundant working fluid for the collector.

Most experimental analyses conducted on air-cooled solar collectors have been with flat-plate type collectors (12, 19). Some of these collectors were made of overlapped glass plates, others used single sheets of corrugated metal, while still others used metallic sheets with built-in fluid circulating channels. The general principle of all these is essentially the same; a black surface faces the sun and absorbs its energy, then heat is transferred to a circulating fluid as it flows over the plate or through fluid channels.

There is usually only one layer of absorbing material facing the sun and therefore heat transfer area is usually low. With air, heat transfer coefficients are generally low, thus requiring large plate temperatures for collecting substantial amounts of energy. These large plate temperatures increase collector heat losses to the atmosphere and therefore reduce its overall efficiency. As a result, larger collector areas are required, increasing initial construction and maintenance costs.

Utilization of porous media (matrices) as an effective absorber for solar collectors offers several advantages. First, such matrices have high heat transfer area to volume ratios, usually accompanied by high heat transfer coefficients. It may then be expected that a porous bed subjected to solar radiation will absorb its radiant energy in depth and result in high heat transfer rates. Higher heat transfer rates, due to larger area to volume ratios result in reduced operating temperatures. A collector operating with low temperature differences

will have less heat loss and hence higher efficiency. Improved efficiency results in a reduced collector size needed for a given energy requirement.

As implied above, an efficient low-cost collector design might be one in which a matrix (porous media) is used as the major absorber. One problem is to select a low-cost and durable porous material that may be easily installed in solar collectors. Duralast filter material is a non-metallic porous material that satisfies these requirements and has several additional advantages. It is lightweight, flexible, readily obtained in large quantities and non-corrosive. The term matrix is used throughout this paper to refer to a layer or bed of porous media having inter-connecting voids.

Accurate theoretical analysis of a matrix solar collector design provides a means of evaluation and prevents costly construction and testing of additional models and prototypes. However, most of the available analytical solutions to heat transfer phenomena in matrix collectors have required complicated manipulation of complex differential and integral equations. Solutions to these equations are usually obtained by a numerical analysis technique. The numerical analysis generally requires the aid of a digital computer for obtaining a solution. Thus, there is a need to develop a simple method to theoretically evaluate the performance of a matrix solar collector.

Knowledge of fluid flow and heat transfer characteristics of the matrix are necessary before analytical analyses can be completed.

Design and construction of a collector prototype is also needed to obtain experimental data that can be used to verify theoretical calculations.

The collector design should be evaluated for its applicability to agricultural crop drying.

Objectives

The objectives of this study are:

1. Develop a simple method to theoretically evaluate the performance of matrix solar collectors.
2. Design and construct a low-cost and efficient matrix solar collector.
3. Analyze the solar collector by theoretical and experimental techniques.
4. Evaluate the collector design for solar peanut crop drying.

Limitations of the Study

Several matrix properties such as volumetric heat transfer coefficient, bed scattering coefficient, and variable radiant exchange factors used in analyses conducted by other investigators (1, 5, 9, 11) were not determined in this study. The developed theory in this study did not require direct knowledge of these parameters. In addition, matrix configuration and limited instrumentation prohibited accurate measurement of bed and fluid temperature profiles within the matrix layer.

Experimental prototype studies used to verify theoretical analyses were conducted on clear days making no attempt to account for diffuse radiation. This procedure was violated to some degree during peanut drying studies because of weather conditions.

In order to hold the scope of this work to a manageable level, no attempt was made to determine effects of collector shape, air inlet location, and size, and collector angle on performance.

CHAPTER II

LITERATURE REVIEW

A study of climatological data reveals that during Oklahoma's peanut drying season (October to November), ambient temperature ranges from 18 °C to 29 °C are quite common. At these temperatures, an increase of 10 °C usually results in a decrease of 20-40% in air relative humidity. This decrease in humidity should provide an adequate vapor pressure differential necessary for proper drying. Researchers have also indicated that 35 °C is a maximum safe drying temperature for peanut curing. These drying criteria indicate a 10 °C temperature rise should be more than adequate for most Oklahoma fall peanut drying conditions.

Beulow (2, 3) and Satcunanathan (16) have shown that a flat-plate solar collector's efficiency increases significantly as temperature rise across the collector decreases. Therefore, use of solar collectors as an energy source for drying peanuts with temperature rises less than 10 °C offers great potential. These small temperature rises needed in peanut drying allow the collector to operate at near maximum efficiency, thus creating an attractive method for efficient utilization of solar energy.

Solar collectors utilizing air as a working fluid have several advantages over those using water when used for agricultural crop drying. One advantage is, corrosion inside collector chambers and

transport ducts are minimal for air solar collectors. Sealing the collector system for leaks is generally not as critical when air is the energy transporting fluid. Since heated air can be directly used for drying, no additional heat exchangers are necessary as they would be with closed water systems.

There is scarce experimental data in literature concerning thermal behavior of radiatively participating porous materials (matrices). However, much work has been done to obtain analytical solutions of such problems. Leung and Edwards (11) formulated an exact solution of simultaneous radiation, conduction, and convection heat transfer for steady-state conditions in a one-dimensional, semi-infinite, isotropic, homogeneous, absorbing, and scattering porous bed. Coppage and London (6) experimentally determined heat transfer and flow friction characteristics of porous media by heating and cooling woven wire meshes and spheres. They expressed the product of the Stanton and Prandtl number as a function of Reynolds number.

Tong and London (18) studied heat transfer and flow characteristics of screen and cross-rod matrices for Reynolds numbers ranging from 5.0 to 100,000 and for matrix porosities of 0.60 to 0.83. Their study was related to the use of matrices as fuel-element geometries for certain types of nuclear reactors.

Detailed analytical solutions for heat transfer in porous beds have been presented by Weiner and Edwards (21). However, as mentioned by Viskanta (20), future development must rest on critical appraisal of analytical results in light of experimental data. Unless more detailed experimental data are obtained, accurate assessment of matrix solar collectors cannot be made. Most analytical solutions mentioned

above, require simplifications be made to reduce governing mathematical relationships.

Beckman (1) has solved the problem analytically by assuming a one-dimensional, steady-state temperature distribution within an isotropic porous bed subjected to collimated and diffuse heat flux and a transparent flowing fluid. The porous bed was assumed to be a gray nonscattering body and to have a constant absorption coefficient. He also assumed a finite volumetric heat transfer coefficient and therefore bed and fluid temperatures were different. In the analysis by Leung and Edwards (11) it was assumed that volumetric heat transfer coefficients were infinite and thus resulted in equal bed and fluid temperatures.

Hamid and Beckman (9) experimentally investigated performance of air-cooled radiatively heated screens by using a small collimating test box with stacked copper wire screens forming the absorbing matrix. Their results were compared with theoretical analysis conducted by Hamid and Beckman (10). The experimental investigation covered a range of flow rates between 1.3 and 11.6 $m^3/(min\text{-}m^2)$. Their experimental and analytical models consisted of a porous bed heated by diffuse longwave and collimated shortwave radiation and cooled by flow of a transparent gas normal to the bed.

Chiou, Duffie and El-Wakil (5) studied slit-and-expanded aluminum-foil matrix solar collectors of the types shown in Figure 1. The unidirectional flow type collector has its upper surface area subjected to cool incoming air thus reducing top cover losses. Chiou's (4) analysis consisted of using experimental data and known functions of the fanning friction factor, Reynolds and Nusselts numbers to

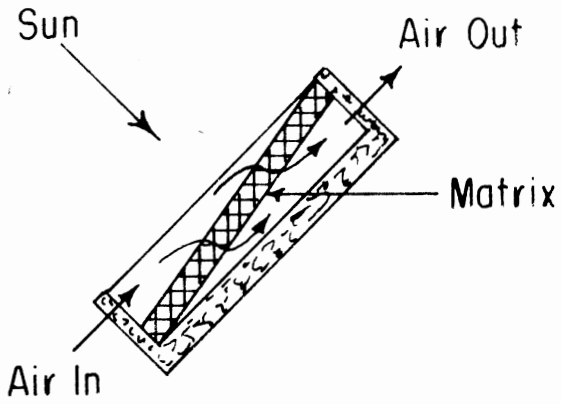

(a) Unidirectional Flow Type

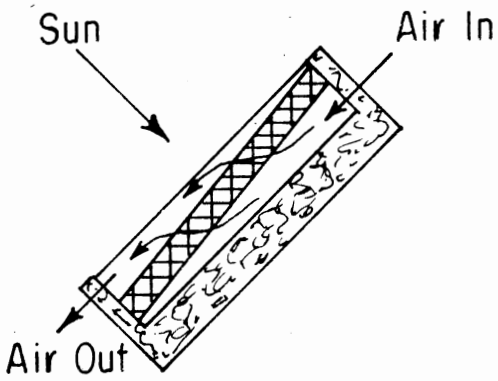

(b) Counterflow Type

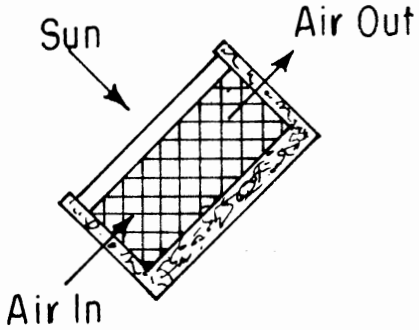

(c) Cross Flow Type

Figure 1. Types of Matrix Solar Collectors Studied by Chiou, Duffie and El-Wakil (5).

analytically evaluate the types of collectors shown in Figure 1. The unidirectional type proved to be most efficient.

Locke (13) and Marco and Han (14) have extensively studied the utilization of porous and matrices in compact heat exchangers used in the aircraft industry. Locke (13) studied heat transfer and friction characteristics of porous media. Marco and Han (14) investigated heat transfer by convection through porous materials.

As indicated above there has been considerable research conducted in analytical studies and some experimental work done on metallic type matrix collectors. However, no information has been found for heat transfer analysis of solar collectors using non-metallic Duralast filter media as the absorber. Neither has a relatively simple analytical solution been developed that may be used to evaluate the performance of a matrix solar collector.

CHAPTER III

EQUIPMENT AND INSTRUMENTATION

Test Model

The following is a description of a small test model constructed and instrumented for measuring the average extinction coefficient and friction loss through Duralast filter media. Duralast filter media is a non-metallic porous material that is used throughout this study as the basic matrix absorber for the solar collector.

Model Construction

A small test box as shown in Figure 2 was constructed from 26 gauge sheet metal rolled into a cylinder with a 929 square centimeter (cm^2) cross-sectional area. The model was constructed to support various depths of test specimens of Duralast filter media. Holes 2.54 centimeters (cm) in diameter were drilled in the model wall above the test specimen to serve as air inlet ports. Wire mesh was placed below the test specimen to create uniform air flow.

For a top cover plate, a single sheet of six mil clear polyethylene was stretched tightly over a plywood ring. Quick removal of the cover plate for changing bed specimens was accomplished by simply slipping the plywood ring over the outside of the test box. The same sheet of polyethylene was also used in tests for measuring effective

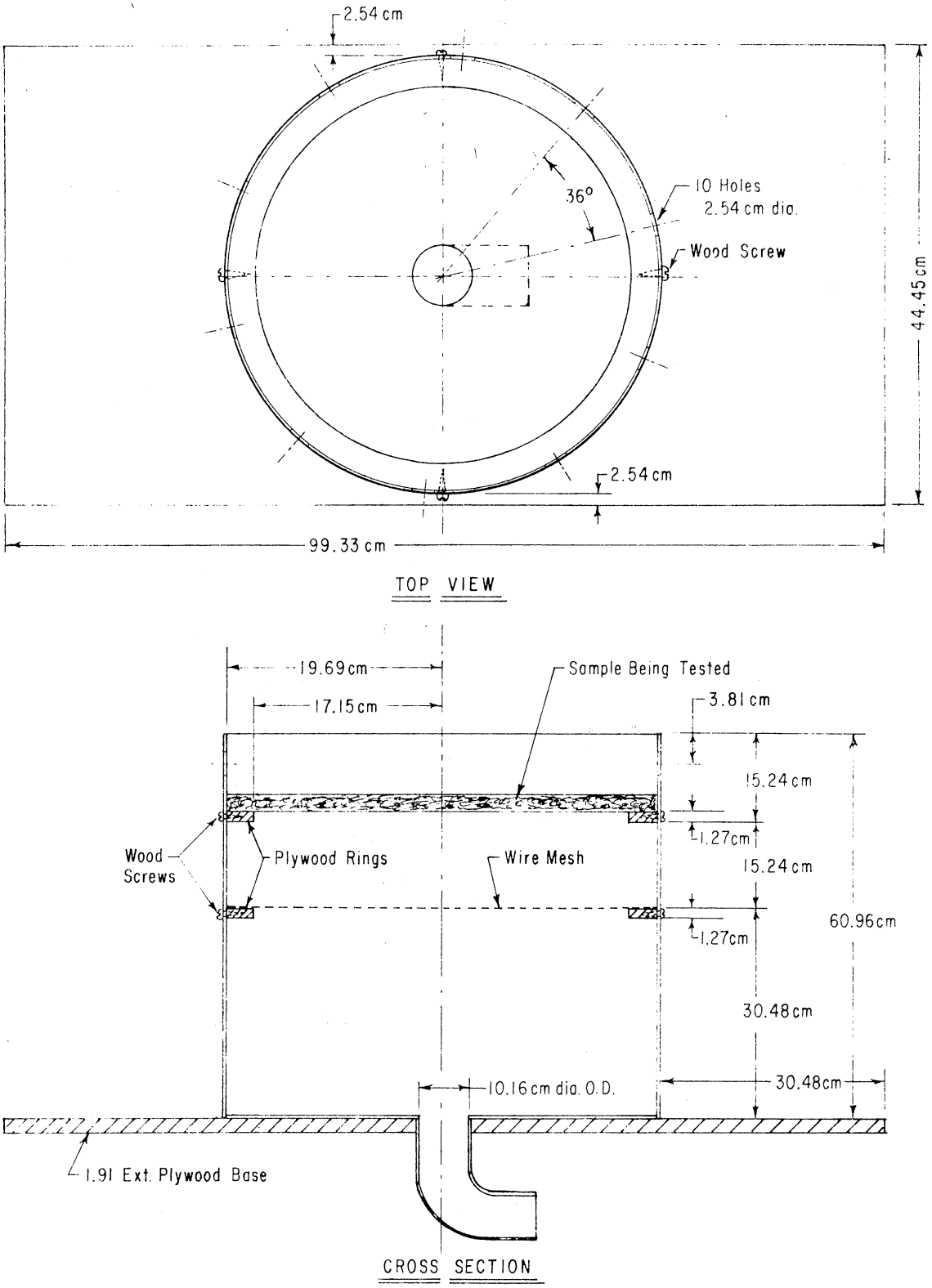

Figure 2. Test Model Working Drawing.

cover transmittance.

Model Instrumentation

A flexible hose was used to connect the test box outlet to the suction side of a small fan. A pitot-static tube was placed in the center of a small copper pipe connecting the hose and fan. The pitot-tube was placed in the pipe 45 diameters downstream from the entrance to provide a fully developed velocity profile. All velocities measured in the model and prototype studies were of fully developed turbulent flow.

Pressure drop through inlet ports around the test box perimeter was considered negligible when compared to pressure drop across deep matrix beds of porous material. A pressure tap was inserted just below the lower surface of matrix specimens. An inclined manometer was connected to this pressure tap and used to measure pressure drop across the matrix bed. Atmosphere pressure was used as measure of pressure above the bed.

An Eppley total radiation pyranometer was located on a platform just beneath the matrix as indicated in Figure 3. Output signals were recorded with a Leeds and Northup potentiometer.

Collector Prototype

Design Criteria

A matrix air-cooled collector design was selected for its high heat-transfer area to volume ratio allowing it to operate at low temperatures. Reduced operating temperatures yield lower collector

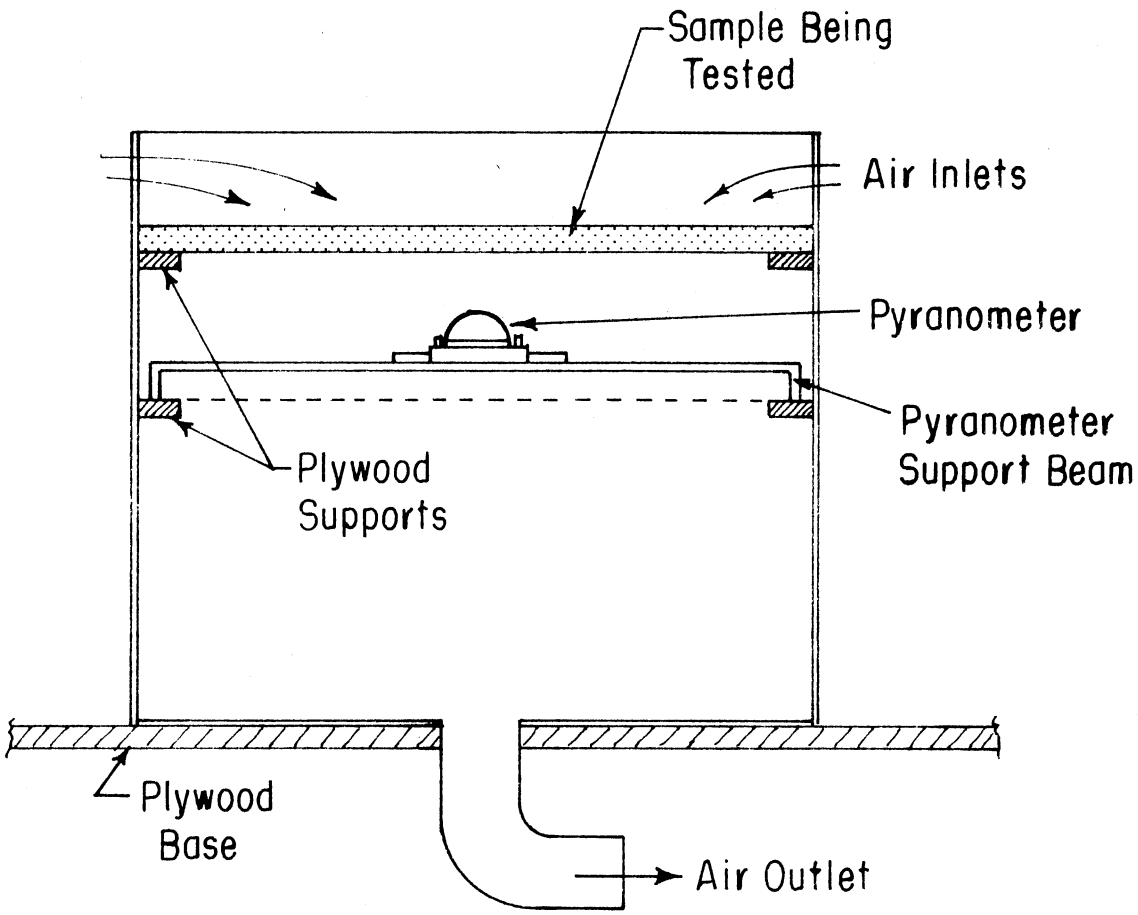

Figure 3. View of Pyranometer Position During Test Model Experiments.

losses and result in higher efficiencies. It is desirable to design a collector with lower cover losses and to minimize collector shading effects during earlier morning and late evening hours. Construction should be simple and cost of materials keep to a minimum. These specifications should result in a low-cost highly efficient solar air-cooled collector that might effectively be applied to agricultural crop drying.

Collector Construction

A wedge-shaped air-cooled matrix solar collector was designed from the previous specifications. Figure 4 is a working drawing of the collector constructed from two 1.22m X 2.44m sheets of 1.27cm plywood. The wedge-shaped sides were designed to minimize shading effects while still providing sufficient air space between the absorber and cover. The collector was covered with six mil clear polyethylene plastic. Expanded metal (Figure 5) was used to support a 1.91cm layer of Duralast filter media 6.4cm below the collector cover. The porous material was sprayed with Krylon flat black paint to improve its absorptivity. The air chamber and plenum duct located beneath the matrix absorber were insulated with styrofoam to reduce heat losses to the surrounding atmosphere. Two sheets of plywood provided all the necessary structural components except for two support beams located on the collector back plate.

Figure 6 shows the collector constructed and connected to an individual peanut drying bin. The suction side of a small straight-blade centrifugal fan was connected by insulated pipe and flexible hose to the collector outlet. The fan pulled air through inlet ports around the collector perimeter and into a space between

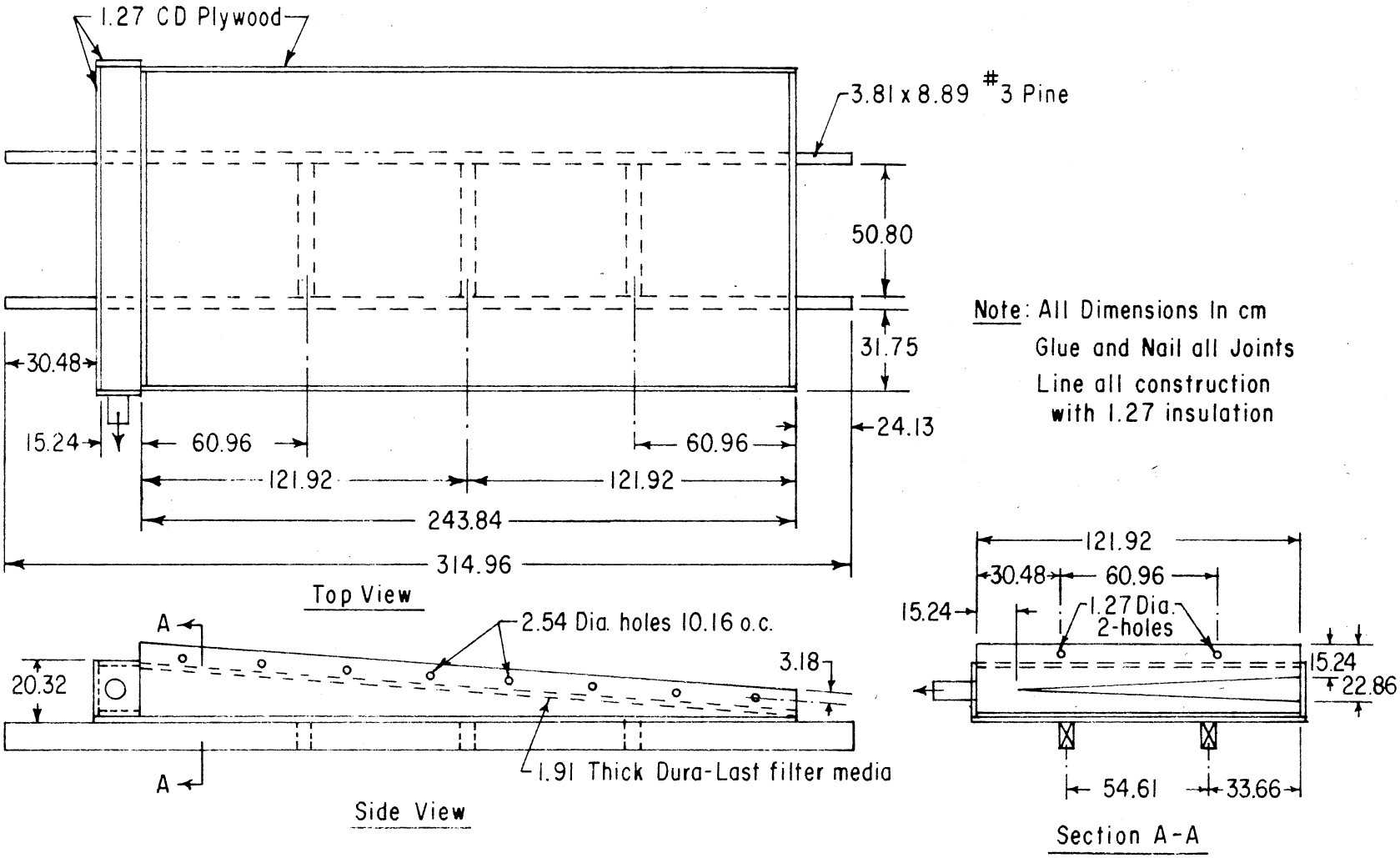

Figure 4. Wedge-Shaped Matrix Solar Collector Working Drawing.

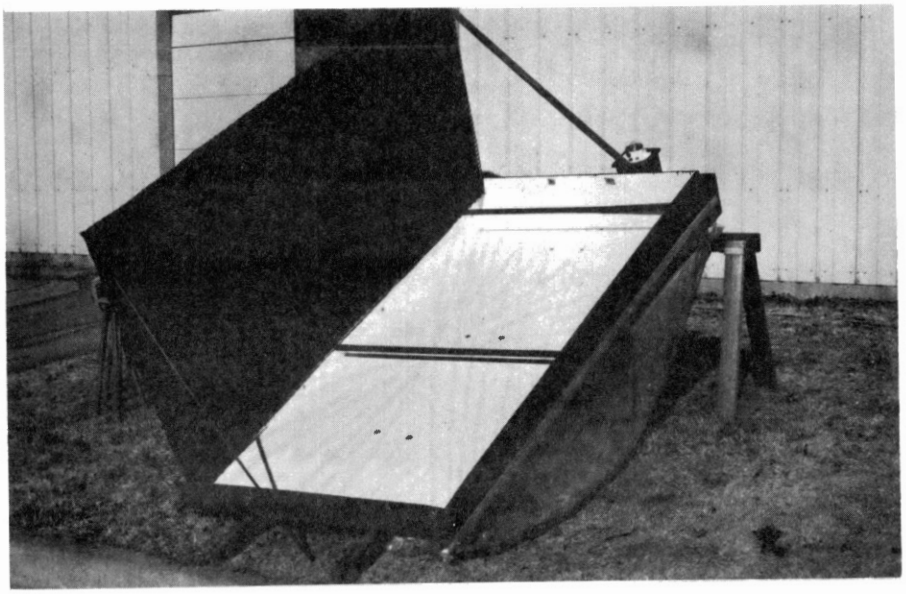

Figure 5. Wedge-Shaped Solar Collector with Absorber Removed to Show Air Chamber Beneath the Matrix Bed.

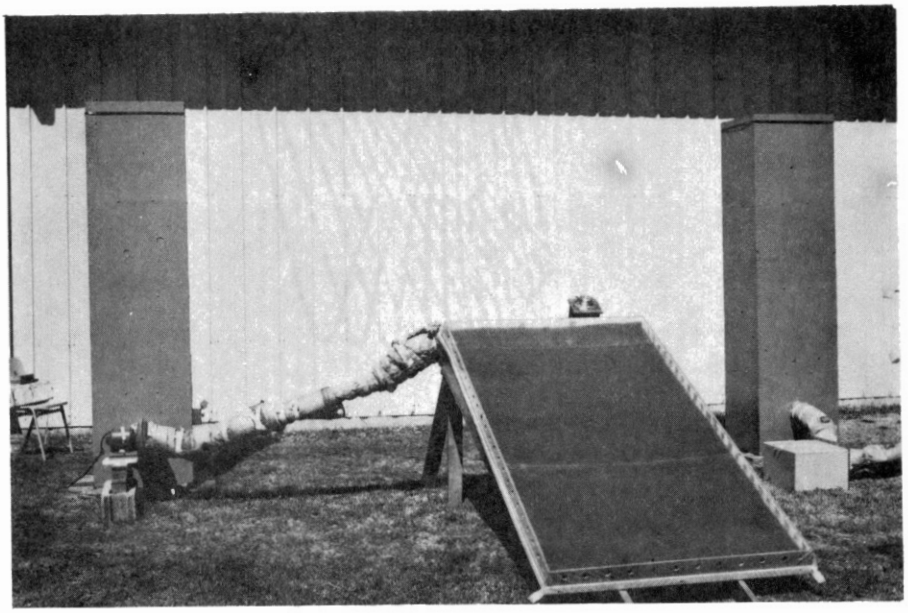

Figure 6. Matrix Solar Collector Connected to Suction Fan and Peanut Dryer.

the matrix bed and cover. Air then passed through the matrix where it was heated by convection. After passing through the matrix absorber, air flowed along the collector floor to an opening in the plenum chamber shown in Figure 7. Air flowed through the plenum chamber to the collector outlet in a direction perpendicular to flow at the plenum inlet. Because of this rapid change in flow direction, a triangular shaped plenum inlet was needed to provide a more uniform air flow through the matrix bed. Immediately after air passed through the triangular inlet shown in Figure 7, it turned and traveled horizontally to the left toward the collector outlet.

Collector Instrumentation

Flexible hose was used to connect a well-insulated circular duct to the collector outlet. The other end of the duct was connected to the suction side of a centrifugal fan. A variable transformer was used to vary fan speed to obtain desired flow rates. Diameter of the duct was reduced from 10.16cm to 5.08cm to increase air flow to a turbulent regime with velocity heads measurable with an inclined manometer. A pitot-static tube was placed in the pipe's center, 25 diameters downstream from the change in cross-section. This was an attempt to provide a fully developed velocity profile. An inclined manometer was used to measure centerline velocity head.

A shielded copper-constantan thermocouple was secured in the centerline of the outlet duct near the collector. Another shielded thermocouple was placed in the atmosphere near the collector test site. A Honeywell temperature recorder was used to constantly monitor inlet and outlet collector temperatures.

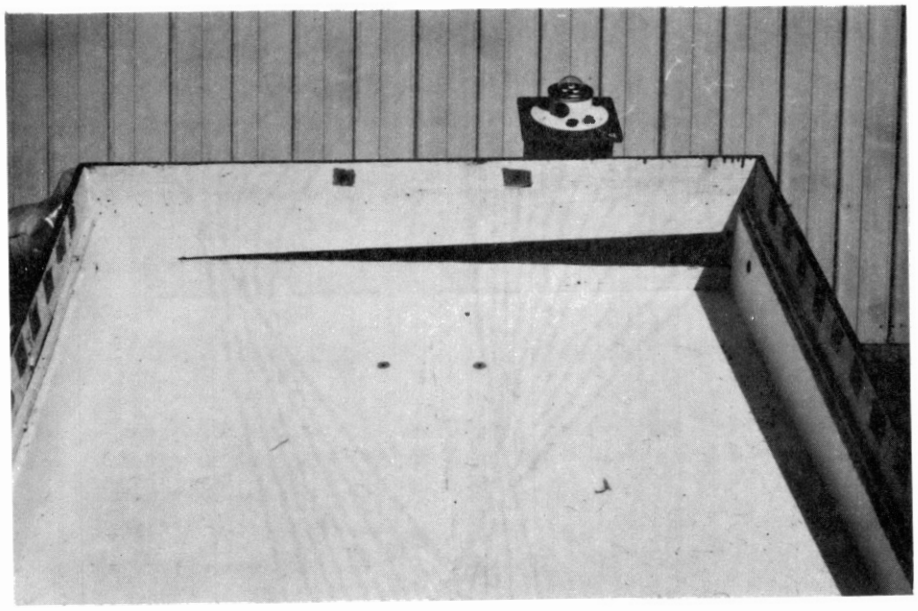

Figure 7. Top View of Collector with Matrix Removed Showing Triangular Plenum Inlet.

An Eppley black and white pyranometer (Figure 7) was placed on the collector base to measure total direct and diffuse insolation. A Leeds and Northup potentiometer was used to record emf signals produced by the pyranometer.

Solar Peanut Drying Equipment

Construction of Collectors

Four, three square-meter (m^2) prototype wedge-shaped matrix solar collectors were constructed from the drawing in Figure 4. The collectors were instrumented using the procedure described in the previous section.

Construction of Peanut Dryers

Four 225 kilogram (Kg) capacity peanut dryers (bins) were constructed from two sheets of 1.27cm exterior grade plywood. Figure 8 is the working drawing used in primary construction. Peanuts were supported in the upper 1.83m of the bin by a perforated steel plate. This created a plenum chamber beneath the perforated floor consisting of a 0.61m cube insulated with styrofoam to prevent excess heat loss. To provide uniform air flow through the drying bed cross-section, angle iron was placed on the inside of bin walls at approximately 0.61m intervals. This was expected to minimize problems typically encountered in small bin sizes with large air velocities along bin walls and corners. Figure 9 shows one of the dryers constructed and instrumented with auxiliary heaters controlled by thermostats.

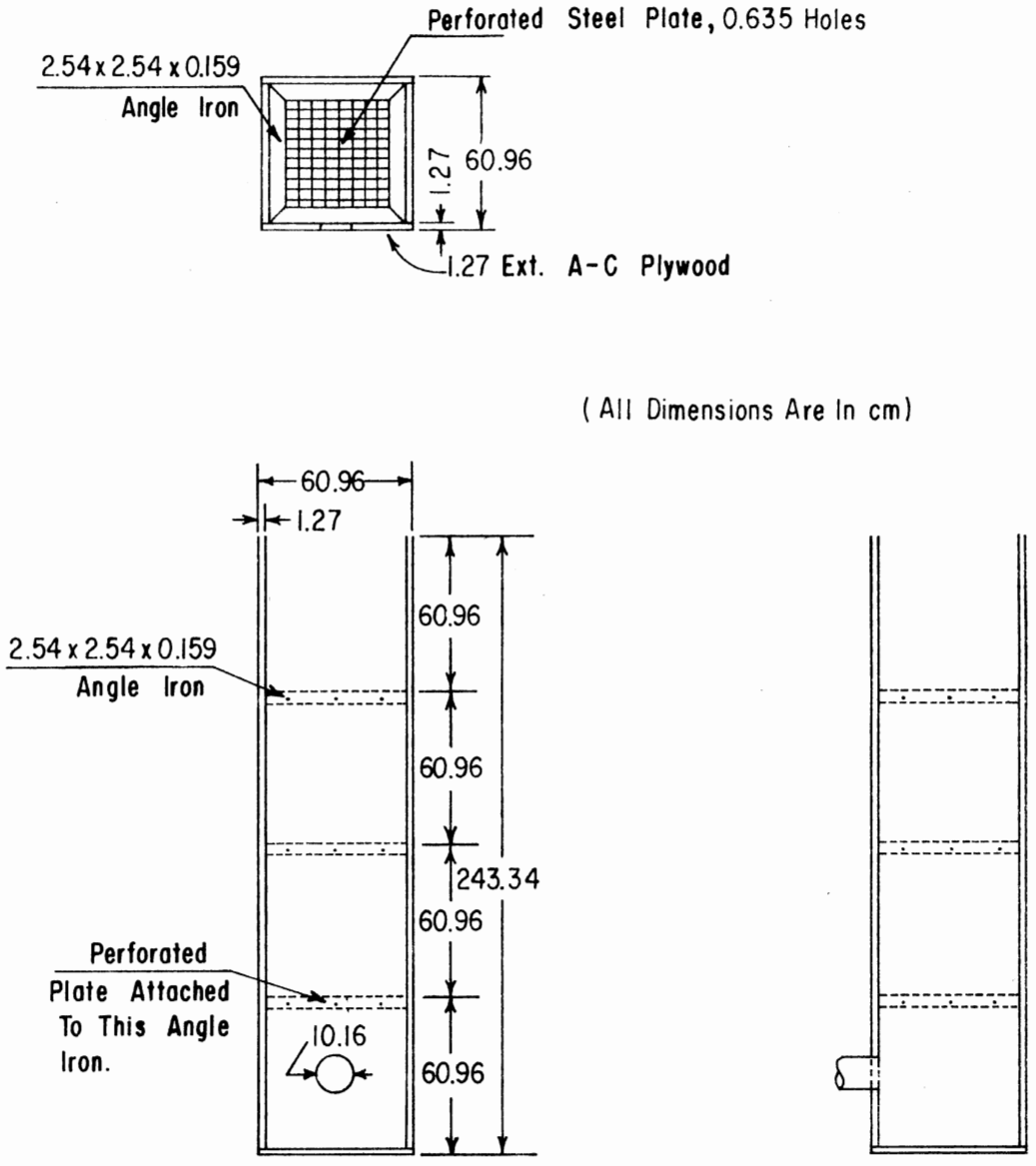

Figure 8. Working Drawing of Peanut Dryer.

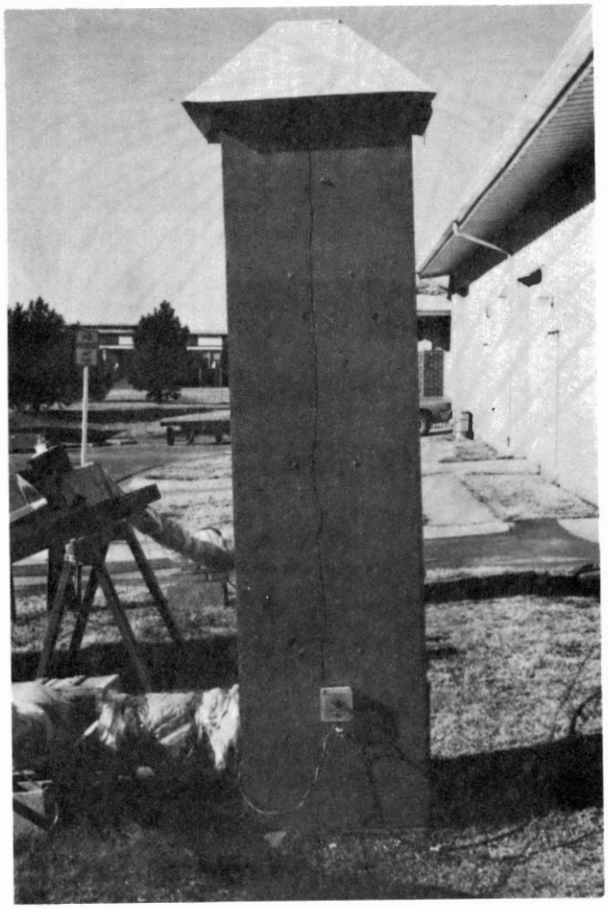

Figure 9. Peanut Dryer Assembled with Auxiliary Heaters Attached.

Dryer Instrumentation

Straight-blade centrifugal fans being used to operate the collectors were connected to individual drying bins as shown in Figure 10. Electrical resistance auxiliary heaters were positioned between fan outlets and drying bins to provide supplemental heat when required. Pitot-static tubes were placed in insulated pipes connecting the fans to collector outlets and an inclined manometer was used to measure the respective centerline velocity heads.

Solar collectors and drying bins were placed on the test site as shown in Figure 11. A 24-point temperature recorder was used to constantly monitor inlet and outlet temperatures of the solar collectors and dryers. Outlet temperature of the dryer was measured by embedding a copper-constantan thermocouple in the upper 15cm of peanut pods.

Relative humidity measurements were made periodically using a sling-psychrometer. Also, a continuous recording of ambient dewpoint temperature was obtained using a dewpoint probe and potentiometer recorder. An Eppley pyranometer was used to record incoming solar radiation during daylight hours. The pyranometer was oriented parallel to the collector angle to eliminate need for angle correction.

Velocity Measurements

For velocity ranges used in this study air could be assumed an incompressible fluid. Bernoulli's equation (15) states for a steady incompressible fluid

$$\frac{1}{2}\frac{v^2}{g_a} + \frac{P}{\rho g_a} + Y = \text{constant} \qquad [1]$$

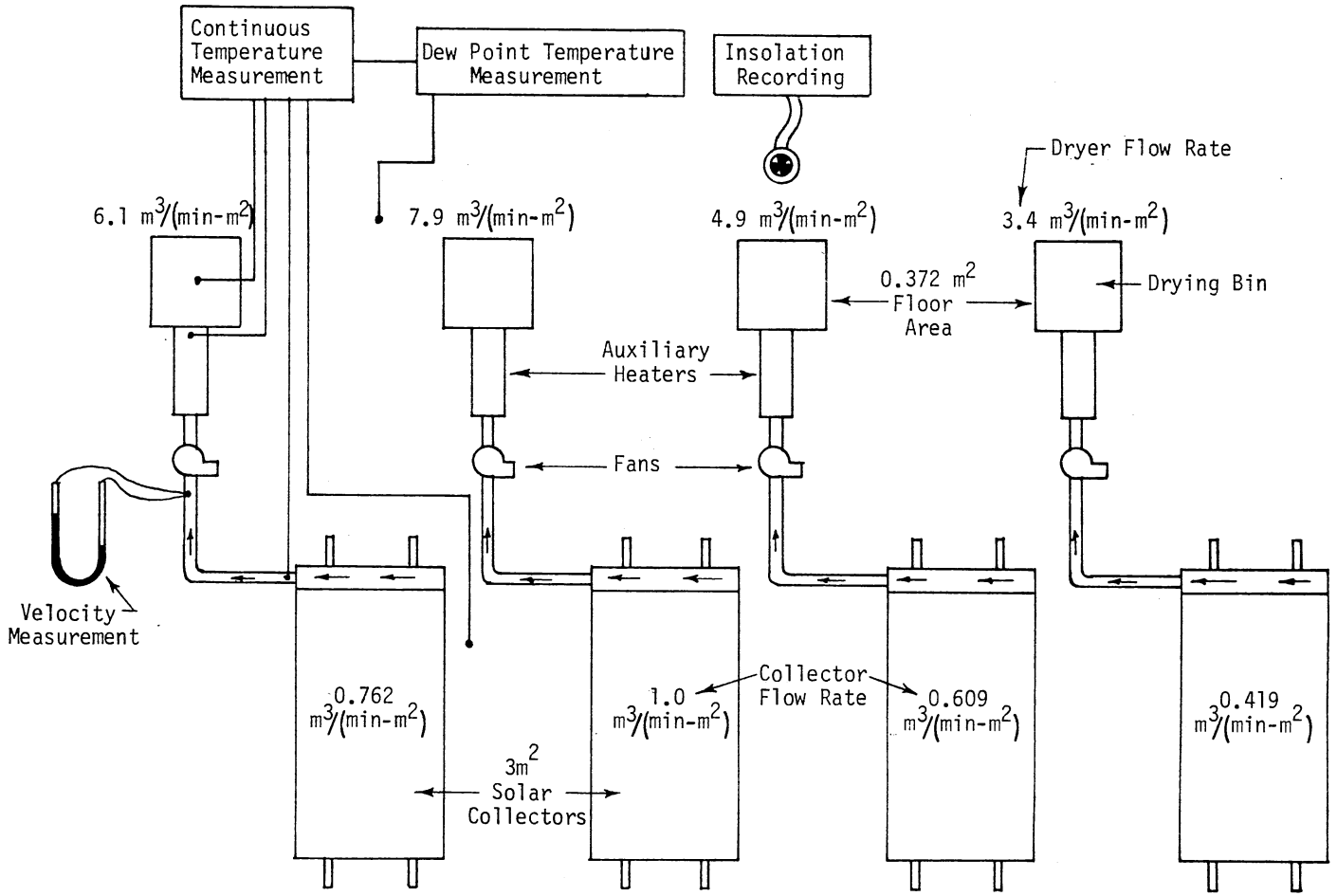

Figure 10. Experimental Layout of Solar Collectors and Dryers at Test Site.

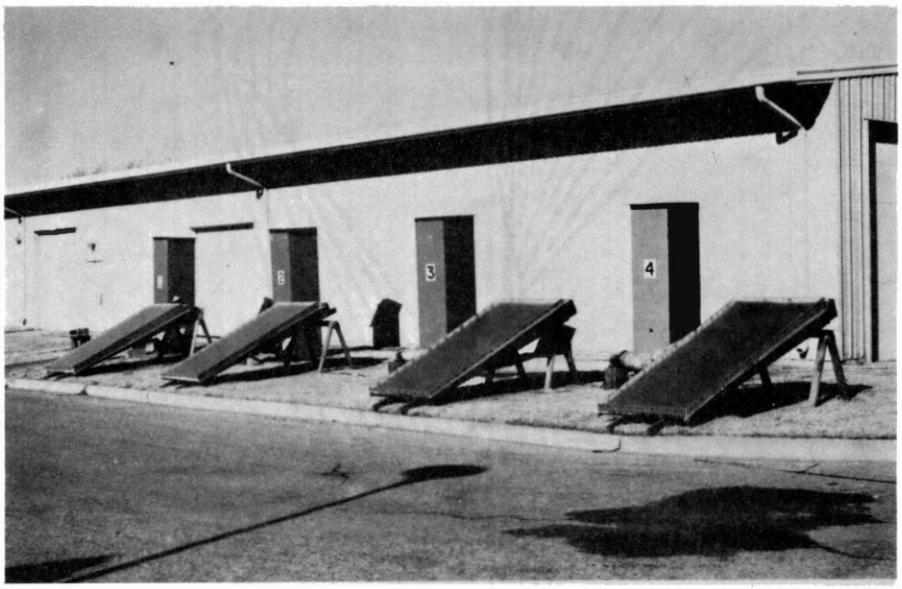

Figure 11. Solar Peanut Dryers and Collectors Assembled on Test Site.

where

v = Fluid velocity, m/sec

P = Static pressure, Pa

ρ = Fluid density, Kg/m^3

g_a = Acceleration of gravity, m/sec^2

Y = Vertical distance above a specified datum, m

All velocity measurements in this study were made by placing a pitot-static tube in the pipe's centerline. Solving equation 1 for this case yields the following expression for centerline velocity, v_∞.

$$v_\infty = [2g_a \Delta h (\rho_f/\rho_a - 1)]^{1/2} \qquad [2]$$

Δh = Velocity head, m

ρ_f = Density of manometer fluid, Kg/m^3

ρ_a = Density of air, Kg/m^3

After centerline velocity has been determined, some estimate of average velocity must be made before flow rate can be calculated. For turbulent flow in smooth pipes, Schlichting (17) has presented ratios of the mean to maximum velocity of 0.79-0.82 for Reynolds number varying from 4,000-110,000. Velocities encountered in this study resulted in Reynolds numbers between 4,000 and 110,000. A velocity ratio of 0.82 was selected for calculations of flow rate in this study.

CHAPTER IV

EXPERIMENTAL DESIGN AND PROCEDURE

Test Model

Theoretical evaluation of the solar collector designed in this study required a knowledge of the matrix's average extinction coefficient. Addition matrix properties which may prove useful in future studies with Duralast filter media are porosity, friction coefficients, and density. The following procedure was used in evaluating these properties.

Determination of Matrix Porosity

Available commercial thicknesses of Duralast filter media were 1.27cm and 1.91cm. Three samples, measuring 8cm X 18cm, of each thickness were coated with Krylon flat black paint and allowed to dry. Then each sample was weighed and submerged in a column of water. Fluid displacement was used as a measure of volume change. Volume of displaced water represented the volume of the sample's solid material.

Bed Friction Loss Characteristics

A pressure tap was placed in the model wall below the matrix bed and used to measure pressure drop across test specimens. Preliminary tests revealed that a relatively thick layer of absorber bed should be

used to provide measurable values of static pressure head. As a result, a thickness of 10.8cm was selected as an adequate bed depth. A randomized block design using three replications was selected for the experiment. Flow rates ranged from 0.55 to 3.95 $m^3/(min\text{-}m^2)$.

Average Extinction Coefficient

Matrix beds were removed from the model and an Eppley black and white pyranometer was positioned just below the edge of bed supports as shown in Figure 3. Bed samples of 1.27cm and 1.91cm thicknesses were used to randomly vary bed depths from zero to 3.81cm. A digital millivolt recorder was used to monitor emf signals from the pyranometer. During each test the matrix surface was oriented perpendicular to the sun's rays. After matrix depth increased sufficiently to absorb all incoming radiation, the beds were removed and a final reading was taken. The average of initial and final readings was used as the value of available insolation during these tests.

Effective transmittance of a single layer of six mil polyethylene was measured using the procedure mentioned above.

Collector Prototype

Collector prototype experiments were conducted within two hours from solar noon and on clear days. This reduced collector shading and diffuse radiation effects. Each test consisted of orienting the collector due south at the normal angle of incidence occurring at solar noon. The collector was initiated and operated at a design flow rate until thermal equilibrium occurred. Inlet and outlet temperatures, insolation (solar radiation), and flow rate were recorded for a time

duration of 30 minutes. Measurement of ambient wet bulb temperature was also recorded to provide calculation of air density. Three replications of each test were conducted in a complete randomized design. Collector flow rates ranged from 0.3 to 2.4 $m^3/(min\text{-}m^2)$.

Solar Peanut Drying

Solar Drying Design

Table I is the experimental block design used for solar drying studies. Dryer flow rates ranged from 3.4-7.9 $m^3/(min\text{-}m^2)$*. Table I lists the collector sizes used for each drying block. The four dryers and corresponding solar collectors were operated simultaneously during each test block. Blocks one-five were conducted using the same collector area ($3m^2$) for each dryer. As shown in Table I, the sixth test block was conducted with three dryers using one-half the original collector area while the fourth dryer continued to utilize full collector area. Reduction in collector area was accomplished by covering the matrix bed with 2.54cm styrofoam insulation. Figures 10 and 11 show the location of solar collectors and dryers during testing.

Drying Procedure

During the first week of October, 1975, freshly harvested Spanish peanut pods with 30% kernel moisture content, wet basis**, were obtained from the Oklahoma State University Agricultural Experiment

---

*Dryer flow rates are based on a dryer floor area of 0.341 m^2.
**All moisture contents reported in this study are wet basis and were obtained by oven-drying the kernels at 130 °C for six hours.

Station at Stratford, Oklahoma. Each dryer was filled with 200 Kg of these pods to a depth of 1.37m. This test was used as a preliminary drying trial to facilitate instrument calibration and adjustment before actual data were collected. More peanuts were obtained on October 8 and actual testing began on October 9.

TABLE I

SOLAR DRYING EXPERIMENTAL DESIGN

Block I. D.	Dryer I. D.	Dryer Flow Rate $m^3/(min\text{-}m^2)$	Collector Area m^2
1, 2, 3, 4, 5	1	6.1	3.0
1, 2, 3, 4, 5	2	7.9	3.0
1, 2, 3, 4, 5	3	4.9	3.0
1, 2, 3, 4, 5	4	3.4	3.0
6	1	6.1	1.5
6	2	7.9	1.5
6	3	4.9	1.5
6	4	3.4	1.5

Peanuts were inverted approximately four days before testing and pods were usually placed in dryers within 24 to 36 hours after combining. The short time period from harvesting to drying did not

allow any visible mold growth to occur.

A typical drying test consisted of placing 200 Kg of freshly harvested pods at 20-30% moisture content in each drying bin. Drying began between 8:00 and 10:00 A. M., on the first day and was ended when estimated final kernel moisture content dropped below 10%. Periodically, average kernel moisture content of the upper 15cm of pods in the drying bin was obtained to aid in determining dryer shutoff times. The drying blocks were conducted at approximately one week intervals.

Solar collectors provided the total heat input between the hours 8:00 A. M., and 4:00 or 5:00 P. M., each day, while auxiliary heaters were operated the remaining time. The solar collectors were pointed due south and tilted 24 degrees from horizontal. In case of relative humidities above 85-90% occurring during mid-day hours, supplemental heat was supplied with auxiliary heaters to insure adequate drying.

Approximately two Kg of pods were collected from each harvested lot and used as milling standards. These standards were dried conventionally at 30.5 °C $\pm$ 1.7 °C to 8-10% final kernel moisture content with a dryer flow rate of 6.0 $m^3/(min\text{-}m^2)$. When each solar drying test was completed, a two Kg sample was taken from each dryer and used for milling tests. Standard and solar drying samples were stored in air-tight containers at 4-5 °C until milling. Samples were removed from this storage 24 hours prior to shelling and allowed to reach ambient room temperature. These samples were shelled in the same order as they were dried in an effort to equilize their storage time. This would hopefully eliminate any difference occurring between samples resulting from storage times.

Milling tests were conducted with United States Department of Agriculture (USDA) Standard Grading Procedures. Three 500-g pod samples were removed from each original two Kg sample and shelled in random order resulting in three milling replicates for each sample. Percent sound splits (%SS), defined as the percent of the original pod sample made up of sound mature splits after shelling, was used as a measure of milling quality.

CHAPTER V

DEVELOPMENT OF THEORY

Several assumptions were made to reduce mathematical relationships governing flow and heat transfer characteristics of the matrix solar collector. It was assumed that axial and horizontal conduction through the non-metallic porous bed could be neglected. The bed was assumed to be a gray nonscattering body and to have a constant absorption coefficient. The bed was considered to have a one-dimensional steady-state temperature distribution within an isotropic porous medium. Only direct radiation effects were considered. However, diffuse radiation also contributes to solar radiation and can become significant in an overcast sky.

Because of low temperature differences between the matrix's lower surface and the outlet air, and between the outlet air and the front side of the collector back plate, heat transfer by radiation between these parts was neglected. Air picks up heat by convection as it makes contact with the top matrix surface. However, most of this air passes directly into the matrix body where it is heated as it makes contact with matrix inter-parts. No attempt was made to separate convection heat transfer on the top matrix surface from that occurring within the matrix bed.

Absorption of radiation by a partially transparent medium can be described by Bouger's law (7), which is based on the assumption that

absorbed radiation is proportional to local intensity in the medium and distance radiation travels through the medium;$dI = \beta I dx$, where β is the extinction coefficient and is assumed a constant in the solar spectrum, I is local intensity, and x is distance traveled through the medium. Integrating the above expression between the limits of zero and L, the bed depth, yields $I_L/I_0 = e^{-\beta L}$. The ratio I_L/I_0 is used to determine the amount of solar radiation passing through the matrix layer (bed) unabsorbed.

Neglecting axial conduction, an energy balance on a fluid element within the bed becomes

$$G\, C_p \frac{\partial T_f}{\partial x} - h_{vx} (T_{bx} - T_{fx}) = 0 \qquad [3]$$

and neglecting diffuse radiation effects, an energy balance on the bed element yields

$$\tau_c I_o\, e^{-\beta x} - h_{vx} (T_{bx} - T_{fx}) - \sigma E_{gx} (T_{bx}^4 - T_c^4) = 0 \qquad [4]$$

where

G = Mass flow rate per unit area, $Kg/(hr\text{-}m^2)$

C_p = Specific heat of fluid, w-hr/(Kg-K)

T_f = Temperature of fluid, K

x = Distance from top of bed surface, m

h_{vx} = Volumetric heat transfer coefficient at point x in the bed, $w/(m^3\text{-}K)$

T_{bx} = Temperature of bed at x, K

T_{fx} = Temperature of fluid at x, K

τ_c = Effective transmittance of collector cover

I_o = Direct solar radiation normal to collector cover, w/m^2

β = Average extinction coefficient of bed, m^{-1}

σ = Stefan-Boltzmann constant, $w/(m^2\text{-}K^4)$

E_{gx} = Radiant interchange factor between collector cover and point x in the matrix layer, m^{-1}

T_c = Temperature of cover plate, K

Equation 3 can be integrated from x = 0 to x = L (where L is the total bed depth) yielding

$$G\ Cp\ (T_{fl} - T_{fo}) - L\ h_{va}\ (T_{ba} - T_{fa}) = 0 \qquad [5]$$

where T_{ba} and T_{fa} are average bed and fluid temperatures, respectively, and h_{va} is defined as $\frac{1}{L}\int_o^L h_{vx}\,dx$. Integrating equation 4 with the same limits of x yields

$$\tau_c\ I_o\ (1 - e^{-\beta L}) - Lh_{va}\ (T_{ba} - T_{fa}) - \sigma\int_0^L E_{gx}\ (T_{bx}^4 - T_c^4)\,dx = 0 \qquad [6]$$

Figure 12 pictorally illustrates the energy balance on the bed element. Because of complexity and difficulty in determining E_{gx} for this type of matrix material, it was assumed $\int_o^L E_{gx}\ (T_{bx}^4 - T_c^4)\,dx$ may be approximated by $e_g\ (T_{ba}^4 - T_c^4)$ where e_g is the radiant interchange factor between two parallel plates and T_{ba} is average bed temperature. This assumption means that reradiation from all points within the matrix layer to the cover was approximated by assuming the matrix a flat plate at average bed temperature. Recall that e_g is expressed as

$$e_g = \frac{1}{1/e_b + 1/e_c - 1} \qquad [7]$$

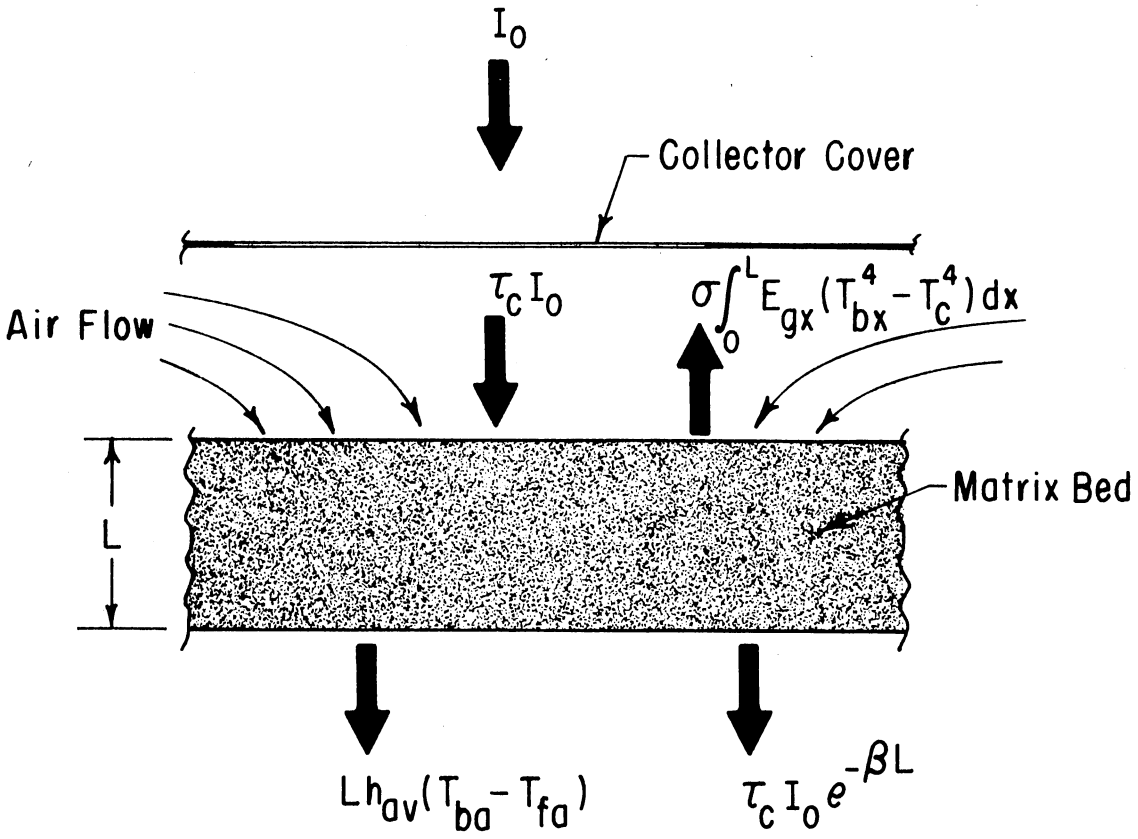

Figure 12. Energy Flow Terms for a Matrix Bed Element.

where

e_b = Emissitivity of bed

e_c = Emissitivity of cover

Equations 3 and 4 must satisfy the boundary condition

$$T_{fx_{x=0}} = T_{fo} \qquad [8]$$

where T_{fo} is temperature of fluid entering the matrix layer. The above boundary condition and use of the Stefan-Boltzmann constant introduces convenient parameters which may lead to obtaining the following dimensionless terms.

T_{fo}^* = Dimensionless temperature ratio, $T_{fo}/T_{fo} = 1$

T_{fl}^* = Dimensionless temperature ratio, T_{fl}/T_{fo}

T_{ba}^* = Dimensionless temperature ratio, T_{ba}/T_{fo}

T_{fa}^* = Dimensionless temperature ratio, T_{fa}/T_{fo}

T_c^* = Dimensionless temperature ratio, T_c/T_{fo}

τ = Optical depth, βx

θ = Dimensionless volumetric heat transfer coefficient, $h_{va}\ T_{fo}/\beta\sigma T_{fo}^4$

Γ = Dimensionless mass flow rate, $G\ Cp\ T_{fo}/\sigma T_{fo}^4$

ψ = Dimensionless direct solar radiation, $I_o/\sigma T_{fo}^4$

When the above dimensionless terms are substituted into equations 5 and 6 they become

$$\Gamma\ (T_{fl}^* - 1) - \tau\theta\ (T_{ba}^* - T_{fa}^*) = 0 \qquad [9]$$

$$\tau_c\ \psi\ (1-e^{-\tau}) - \tau\theta\ (T_{ba}^* - T_{fa}^*) - e_g\ (T_{ba}^{*4} - T_c^{*4}) = 0 \qquad [10]$$

Values of G, Cp, I_o, τ_c, e_g and τ are usually given or can be easily determined by measuring bed depth and the average matrix extinction coefficient. For matrix solar collectors considered in this study (unidirectional), matrix inlet air temperature (T_{fo}) was assumed to be equal to temperature of atmospheric air, which is known for a given condition. With T_{fo} known, corresponding values of ψ can be calculated. Volumetric heat transfer coefficients (h_{va}) for matrices are generally difficult to determine experimentally and vary widely with matrix type and configuration. Therefore, values of the dimensionless volumetric heat transfer coefficient θ, in equation 9 and 10 are usually unknown. However, since dimensionless flow rate Γ, is known, the term $\Gamma(T_{fl}^* - 1)$ in equation 9 can be substituted directly into equation 10 for $\tau\theta\ (T_{ba}^* - T_{fa}^*)$ yielding equation 11.

$$\tau_c\psi\ (1 - e^{-\tau}) - \Gamma\ (T_{fl}^* - 1) - e_g\ (T_{ba}^{*4} - T_c^{*4}) = 0 \qquad [11]$$

Equation 11 has three unknowns, T_{fl}^*, T_{ba}^*, and T_c^*. Assumptions have to be made to reduce the number of unknowns to one (T_{fl}^*) in equation 11.

The matrix collector considered in this study was designed to have small top cover losses. After making contact with the matrix's top surface, cool incoming air flowed immediately into the matrix bed. As a result, the collector cover's underside was always in contact with cool ambient air. Therefore, temperature of the cover plate was assumed equal to temperature of the ambient air, $T_c = T_{fo}$. This yields a value of $T_c^* = 1$.

Preliminary experiments with the test model in Figure 2 indicated that bed temperatures at depths up to 0.0381m were usually within 1K

of fluid leaving the matrix. Hamid and Beckman's (9) study of heat transfer in porous beds indicates that average theoretical bed temperature can be approximated to be equal to fluid temperature leaving the bed. This assumption contains an error of 3-5% for the range of flow rates and optical depths used in this study. From the above analogy, T_{ba} is approximated by T_{fl} and hence $T_{ba}^* = T_{fl}^*$.

Substituting $T_c^* = 1.0$ and $T_{ba}^* = T_{fl}^*$ into equation 11 yields equation 12.

$$\tau_c \psi \ (1 - e^{-\tau}) - \Gamma \ (T_{fl}^* - 1) - e_g \ (T_{fl}^{*4} - 1) = 0 \qquad [12]$$

Equation 12 can be solved for T_{fl}^* implicitly by successive iterations.

Bed efficiency is defined as the ratio of actual temperature rise to maximum temperature rise. Equation 13 was used to calculate bed efficiency for this study.

$$\eta_b = \frac{\Gamma \ (T_{fl}^* - 1)}{\tau_c \psi} \ (100), \ \% \qquad [13]$$

As heated air leaving the bed at temperature T_{fl} passes through the collector ducts, heat loss through collector walls and floor reduces air temperature to some value, T_{fe}, at the outlet. Assuming fluid properties can be evaluated at an average temperature of T_{fl} and T_{fe}, the following energy balance yields a direct solution of T_{fe}.

$$\Gamma \ (T_{fe}^* - 1) = \Gamma \ (T_{fl}^* - 1) + \tau_c \psi e^{-\tau} - \phi \ \left(\frac{T_{fl}^* + T_{fe}^*}{2} - 1\right) \qquad [14]$$

where

T_{fe}^* = Dimensionless temperature ratio, T_{fe}/T_{fo}

$\phi = A_L \ U_L \ T_{fo}/\sigma T_{fo}^4$

A_L = Heat transfer area subject to conduction per unit of collector area, m^2/m^2

U_L = Overall heat transfer coefficient for collector walls and back plate, $w/(m^2\text{-}K)$

The term $\tau_c \psi e^{-\tau}$ in equation 14 represents the amount of radiant energy passing through the matrix unabsorbed. For relatively thick layers of matrices with moderate extinction coefficients this term usually represents a small portion of total radiation available at the bed's top surface.

After solving equation 14 explicitly for T_{fe}^*, overall collector efficiency can be calculated using equation 15.

$$\eta_c = \Gamma \frac{(T_{fe}^* - 1)}{\psi} (100), \% \qquad [15]$$

Collector efficiency is defined as the ratio of heat gained by air passing through the collector divided by total available insolation normal to the collector's surface.

CHAPTER VI

DATA ANALYSIS AND RESULTS

Matrix Properties

Matrix Porosity and Density

Porosity is one of the most important characteristics of a porous medium (matrix). Total porosity of a matrix is defined as the ratio of void volume to total volume. Effective porosity is defined as the ratio of interconnected void volume to the total volume (15). The matrix used in this study, Duralast filter media, was unconsolidated (interconnected voids) and therefore assumed to have equal total and effective porosities.

Equation 16 was used to calculate matrix porosity from the experimental data in Table II.

$$\lambda = \frac{V_i - V_w}{V_i} \qquad [16]$$

where

λ = Porosity

V_i = Total sample volume, cm^3

V_w = Volume of water displaced by submerged sample, cm^3

Calculated values of porosity are listed in Table II. The average porosity was 0.955 and all experimental values were within 0.31% of

the average.

Heat transfer and flow analysis of a matrix usually requires knowledge of the material's density. Apparent density (ρ_b, bulk density) of a porous medium is defined as the total mass divided by the material's bulk volume. Equation 17 was used to calculate apparent density of the samples listed in Table II. Values of apparent density ranged from 0.0518 g/cm^3 to 0.0533 g/cm^3 with an average of 0.0526 g/cm^3.

TABLE II

MATRIX POROSITY AND DENSITY

Sample I. D.	Sample Thickness cm	Total Sample Volume cm^3	Volume of Solid cm^3	Mass of Sample g	Porosity	Apparent Density g/cm^3	Specific Density g/cm^3
1	1.91	282.9	13.5	14.75	0.952	0.0521	1.09
2	1.91	284.8	12.5	14.75	0.956	0.0518	1.18
3	1.91	291.5	14.2	16.50	0.953	0.0535	1.09
1	1.27	170.4	7.2	8.88	0.958	0.0521	1.24
2	1.27	177.5	8.0	9.40	0.955	0.0530	1.18
3	1.27	174.4	7.7	9.53	0.956	0.0533	1.24

$$\rho_b = \frac{m_b}{V_i} \qquad [17]$$

where

ρ_b = Apparent matrix density, g/cm^3

m_b = Mass of matrix sample, g

Another useful characteristic of a porous medium is specific density or density of the actual solid. Specific density (ρ_s) of the matrix used in this study is defined by equation 18.

$$\rho_s = \frac{\rho_b}{1 - \lambda} \qquad [18]$$

Knowledge of matrix porosity and apparent density were needed for calculating specific density. Table II contains values of specific density that ranged from 1.09 g/cm^3 to 1.24 g/cm^3 with an average of 1.17 g/cm^3.

Porosity was the only matrix physical property used in theoretical evaluation of the solar collector. However, apparent and specific densities were measured to provide additional information that might be useful in future study.

Matrix Friction Loss Characteristics

When evaluating the performance of a solar collector, it is important to know friction loss characteristics of the fluid channels. This will provide knowledge of how much energy is required for transporting fluid through the collector. In a matrix solar collector, friction loss through the absorber is usually a large percentage of the total friction loss through the collector. Therefore, in most cases, knowledge of matrix friction loss characteristics is adequate for collector evaluation.

Data for friction loss through Duralast filter media are shown in Table III. The Reynolds number and Fanning friction factor listed in

TABLE III

MATRIX FRICTION LOSS CHARACTERISTICS

Rep	Air Velocity u (m/sec)	Reynolds Number Re	Pressure Drop dp/dz (Pa/m)	Friction Factor (Fanning) f
1	0.0091	3.27	0.92	28.14
2	0.0098	3.52	1.15	30.13
3	0.0111	4.00	0.92	18.74
1	0.0117	4.22	1.27	23.20
2	0.0111	4.00	0.92	18.76
3	0.0128	4.61	1.15	20.14
1	0.0148	5.34	1.62	18.45
2	0.0148	5.33	1.73	19.78
3	0.0148	5.33	1.73	19.77
1	0.0216	7.78	3.23	17.38
2	0.0234	8.43	3.58	16.35
3	0.0227	8.21	2.77	13.32
1	0.0366	13.22	6.81	12.70
2	0.0369	13.25	6.23	11.51
3	0.0373	13.39	6.46	11.69
1	0.0392	14.13	7.62	12.43
2	0.0387	13.91	8.54	14.32
3	0.0389	13.97	7.16	11.89
1	0.0598	21.57	15.12	10.58
2	0.0598	21.48	13.85	9.73
3	0.0597	21.44	14.08	9.93
1	0.0626	22.58	16.28	10.40
2	0.0625	22.45	16.16	10.40
3	0.0625	22.44	15.81	10.17
1	0.0643	23.20	16.51	9.99
2	0.0641	23.04	16.97	10.37
3	0.0641	23.03	16.51	10.09

Table III were calculated using equations 19 and 20. The average matrix filament diameter was measured to be 0.0284cm. This value was the average of ten random samples with diameters ranging from 0.0213cm to 0.0368cm.

$$Re = 4r_h \rho_a u/\mu \quad [19]$$

$$f = 2r_h (-dp/dz)/\rho_a u^2 \quad [20]$$

where

r_h = Hydraulic radius of matrix, $r_h = D_f \lambda/4 (1-\lambda)$, m

D_f = Average diameter of matrix filaments, m

λ = Porosity

ρ_a = Density of air, kg/m^3

u = Velocity of air through matrix voids, m/sec

μ = Dynamic viscosity of air, kg/(m-sec)

dp/dz = Pressure drop across matrix layer per unit depth, Pa/m

A plot of Reynolds number versus friction factor on log-log coordinates is shown in Figure 13. A least squares regression analysis of the data in rectangular, semi-log, and log-log coordinate systems indicated that log-log coordinates yielded the best fit. The friction factor was found to vary with the -0.464 power of the Reynolds number. Equation 21 shows the correlation of f with Re.

$$f = 42.4\ Re^{-0.464} \quad [21]$$

The regression correlation coefficient was 0.923 with a standard deviation of 1.10.

Chiou (4) studied the effects of Reynolds number on friction loss

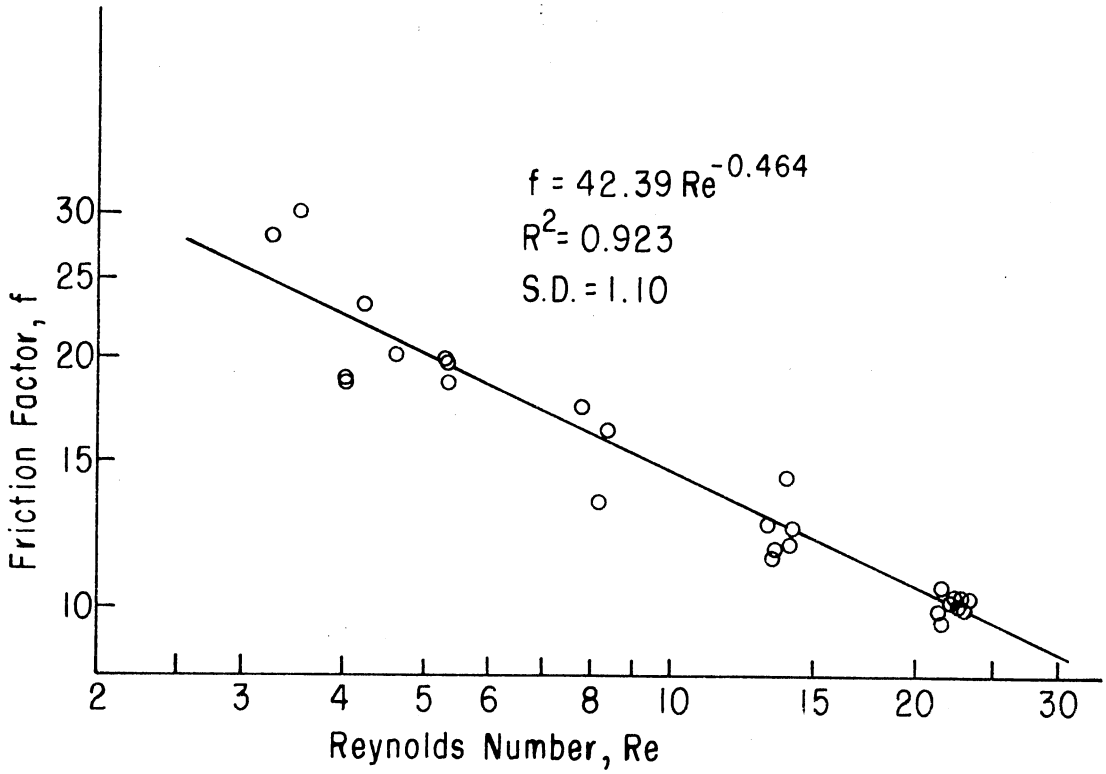

Figure 13. Fanning Friction Factor as a Function of Reynolds Number for Duralast Filter Media.

through slit-and-expanded aluminum-foil matrices. One type of matrix (Type II) used in his study had a porosity (0.962), very similar to that that of Duralast filter media (porosity = 0.955). He expressed the flow friction coefficient f, for Type II matrix by equation 22.

$$f = 38.5\ Re^{-0.96} + 1.42 \qquad [22]$$

Equations 21 and 22 were compared for Reynolds numbers between 3.0 and 30.0. Friction loss coefficients for Duralast filter media were found to be 2.0-4.0 times as high as those for Chiou's (4) Type II matrix. Coppage and London (6) reported for wire-screen matrices, that St $Pr^{2/3}$ was of the order f/10. This indicates that heat transfer capability of Duralast filter media is 2.0-4.0 times that of the aluminum-foil matrix used by Chiou (4).

Average Extinction Coefficient

Table IV contains data for determining the matrix average extinction coefficient. As developed in chapter V, the extinction coefficient (β) is defined as the slope of the curve of the logarithm ratio of emerging to incident energy versus thickness. Data from Table IV are plotted on semi-log coordinates in Figure 14. Least-squares regression yielded an average extinction coefficient of 187.8 m^{-1} with a regression correlation coefficient of 0.992 and standard deviation of 0.281. Theoretically, the intercept coefficient of 0.954 in Figure 14 should actually be equal to 1.00; however, this difference is partially due to experimental error encountered in measuring bed depth. Bed thicknesses exceeding 0.038m absorbed over 99.9% of incident radiant energy.

TABLE IV

MATRIX EXTINCTION COEFFICIENT

Bed Thickness L (m)	Ratio of Emerging to Incident Energy I_1/I_0
0.000	1.000
0.0127	0.0870
0.0191	0.0322
0.0254	0.0054
0.0381	0.0009

Effective Transmittance of Cover

Three replications of measuring cover transmittance of the six mil polyethylene yielded values of 0.877, 0.884, and 0.895 with an average of 0.885. These data produced a standard deviation of 0.009. In their study of greenhouse covering materials, Duncan and Walker (8) list values of 0.85-0.88 for effective transmittance of six mil clear polyethylene. These values agree quite well with those measured in this study.

Matrix Solar Collector

Theoretical Analysis

Equations 11, 12, 13, 14 and 15 derived in chapter V were solved

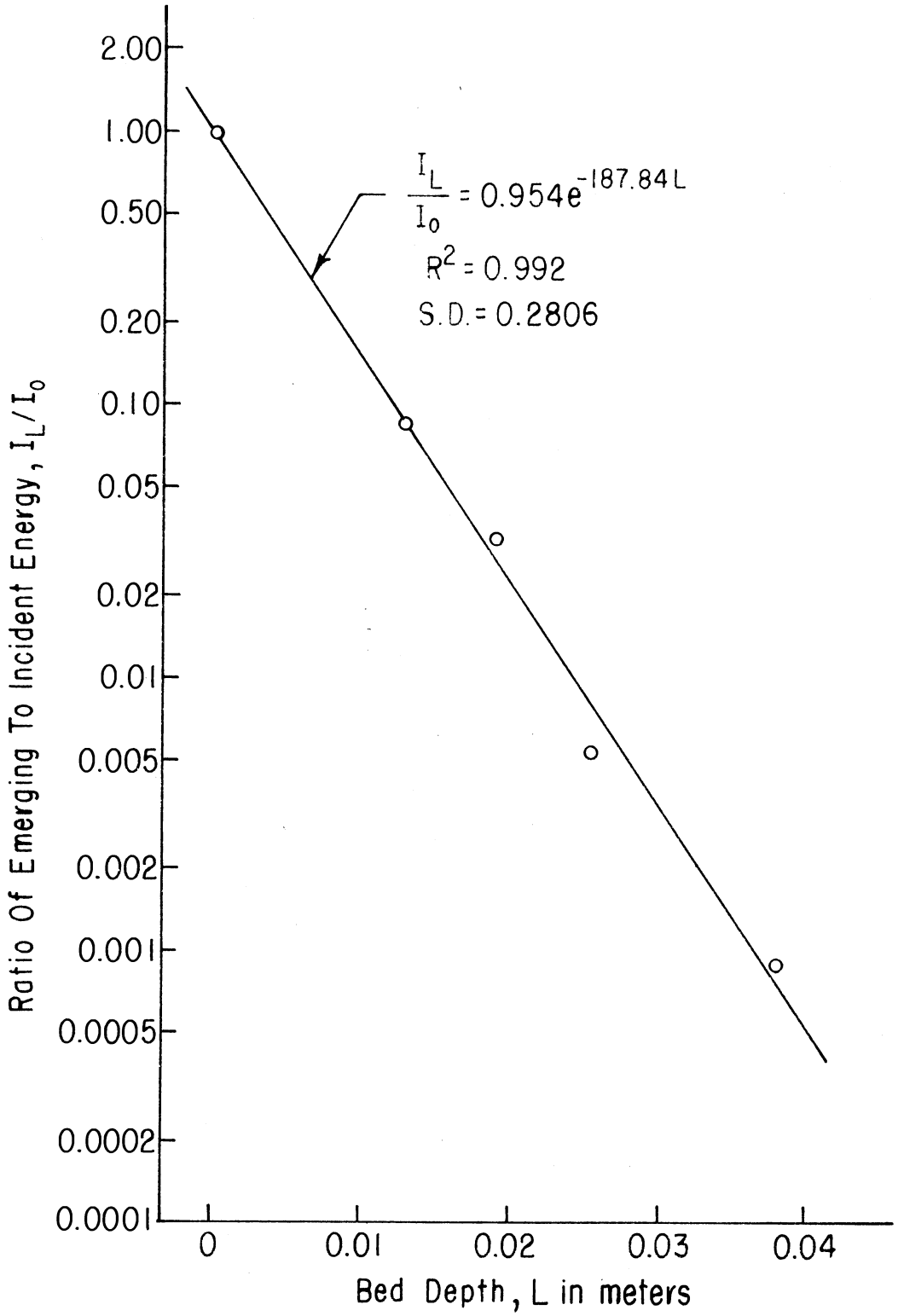

Figure 14. Ratio of Emerging to Incident Energy as a Function of Matrix Bed Depth for Duralast Filter Media.

simultaneously for atmospheric conditions similar to those encountered in actual experiments. This provided adequate comparison of theoretical to experimental analysis. Listed below are numerical values of environmental conditions and collector physical parameters used in the theoretical collector analysis.

$e_b = 0.95$

$e_c = 0.90$

$\tau_c = 0.885$

$T_{fo} = 305.2$ K

$I_0 = 916$ w/m^2

$A_L = 1.58$ m^2/m^2

$U_L = 1.68$ w/(m^2-K)

$\psi = Io/\ \sigma T_{fo}^4 = 1.87$

$\phi = A_L\ U_L\ T_{fo}/\ \sigma T_{fo}^4 = 1.65$

Results of the theoretical analysis are listed in Table V. Effects of dimensionless flow rate on bed and collector efficiencies are shown in Figure 15. At a dimensionless flow rate of 31.2, bed efficiency is 13.3% higher than collector efficiency. Figure 15 illustrates that increasing dimensionless flow rate beyond 20 results in little increase in bed or collector efficiency.

Experimental Analysis

A least squares regression analysis was used to fit the experimental data to best fit curves on rectangular, semi-log, and log-log coordinates. Comparison of the regression correlation coefficient, coefficient of variance, standard error, and F statistic in analysis

TABLE V

THEORETICAL ANALYSIS*

Dimensionless Flow Rate Γ	Dimensionless Temperature T_{fe}^*	Bed Efficiency η_b, %	Collector Efficiency η_c, %
3.46	1.133	41.7	24.7
6.93	1.119	60.2	44.1
10.39	1.099	69.9	55.0
13.86	1.083	75.7	61.8
17.32	1.071	79.5	66.3
20.80	1.062	82.2	69.5
24.25	1.055	84.2	72.0
27.71	1.050	85.8	73.9
31.18	1.045	86.9	75.3

* $\psi = I_0 / \sigma T_{fo}^4 = 1.87$, $T_{fo} = 305.2$ K

$\Gamma = G\, C_p\, T_{fo} / \sigma T_{fo}^4$

$T_{fe}^* = T_{fe} / T_{fo}$

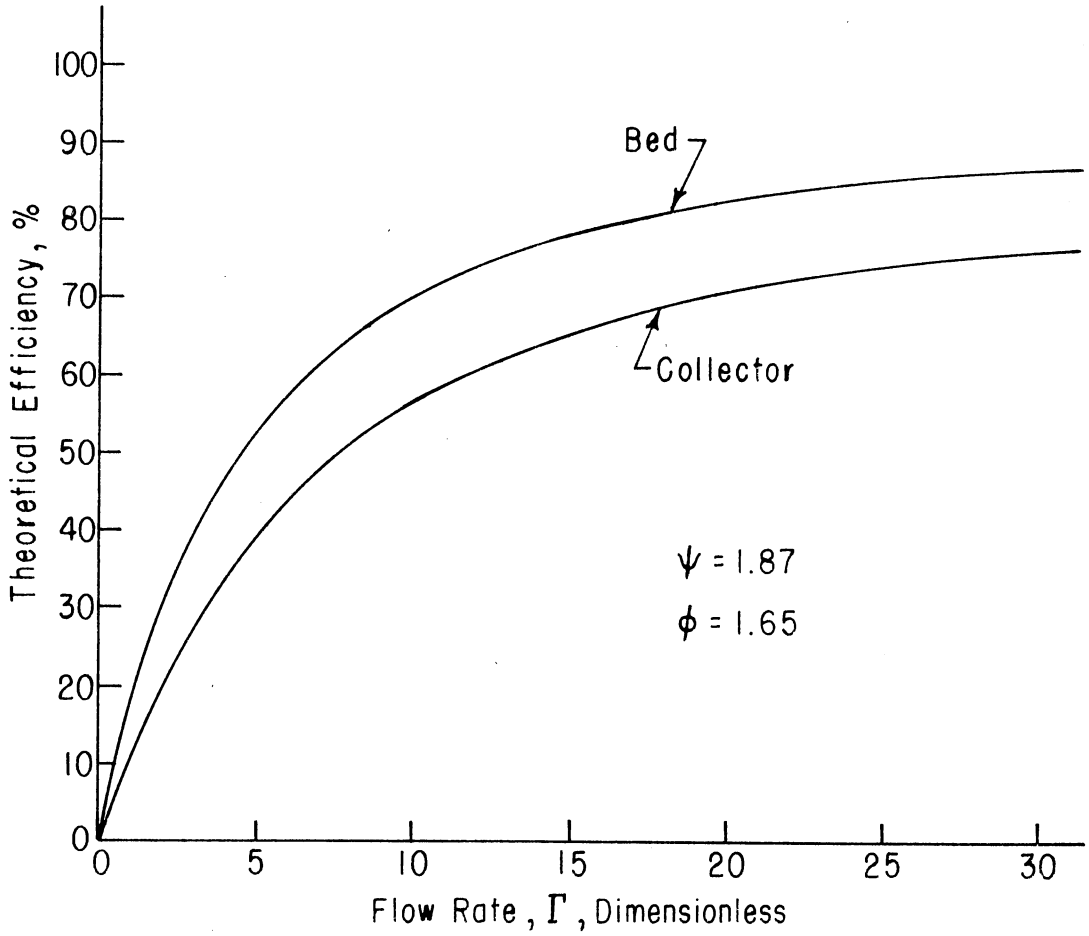

Figure 15. Theoretical Bed and Collector Efficiency as a Function of Dimensionless Flow Rate.

of variance of regression coefficients were used to select best fit equations to represent observed data.

Table VI is a condensed record of experimental data recorded during prototype studies conducted in June, 1976. Insolation during any test varied not more than 8% from its average value over the test period. Insolation for all tests ranged from 793 w/m^2 to 985 w/m^2 while ambient temperature varied from 299.0 K (25.8 °C) to 307.1 K (33.9 °C). The average dimensionless insolation ψ, in Table VI, is 1.87 and equals the value used in the theoretical analysis. Average ambient temperature of observed data was 304.4 K (31.2 °C). This compares quite well to the value of 305.2 K (32.0 °C) used for theoretical analysis.

A plot of observed data for collector efficiency as a function of dimensionless flow rate is shown in Figure 16. Equation 23 is the empirical equation selected to fit the data.

$$\eta_c = 57.7\ (1 - e^{-0.148\Gamma}) \qquad [23]$$

The above equation was selected because it satisfied the boundary condition, $\eta_c = 0$ at $\Gamma = 0$, and fit the data quite well. Analysis indicated a regression correlation coefficient of 0.971 and a standard deviation of 2.62.

Theoretical collector efficiencies calculated in Table V are plotted in Figure 16. Predicted collector efficiency fit the observed data for dimensionless flow rates less than 5.0. However, experimental efficiencies at dimensionless flow rates of 10.4 and 31.2 were 17.5 and 24.0% lower, respectively, than theoretical values. From observing these values and Figure 16, error in predicting collector

TABLE VI

OBSERVED COLLECTOR DATA

Dimensionless Insolation ψ	Dimensionless Flow Rate Γ	Dimensionless Temperature T_{fe}^*	Collector Efficiency η_c, %
1.73	3.81	1.111	24.6
2.10	3.95	1.130	24.5
1.71	3.96	1.108	25.2
1.96	7.05	1.106	37.9
1.86	7.36	1.101	39.9
1.82	7.43	1.094	38.4
1.94	9.78	1.095	48.1
1.87	9.82	1.083	44.0
1.61	9.85	1.072	43.9
1.98	21.93	1.052	57.8
1.86	21.96	1.045	53.8
1.89	22.28	1.044	52.1
1.82	29.24	1.036	57.3
1.96	29.89	1.040	60.4
1.88	30.80	1.033	54.1

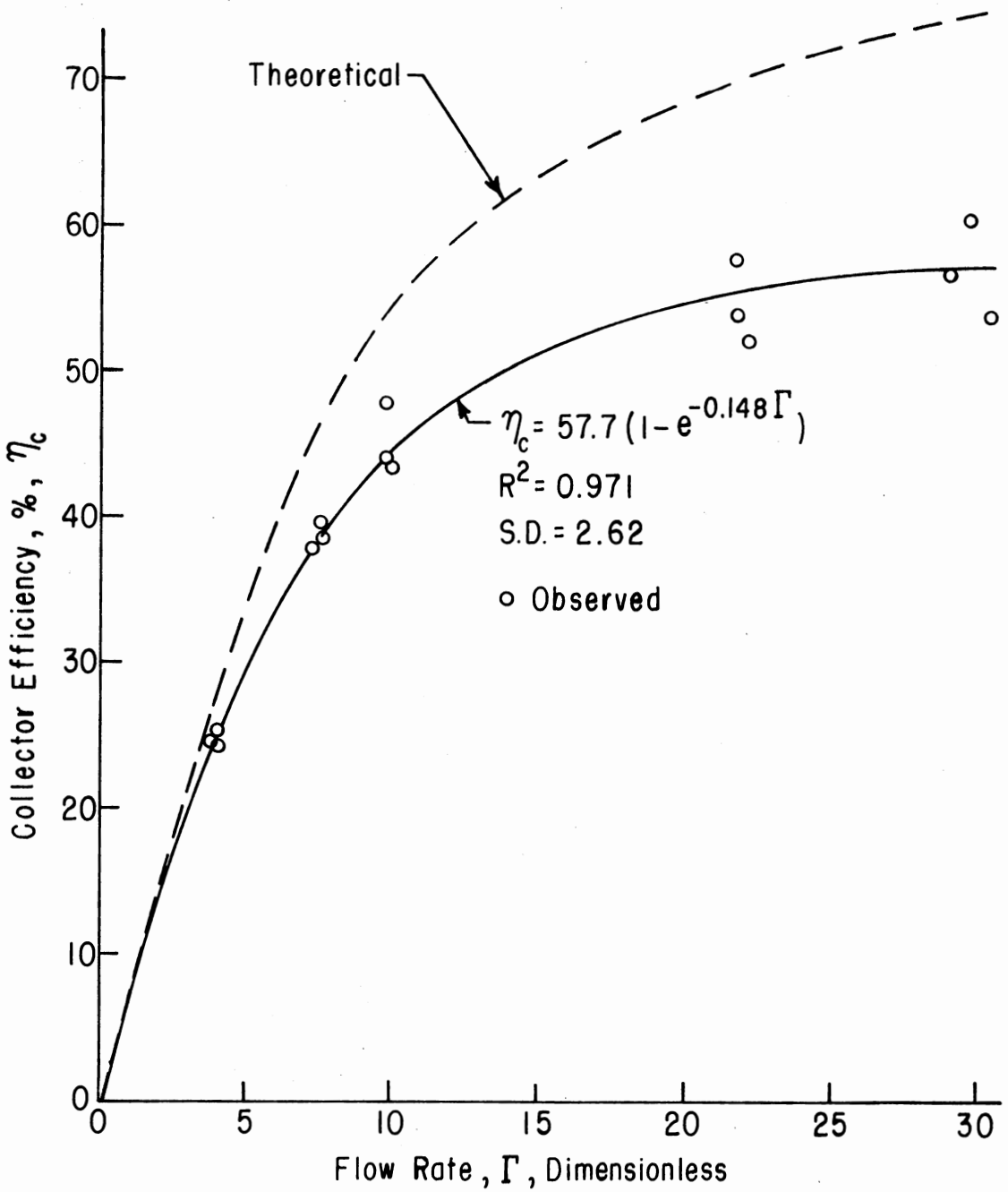

Figure 16. Observed and Theoretical Collector Efficiency as a Function of Dimensionless Flow Rate for Wedge-Shaped Matrix Solar Collector.

efficiency appears to be related to collector flow rate. Before an attempt to identify sources of error, experimental data from another reference (9) was used to further test accuracy of the analytical solution.

Hamid and Beckman's (9) study of performance of air-cooled radiatively heated screen matrices dealt with a similar design as the one used in this study. A small test box was constructed and two different specimens of stacked wire screens were subjected to collimated radiant flux and a normal flow of atmospheric air. They compared their experimental data with analytical results from previous research (10) on transpiration cooling of radiatively heated porous beds. Figure 17 illustrates the accuracy they obtained in analytically predicting matrix bed efficiency as a function of collector dimensionless flow rate.

Using the theoretical analysis developed in chapter V, bed efficiency of Hamid and Beckman's (9) matrix (specimen B) was calculated and is shown in Figure 17. Duplicate environment and boundary conditions were used. However, their analysis considered both direct and diffuse radiant flux and treated them separately. The solution developed in this study considered a total incident radiant flux equal to the combined value of direct and diffuse radiation used by Hamid and Beckman (10).

Comparison of the curves in Figure 17 was used to verify the assumptions and approximations presented in chapter V for calculating bed efficiency. However, prediction of collector efficiency, as described earlier, using these assumptions results in considerable error, as much as 24%.

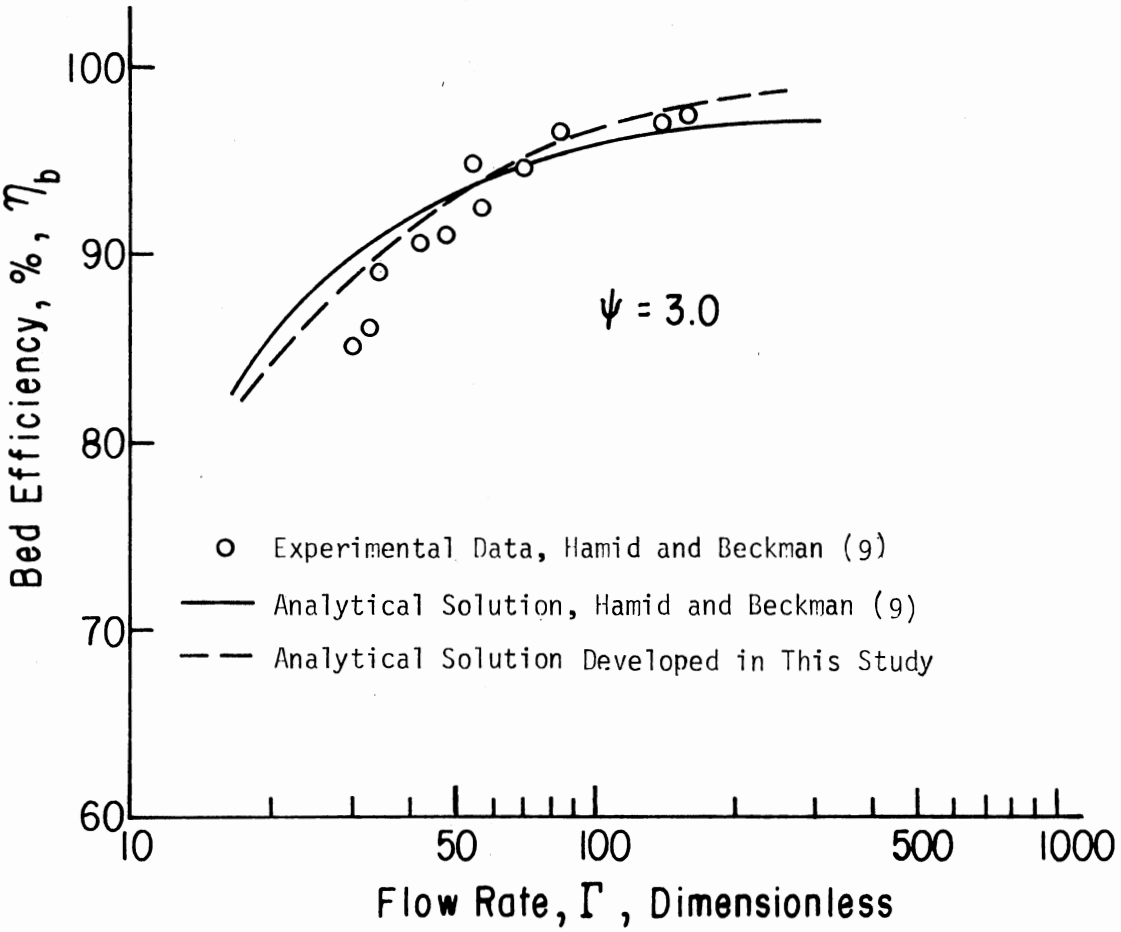

Figure 17. Bed Efficiency as a Function of Dimensionless Flow Rate for Experimental Data and Analytical Solution from Reference (9) and the Analytical Solution from This Study.

One source of error could arise from the assumption of one-dimensional steady flow normal to the matrix. Location and size of inlet ports around the collector perimeter causes non-uniform air flow through the matrix bed. Turbulence of air at high velocities as it passes through inlet ports results in a three-dimensional flow regime through the matrix. This causes non-uniform horizontal temperature gradients and heat flow through the matrix by conduction and convection.

Another possible factor resulting in large prediction errors at high flow rates is that the triangular-shaped plenum inlet was designed for low to moderate flow rates (0.5 $m^3/(min\text{-}m^2)$ to 1.0 $m^3/(min\text{-}m^2)$). This results in non-uniform air flow when flow rate varies widely from its original design condition. Non-uniform air flow through the matrix will create hot spots or concentrated areas of high temperature, thus causing excess heat loss by reradiation and convection to the collector cover.

Another probable cause for prediction error could be the lack of air flow through the matrix in the corners and in narrow widths adjacent to collector side walls. No attempt was made in the analytical solution to account for the lack of air flow through portions of the matrix. In summary, non-uniformity of air flow through the matrix is probably the most important factor that affects accurate prediction of collector performance.

Experimental data and the analytical solution showing effects of dimensionless flow rate on collector outlet temperature ratio are plotted in Figure 18. Data were transformed to log-log coordinates and least squares regression was used to determine the coefficients in

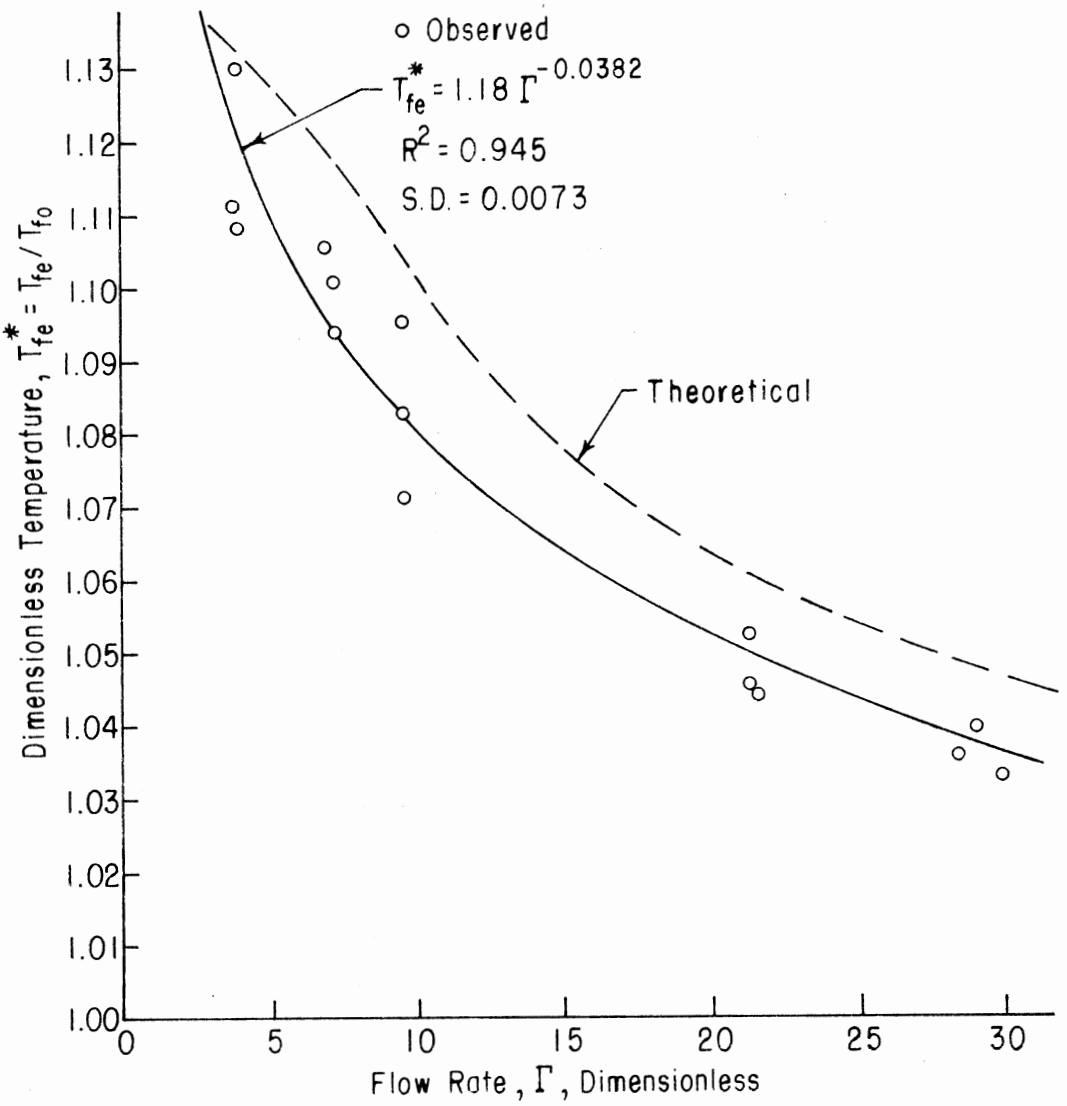

Figure 18. Effects of Dimensionless Flow Rate on Dimensionless Temperature Ratio for Observed Data and Theoretical Solution of Matrix Solar Collector.

equation 24.

$$T_{fe}^* = 1.18\Gamma^{-0.0382} \quad [24]$$

The regression correlation coefficient and standard deviation were 0.945 and 0.007, respectively.

Figure 19 shows the effect of dimensionless temperature ratio, T_{fe}^*, on collector efficiency. A second degree polynomial was found to produce the best fit equation. However, one should use equation 25 with extreme caution when extrapolating beyond the range of this study.

$$\eta_c = 4829\ T_{fe}^* - 2404\ (T_{fe}^*)^2 - 2367 \quad [25]$$

The correlation coefficient and standard deviation for equation 25 are given in Figure 19.

Collector Study in Solar Peanut Drying

Figures 20 and 21 show solar radiation intensity recorded for one day of each drying block. Insolation for blocks one, two and six indicate clear days while tests three and four reveal slight overcast during early morning and mid-afternoon hours. Block five experienced dense overcast during the entire day. Figure 22 shows collector outlet temperature varying with time of day for various flow rates of block one. A 42 °C temperature rise was recorded for the collector operating at 0.40 $m^3/(min\text{-}m^2)$. A 10 °C and greater temperature rise was observed for the collector operating at 0.97 $m^3/(min\text{-}m^2)$ for an entire eight-hour period.

Figure 23 illustrates daily accumulated efficiency varying with

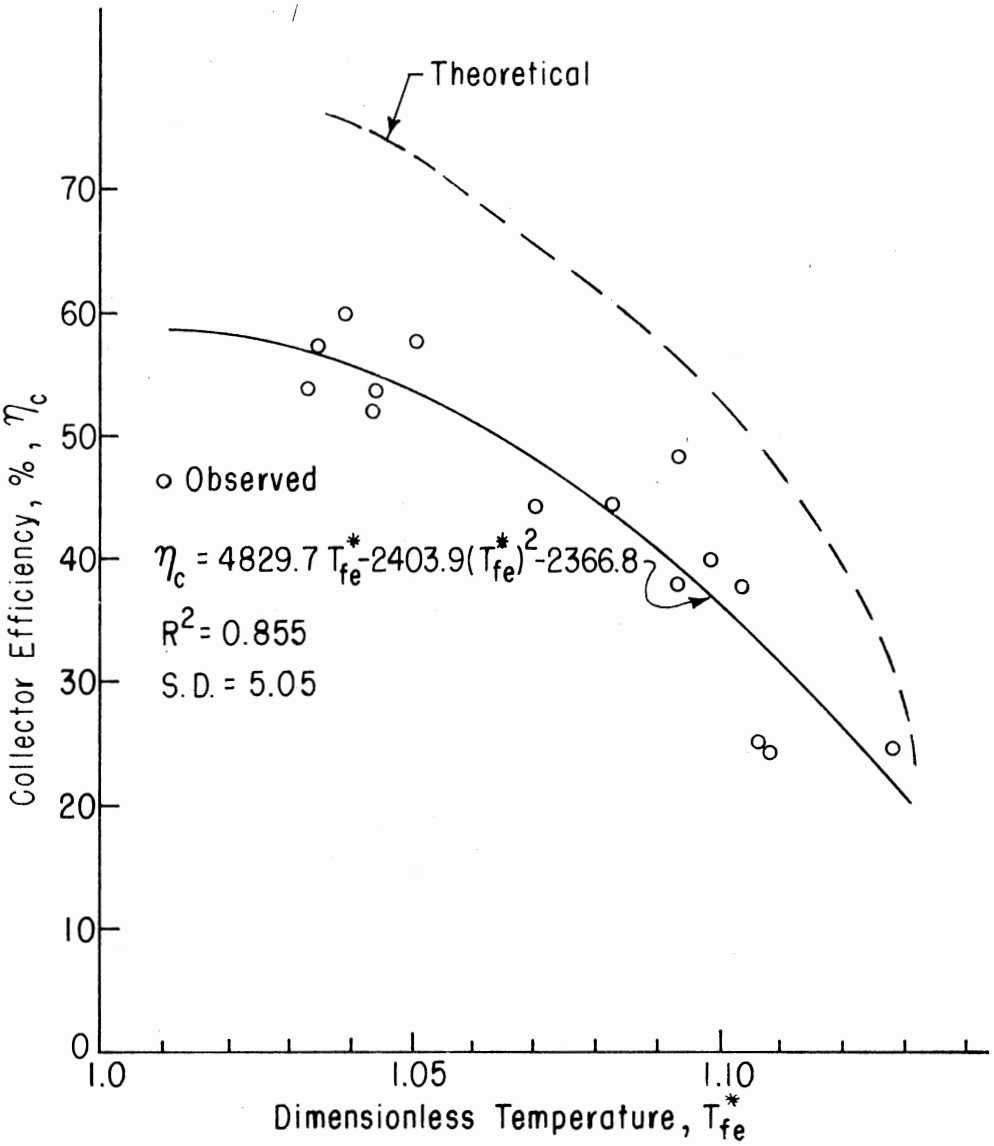

Figure 19. Observed and Theoretical Collector Efficiency as a Function of Outlet Dimensionless Temperature Ratio.

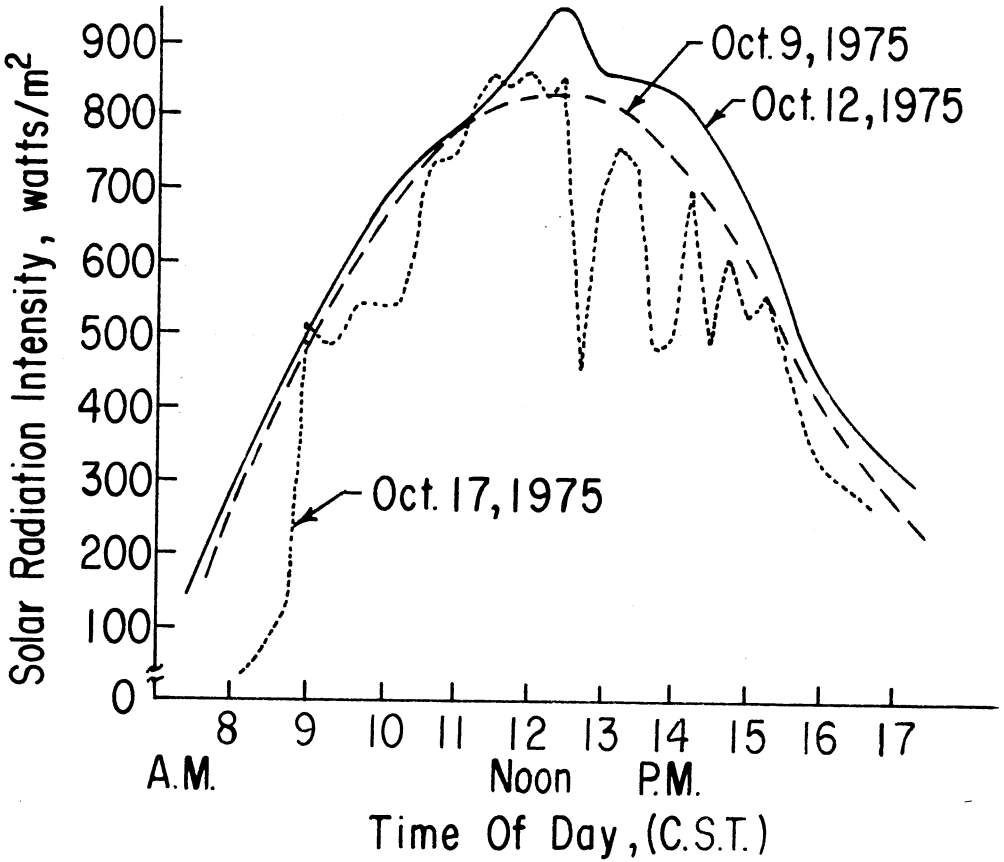

Figure 20. Daily Solar Radiation on a Flat Surface Tilted South 24° from Horizontal, Stillwater, Oklahoma.

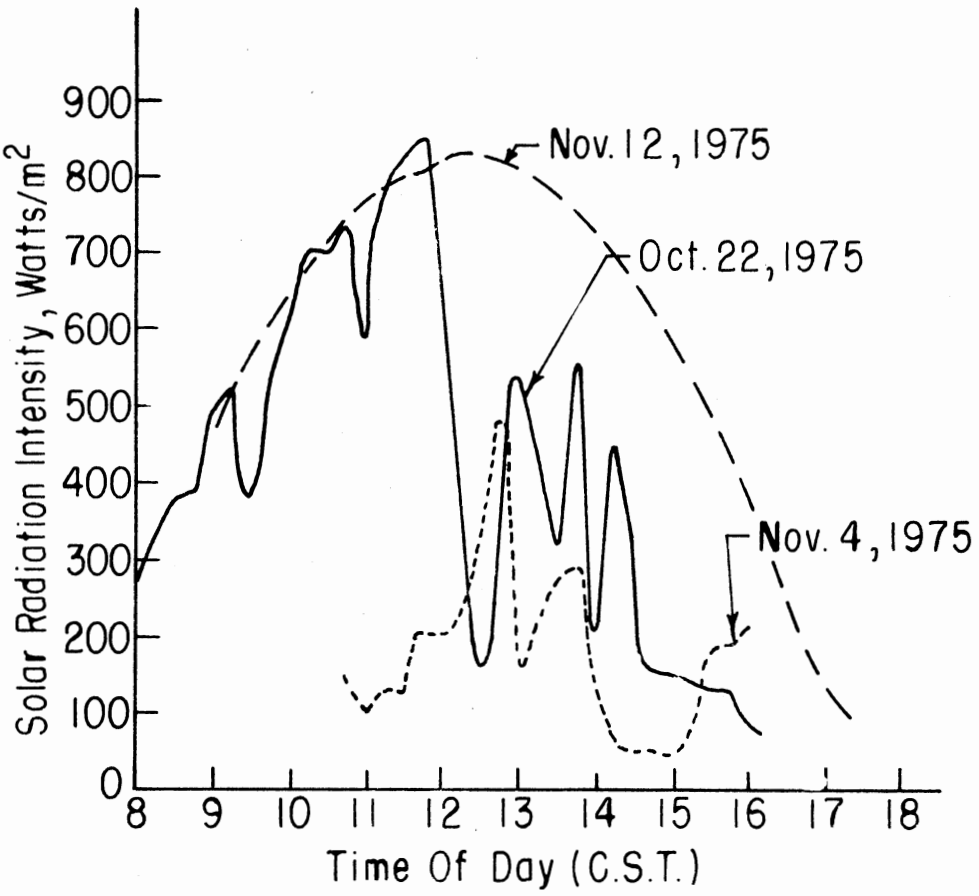

Figure 21. Solar Radiation on a Flat Surface Tilted South 24° from Horizontal, Stillwater, Oklahoma.

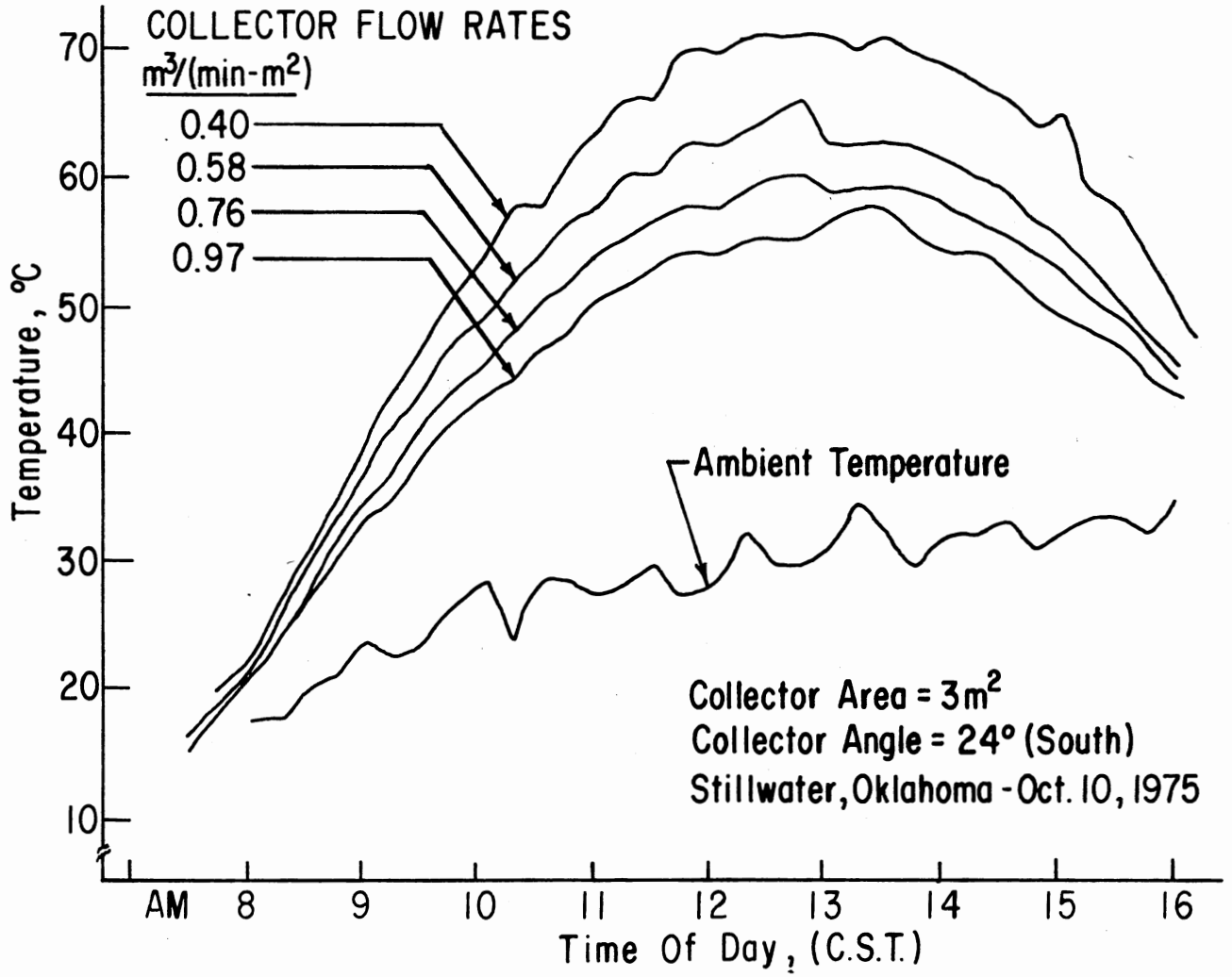

Figure 22. Collector Outlet Temperature as a Function of Time for Varying Flow Rates.

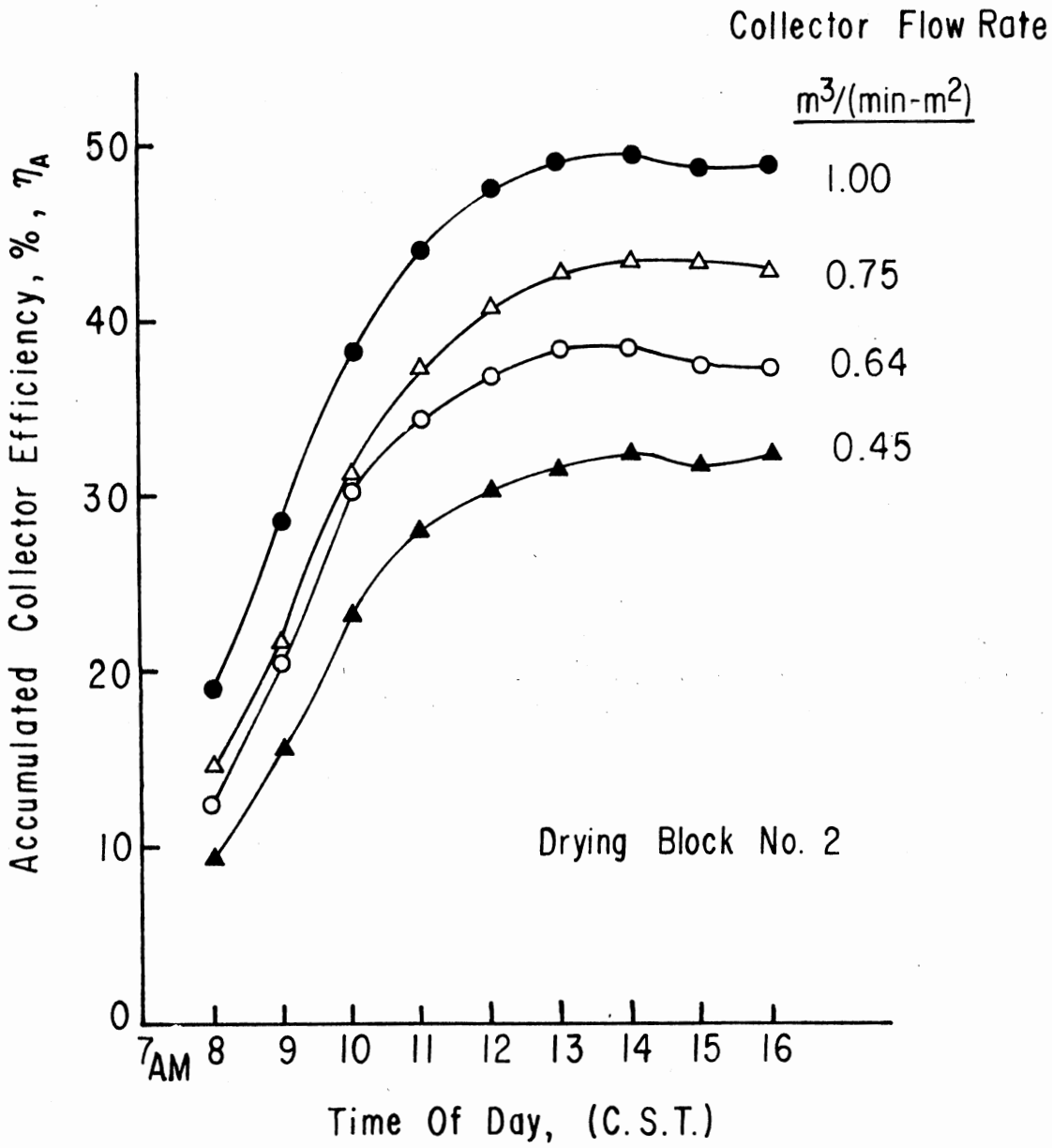

Figure 23. Accumulated Collector Efficiency as a Function of Time for Varying Flow Rates.

collector flow rate and time of day. Accumulated efficiency is defined as the percent of total available solar radiation that has been effectively captured since the collector was activated. Collector efficiency during early morning hours was lower than expected, while late afternoon efficiencies remained relatively high. This phenomenon is due because much of the energy gained during early morning hours is needed to heat the collector body, while a reverse process occurs during late evening hours.

Appendix A lists temperature rise, instantaneous collector efficiency, insolation, and accumulated collector efficiency recorded for the second day of block two. Figure 24 shows effects of flow rate on accumulated collector efficiency during solar drying studies. Drying with a flow rate of 1.0 $m^3/(min\text{-}m^2)$ captured 50% of the sun's total available energy between the hours of 8:00 A. M. and 4:00 P. M.

Data points recorded during the sixth block are also shown in Figure 24. However, these points are not indicative of accurate data and were not included in the regression analysis. Flow rate for these points were calculated assuming all air flowed through half the collector area. Portions of air leaked around the insulation used to cover the collector absorber. Therefore actual flow rates for these data are suspected to be less than shown in Figure 24.

Solar Peanut Drying

Drying temperature-time relationships for blocks one-six are shown in Appendix B. Dryers operating at 7.9 and 6.1 $m^3/(min\text{-}m^2)$ usually obtained the design final moisture content after one or two days and therefore their temperatures are not shown for the

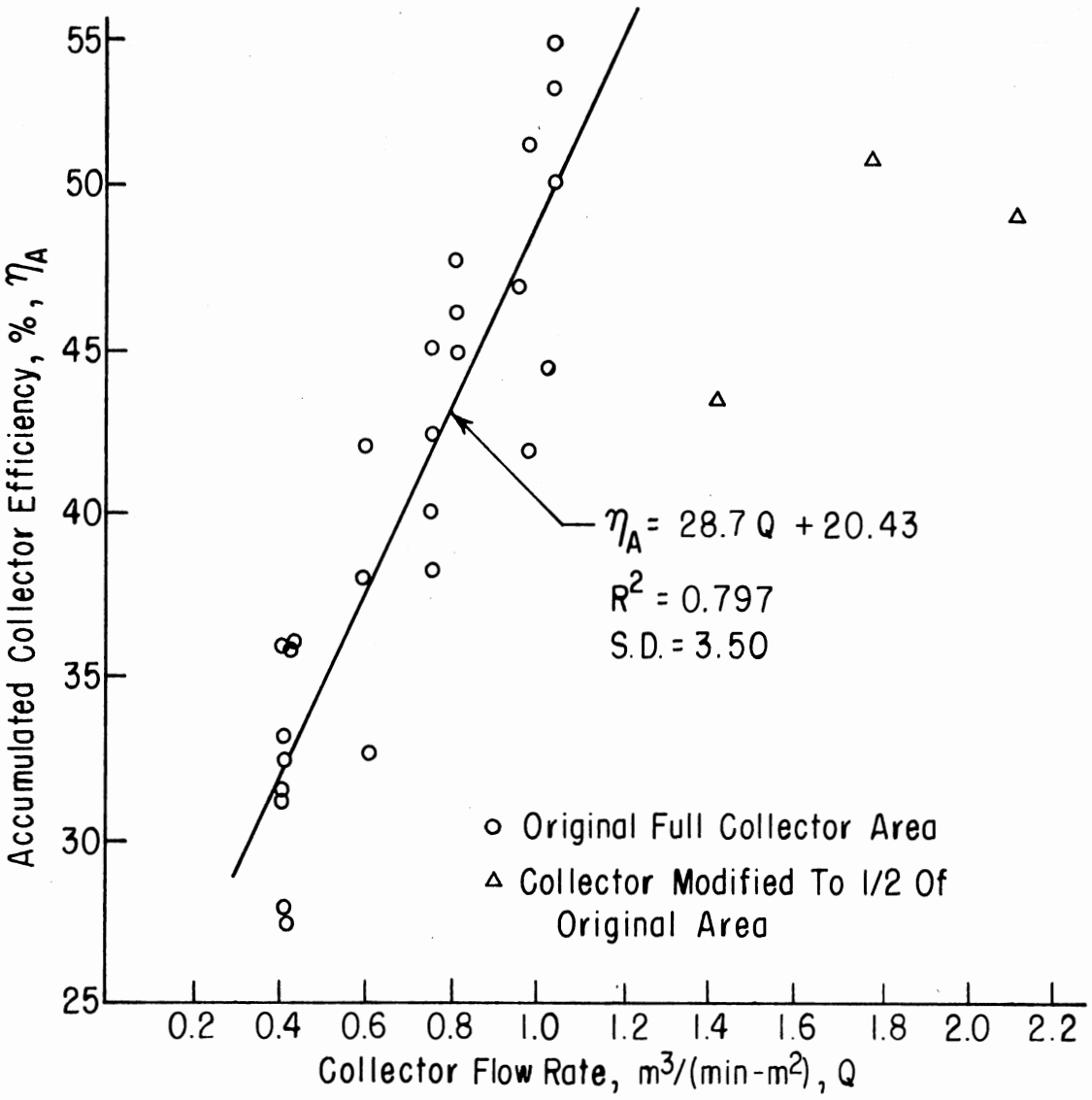

Figure 24. Accumulated Collector Efficiency as a Function of Flow Rate for Solar Peanut Drying Study, October-November, 1975.

remaining time. Auxiliary heaters were used to maintain a constant drying temperature of approximately 28 °C during night-time hours for all dryers. Figure 31 shows a maximum temperature rise of 26 °C for the dryer operating at 7.9 $m^3/(min\text{-}m^2)$ while 3.4 $m^3/(min\text{-}m^2)$ resulted in a 34 °C maximum temperature rise. Instrumentation problems prohibited accurate data collection for the first day of block one and thus only ambient temperature is shown. Shortage of harvested peanuts during blocks three and four resulted in only three dryers operating during these tests.

Collector outlet temperatures were slightly higher than those shown for dryers. This was because of heat lost through dryer plenum walls and connecting ducts. Generally, collector outlet temperatures were 1 °C to 3 °C higher, being inversely related to flow rate.

Figure 25 shows a recording of ambient relative humidity during drying. Relative humidity during block five was not recorded but was estimated to be 95-100% because of rain.

Tabular results of dryer flow rate, drying time, percent sound splits (% SS), United States Department of Agriculture (USDA) grade, initial and final moisture contents for each testing block are presented in Table VII. Average drying rates of all treatments and blocks ranged from 0.18 to 0.45% wet basis per hour, all of which were below the usual allowable maximum of 0.50% per hour.

Figure 26 shows kernel moisture content varying with drying time at selected bin depths for test block six. A considerable moisture gradient developed through the bin after drying was initiated. This gradient increased during the first 20 hours of drying and then decreased with time. Figure 26 indicates a 5% moisture gradient was

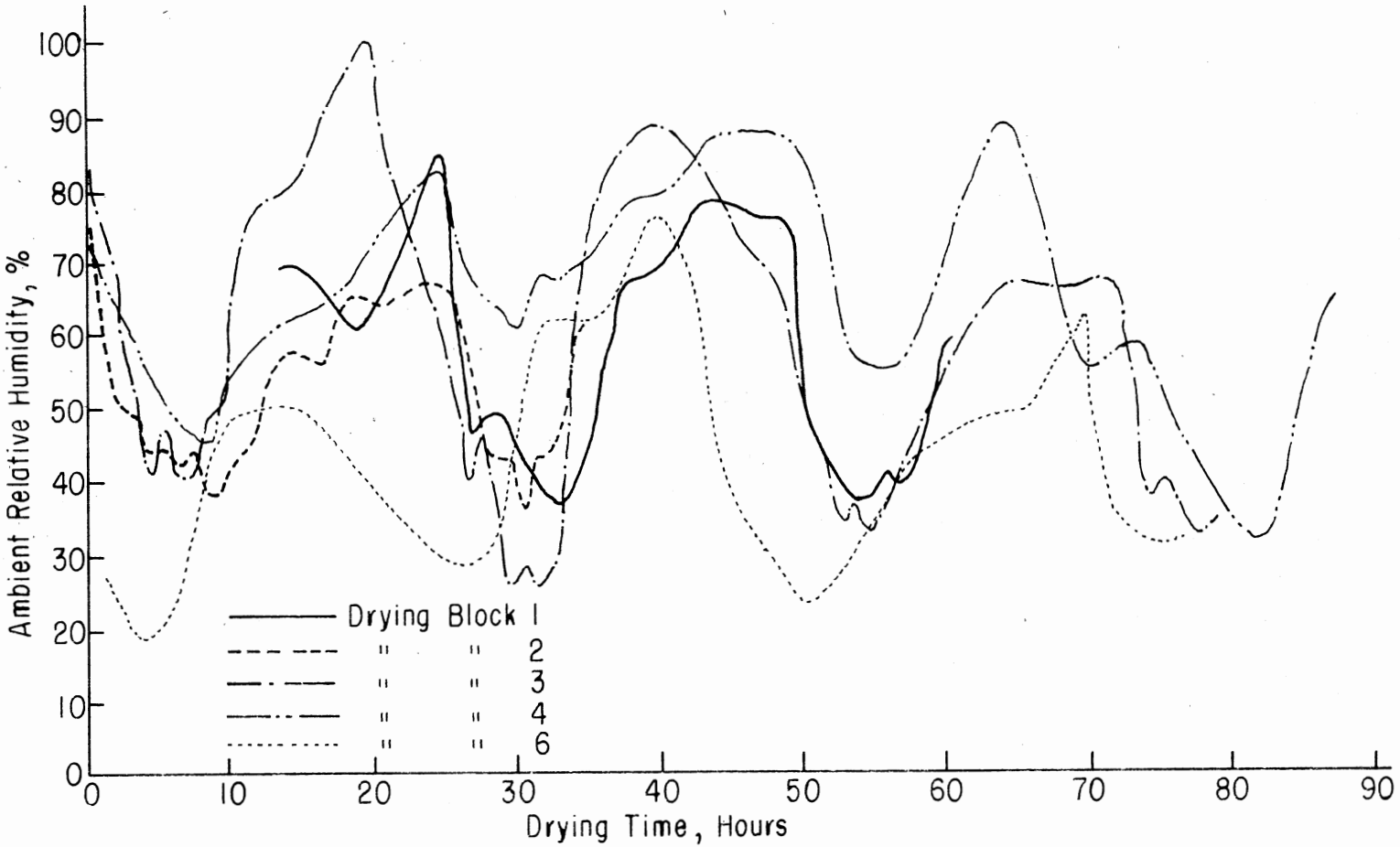

Figure 25. Ambient Relative Humidity as a Function of Drying Time for Solar Peanut Drying Study, October-November, 1975.

TABLE VII

AVERAGES OF SOLAR DRYING TESTS

Block I. D.	Dryer I.D.	Dryer Flow Rate $m^3/(min\text{-}m^2)$	Initial Moisture Content % w.b.	Drying Time Hr	Final Moisture Content % w.b.	Shelling Moisture Content % w.b.	Average Drying Rate %/Hr	Sound* Splits %	USDA* Grade %
1	1	6.1	19.70	34.5	5.60	5.80	0.41	9.16	64.22
1	2	7.9	20.30	32.5	5.77	6.61	0.45	6.82	63.67
1	3	4.6	19.50	35.5	6.35	6.60	0.37	7.10	62.87
1	4	3.2	19.15	59.5	8.53	12.19	0.18	0.70	
2	1	6.1	17.03	25.5	7.47	7.24	0.38	8.44	66.03
2	2	7.9	17.30	25.0	7.87	8.00	0.38	5.82	65.76
2	3	4.8	17.50	27.0	8.37	7.70	0.34	8.27	66.36
2	4	3.3	17.50	48.0	7.30	7.43	0.21	6.34	66.56

TABLE VII (Continued)

Block I. D.	Dryer I.D.	Dryer Flow Rate $m^3(min\text{-}m^2)$	Initial Moisture Content % w.b.	Drying Time Hr	Final Moisture Content % w.b.	Shelling Moisture Content % w.b.	Average Drying Rate %/Hr	Sound* Splits %	USDA* Grade %
3	1	6.1	26.37	65.7	5.03	5.50	0.33	12.27	66.89
3	2	7.9	26.97	54.0	5.40	4.84	0.40	12.93	66.95
3	3	--	--	--	--	--	--	--	--
3	4	3.3	26.23	77.5	5.61	4.31	0.27	13.95	67.15
4	1	6.1	26.67	75.0	7.03	6.26	0.26	11.06	66.26
4	2	7.8	26.10	56.0	7.50	6.72	0.33	8.93	65.75
4	3	--	--	--	--	--	--	--	--
4	4	3.3	25.93	105.7	7.53	6.18	0.17	11.31	66.97
5	1	6.0	21.66	34.7	9.42	8.92	0.35	6.90	66.30
5	2	7.8	22.49	30.0	9.87	9.31	0.42	6.00	64.64
5	3	4.8	22.72	36.0	7.84	8.40	0.41	6.24	63.75
5	4	3.5	23.02	63.5	9.30	8.63	0.22	7.31	65.69

TABLE VII (Continued)

Block I.D.	Dryer I.D.	Dryer Flow Rate $m^3/(min\text{-}m^2)$	Initial Moisture Content % w.b.	Drying Time Hr	Final Moisture Content % w.b.	Shelling Moisture Content % w.b.	Average Drying Rate %/Hr	Sound* Splits %	USDA* Grade %
6	1	6.5	25.80	49.5	8.05	7.36	0.36	10.67	68.78
6	2	7.8	26.78	45.5	8.47	7.62	0.40	10.74	69.35
6	3	5.2	25.15	50.7	10.96	9.96	0.28	6.11	70.08
6	4	3.2	26.67	75.0	9.23	8.30	0.23	10.24	70.36

* Values are averages of 3 milling replicates

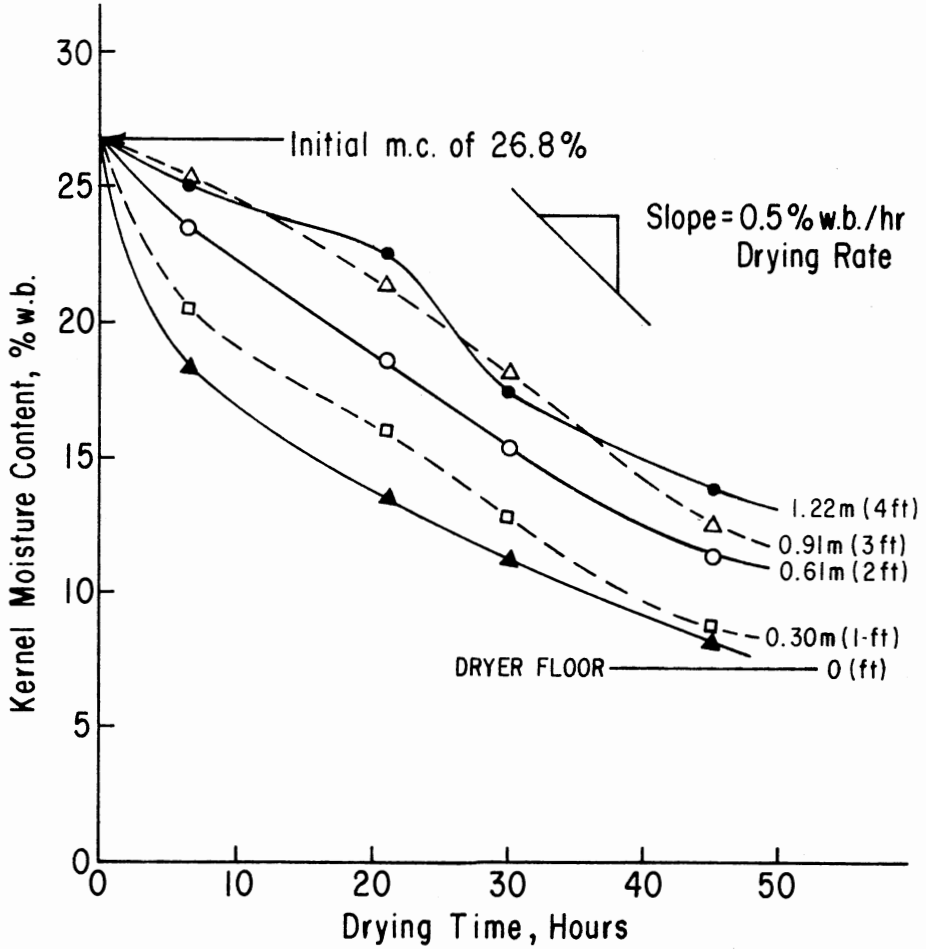

Figure 26. Relation of Kernel Moisture Content with Drying Time for Various Bin Depths, Test Block #6 with Dryer Flow Rate of 7.9 $m^3/(min\text{-}m2)$.

still present when drying stopped.

These moisture gradients caused extreme difficulty in obtaining representative final moisture contents. Therefore, it was necessary to adjust milling values (% SS, etc.) to a common final moisture content before testing for significant difference between dryer flow rates. All block and standard data were combined and used to conduct a least squares regression analysis between percent sound splits (% SS) and final kernel moisture content. Analysis was conducted in rectangular, semi-log, and log-log coordinate systems. Comparison of regression correlation coefficients, coefficient of variance and standard error indicated a simple linear relationship fit the data. The slope coefficient of 1.54 in the linear equation shown in Figure 27 was used to adjust all percent splits to a common final moisture content of 8%. Table VIII contains original percent split values and their respective adjusted means.

After adjustments for moisture content were made, an analysis of variance was conducted to determine if there was a significant difference in percent splits between dryer flow rates for the solar and standard tests. Results of that analysis are shown in Table IX. Analysis indicated a significant difference between blocks at the 95% confidence level. However, analysis of variance indicated no significant difference between mean percent splits for different drying treatments (dryer flow rates). Average adjusted percent splits ranged from 7-8%. Figure 28 shows the relative magnitude of percent sound splits for each treatment compared to the standard.

Since all collectors were of equal size, drying temperature

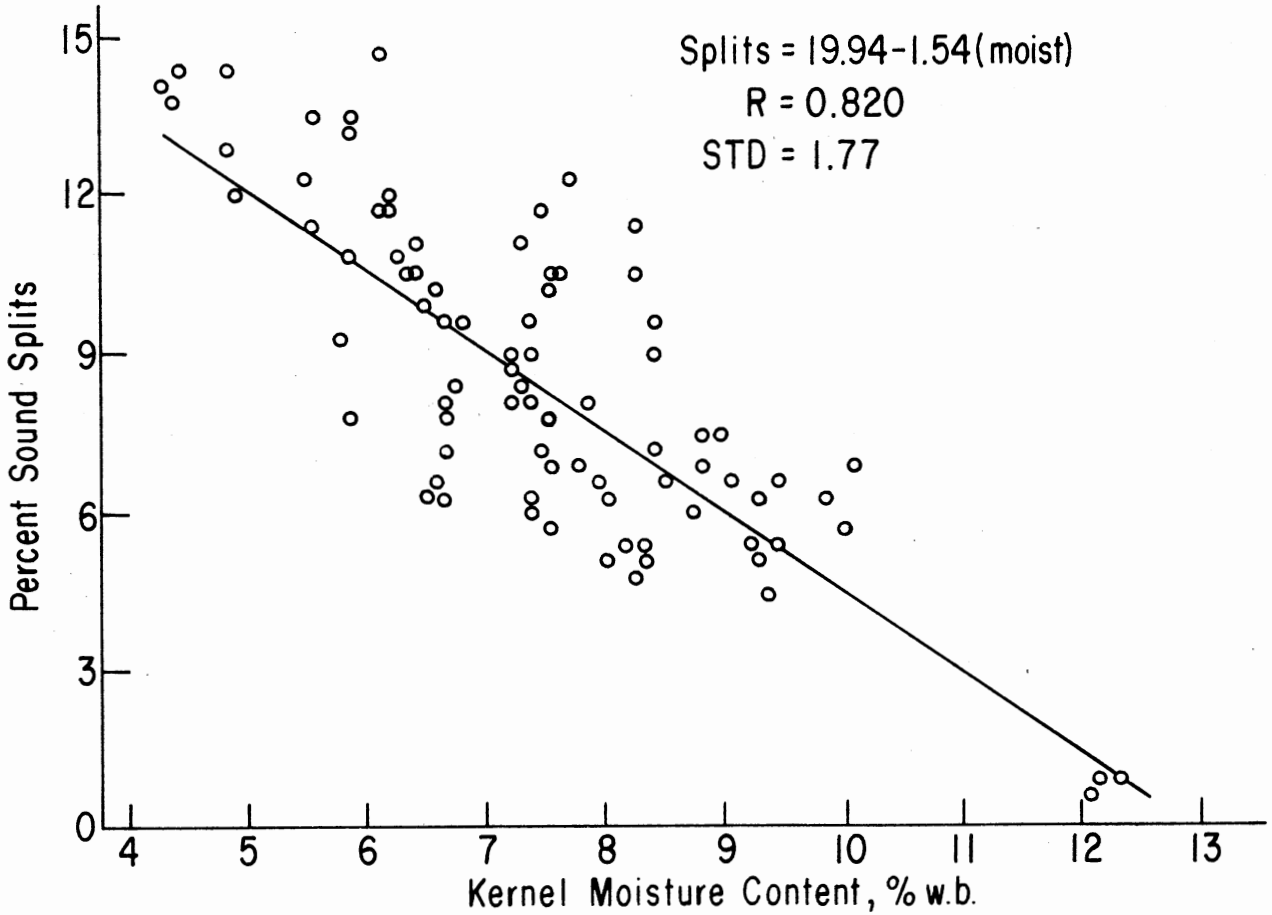

Figure 27. Effect of Final Kernel Moisture Content on Percent Sound Splits for Solar Drying Tests and Standard.

TABLE VIII

ADJUSTED PERCENT SOUND SPLITS

Block I. D.	Dryer I. D.	Final Moisture Content % w.b.	Observed Percent* Sound Splits	% Sound Splits Adjusted to 8% M.C.
1	1	5.80	9.16	5.75
1	2	6.61	6.82	4.67
1	3	6.60	7.10	4.95
1	4	12.19	0.70	7.16
2	1	7.24	8.44	7.26
2	2	8.00	5.82	5.82
2	3	7.70	8.27	7.81
2	4	7.43	6.34	5.46
3	1	5.50	12.27	8.41
3	2	4.84	12.93	8.05
3	--	--	--	--
3	4	4.31	13.95	8.25
4	1	6.26	11.06	8.38
4	2	6.72	8.93	6.95
4	3	--	--	--
4	4	6.18	11.31	8.50
5	1	8.92	6.90	8.32
5	2	9.31	6.00	8.02
5	3	8.40	6.24	6.85
5	4	8.63	7.31	8.28
6	1	7.36	10.67	9.68
6	2	7.62	10.74	10.15
6	3	9.96	6.11	9.14
6	4	8.30	10.24	10.70
1	Standard	8.25	4.91	5.30
2	Standard	7.50	6.75	5.98
3	Standard	7.33	8.44	7.40
4	Standard	6.47	10.13	7.76
5	Standard	9.36	4.96	7.06
6	Standard	5.92	13.60	10.39

* Values are averages of 3 milling replications

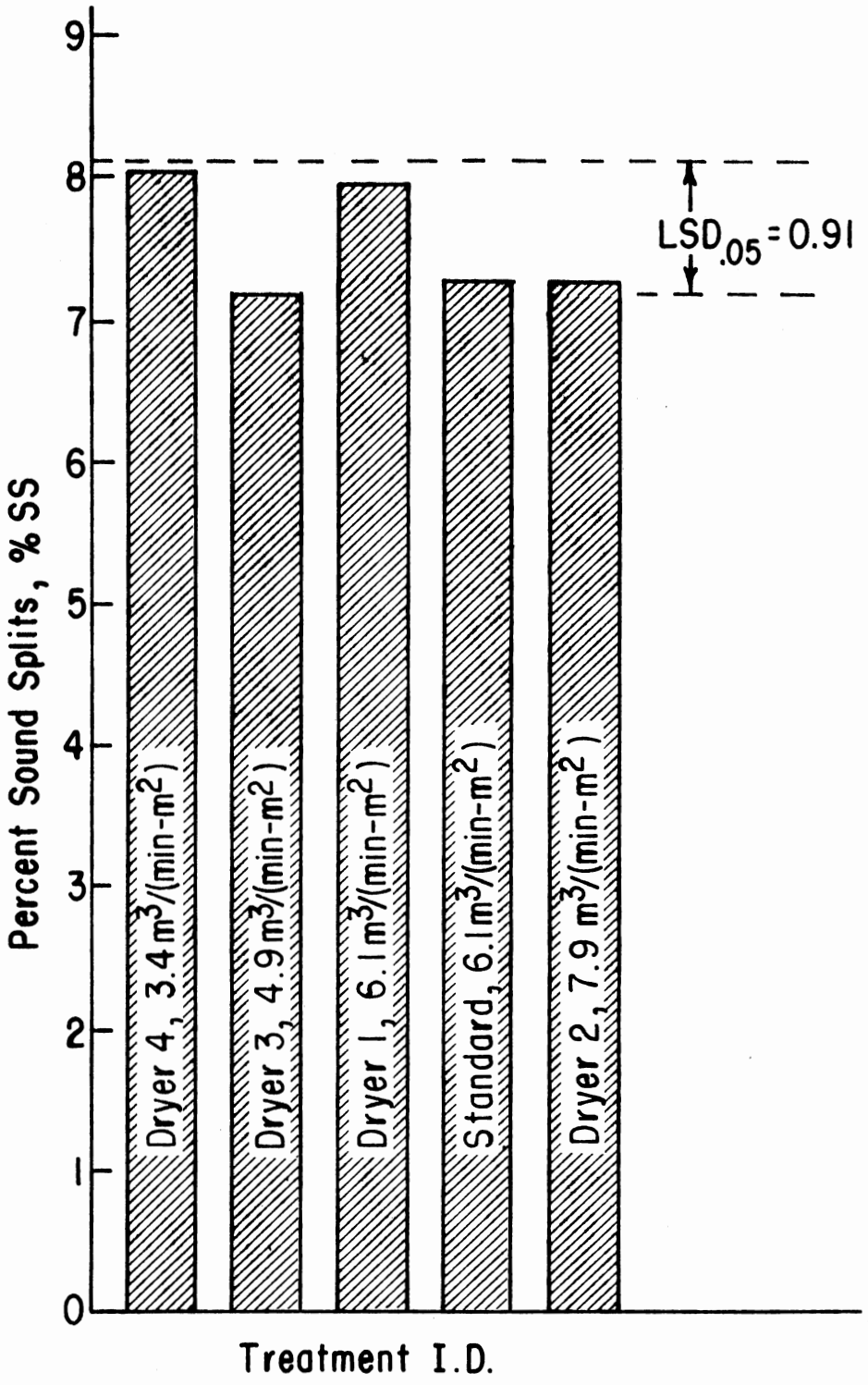

Figure 28. Percent Sound Split Averages for Solar Drying Treatments and Standard.

varied inversely with flow rate. As a result, average drying rates for various replicates differed by small amounts and none exceeded 0.5%/hr. These relatively low drying rates coupled with experimental error and significant block differences are major factors attributing to non-significant percent splits difference between treatments. It is important in referring to Figure 28 to note that the standard produced one of the lowest percent splits values.

TABLE IX

ANALYSIS OF VARIANCE FOR ADJUSTED PERCENT SOUND SPLITS OF SOLAR DRYING STUDY

Source	df	Sum of Squares	Mean Square	F Calc.
Block	5	171.97	34.39	21.44*
Treatment	4	11.61	2.90	1.81
Experimental Error	18	28.87	1.60	2.01*
Sampling Error	56	44.76	0.80	
Corrected Total	83	257.21	3.10	

* Statistically significant at the 95% confidence level

When 7,200 Kg of Spanish peanut pods were dried during solar tests and graded at a local commercial plant, percent sound splits and dollar worth value of those pods were comparable to those dried commercially.

Economic Analysis

A solar collector system can economically be incorporated into a solar peanut drying operation when cost per unit of collected energy (solar energy cost) is less than cost of available conventional energy sources. A unique advantage of the wedge-shaped matrix collector is that it requires no additional fans or pumps. Therefore, only costs of construction materials and annual maintenance for a given life expectancy were considered. The following given conditions were used to develop an economic analysis for solar drying during fall months for central Oklahoma.

Date of analysis	August, 1976
Location	Central Oklahoma
Time considered	Aug., Sept., Oct. and Nov.
Initial collector construction cost	$\$20.00/m^2$
Annual maintenance cost	$\$2.00/m^2$
Daily collector efficiency	44%
Capital recovery interest rate	10%
Life expectancy	10 years
Number of operating days	1-120 days
Average available solar radiation on a horizontal surface from Aug.-Nov.	5.18 kw-hr/(m^2-day)

Results of the economic analysis are presented in Table X.

Annual on-the-farm peanut drying in central Oklahoma usually occurs during the months of October and November. A single farmer can generally operate 10-20 days per year in drying his own peanuts. Ten

to 20 annual operating days results in solar energy costs of 12 to 23¢/(kw-hr), respectively. Continuous operation of the solar collector from August to November reduces solar energy costs to 1.9¢/(kw-hr). Solar energy costs for the example in Table X can be further reduced by operating the collector continuously from August to March. This results in a solar energy cost of 1.2¢/(kw-hr). Therefore, before a solar peanut drying system can become economically feasible, other uses for the collectors must be found during the off-drying season. Heating livestock and human residencies, and drying other crops are ways to increase use of the solar collectors during the off-drying season.

TABLE X

ECONOMIC ANALYSIS FOR WEDGE-SHAPED MATRIX SOLAR COLLECTOR (AUGUST, 1976)

Number of Operating Days Days/Yr	Cost of Solar Energy $/(kw-hr)
1	2.300
10	0.230
20	0.115
30	0.077
60	0.038
120	0.019

Cost of solar energy will increase considerably if there is a need for storage and standby conventional systems. No attempt was made in this study to evaluate the effects storage and auxiliary systems on cost of solar energy.

CHAPTER VII

SUMMARY AND CONCLUSIONS

Summary

The basic objective of this study was to design and construct a low-cost efficient wedge-shaped matrix solar collector and verify a simple theoretical analysis of the collector with observed data. This required assumptions be made in estimating collector cover temperature and matrix bed temperature distributions.

A matrix solar collector was designed and constructed for an initial materials cost of $\$20.00/m^2$. A series of tests were conducted to evaluate physical properties of 1.91cm Duralast filter media being used as the absorber. Experiments were also conducted to obtain actual data on collector efficiency. Collector flow rates ranged from 0.30 to 2.52 $m^3/(min\text{-}m^2)$. These data were used to verify a theoretical analysis of the collector.

Four 3.0 m^2 of these matrix solar collectors were incorporated into a pilot solar peanut drying operation to test their applicability in solar crop drying. Over 7,200 Kg of freshly harvested Spanish peanut pods were dried from original moisture contents of 20-30%, wet basis, to 8-10% during the month of October, 1975. Analysis revealed the collectors operating at 1.0 $m^3/(min\text{-}m^2)$ effectively captured over 50% of available insolation for an 8-hour period each day. An

economic analysis was conducted for solar drying in central Oklahoma.

Conclusions

The following conclusions were based on interpretation of observed and analytical data analyses conducted by the author. Extreme caution should be taken when extrapolating values beyond the scope of this study.

1. Bed efficiency was theoretically predicted with 94% accuracy.
2. Collector efficiency of the design used in this study was theoretically predicted with a maximum error of 24%. However, error in predicting collector efficiency decreased with flow rate.
3. The simplified theoretical analysis can be used to evaluate matrix solar collector performance for flow rates less than 0.15 $m^3/(min\text{-}m^2)$ with a maximum error of 16%.
4. The collector design utilizing a 1.91cm layer of Duralast filter media for a matrix absorber yielded a low-cost ($\$20/m^2$) efficient (maximum efficiency of 60%) solar collector that may be used for agricultural crop drying.
5. A solar peanut drying system using matrix solar collectors can become economically feasible if other uses are found for the collectors during the off-drying season.
6. The collector was successfully incorporated into a peanut drying operation and utilized over 50% of available insolation for eight hours each day.
7. A collector area three to five times that of dryer floor area

provided sufficient temperature rises (greater than 10 °C) needed for adequate peanut drying in central Oklahoma.

8. Operating the collector above 1.5 $m^3/(min\text{-}m^2)$ did not result in any significant increase in efficiency.

Recommendations for Future Study

Theory developed in this study accurately predicts bed efficiency, however, when applied to solar collector performance, it results in considerable error. Therefore, additional research is needed to determine effects of collector shape and the location and size of air inlets on matrix solar collector performance. Research is needed to determine effects of wind, shading, angle of incidence, and diffuse radiation on matrix collector performance.

Considerable research has been conducted in analytically evaluating thermal performance of porous media. However, little experimental data is available in applying these materials to matrix solar collector design. This implies additional research is needed to experimentally investigate matrix solar collectors on a large scale basis.

Additional study is needed in determining economic feasibility of matrix solar collectors for agricultural crop drying. Environmental control systems should be thoroughly investigated for economical application to solar crop drying.

SELECTED BIBLIOGRAPHY

1. Beckman, W. A. "Radiation and Convection Heat Transfer in a Porous Bed." Journal of Engineering for Power, Trans. ASME, Series A, Jan. 1966, 90; 51.

2. Beulow, F. H. "Solar Energy Collector Designs." Trans. of ASAE, 1962, No. 1, 5; 1, 2 and 5.

3. Beulow, F. H., and J. S. Boyd. "Heating Air by Solar Energy." Agricultural Engineering, Jan. 1967, 28-30.

4. Chiou, J. P. "Heat Transfer and Flow Friction Characteristics of Metallic Foil Matrixes Using Radiation as the Heat Source and Their Application to the Design of Solar Collectors." University of Wisconsin, Unpublished Ph.D. Thesis, 1964.

5. Chiou, J. P., J. A. Duffie, and M. M. El-Wakil. "A Slit-and-Expanded Aluminum-Foil Matrix Solar Collector." ASME Paper No. 64-WA/Sol-10.

6. Coppage, J. E., and A. L. London. "Heat Transfer and Flow Friction Characteristics of Porous Media." Chemical Engineering Progress, No. 2, 52; 57-63F.

7. Duffie, J. A., and W. A. Beckman. Solar Energy Thermal Processes. John Wiley and Sons, Inc., New York, 1974.

8. Duncan, G. A., and J. N. Walker. "Selection of Greenhouse Covering Materials." Trans. of ASAE, 1975, 703-710.

9. Hamid, Y. H., and W. A. Beckman. "Performance of Air-Cooled Radiatively Heated Screen Matrices." ASME Paper No. 70-WA/Sol-1.

10. Hamid, Y. H., and W. A. Beckman. "Transpiration Cooling of Radiatively Heated Porous Bed." ASME Paper No. 69-WA/Sol-6.

11. Leung, A. T., and D. K. Edwards. "Simultaneous Radiation, Conduction, and Convection in a Spectrally Selective, Emitting and Scattering Porous Bed." Journal of Heat Transfer, Trans. of ASME, Series C, May 1966, 88; 231.

12. Liu, B. Y. H., and R. C. Jordan. "The Long-Term Average Performance of Flat-Plate Solar Energy Collectors." Solar Energy, 7; 53 (1963).

13. Locke, G. L. "Heat Transfer and Flow Friction Characteristics of a Porous Solid." Tech. Report No. 10, Department of Mechanical Engineering, Stanford University, 1950.

14. Marco, S. M., and L. S. Han. "An Investigation of Convection Heat Transfer in a Porous Medium." ASME Tech. Paper No. 55-A-104, 1955.

15. Parker, J. D., J. H. Boggs and E. F. Blick. Introduction to Fluid Mechanics and Heat Transfer. Addison-Wesley Publishing Co., Inc., Reading, Mass., 1970.

16. Satcunanathan, S. N., and S. Deonarine. "A Two-Pass Solar Air Heater." Solar Energy, 1973, 15; 41-49.

17. Schlichting, H. Boundary Layer Theory. McGraw-Hill Book Co., Inc., New York, 1968.

18. Tong, L. S., and A. L. London. "Heat-Transfer and Flow-Friction Characteristics of Woven-Screen and Crossed-Rod Matrixes." Trans. of ASME, 1957, 79; 1558-1570.

19. United Nations Conference on New Sources of Energy, Rome, 1961. Papers Nos. 5/3; 5/30; 5/67; 5/93; 5/94; 5/112; 5/114.

20. Viskanta, R. "Radiation Transfer and Interaction of Convection with Radiation Heat Transfer." Advances in Heat Transfer ed., Irvine, T. F., Jr., and Hartnett, J. P., 1966, 3; 247.

21. Weiner, M. M., and D. K. Edwards. "Simultaneous Conduction, Convection, and Radiation in a Porous Bed." Proceedings of the 1963 Heat Transfer and Fluid Mechanics Institute, Stanford University Press, Stanford, California, 1963, 236.

APPENDIXES

APPENDIX A

MATRIX SOLAR COLLECTOR DATA

TABLE XI

SOLAR COLLECTOR PERFORMANCE DURING SOLAR PEANUT DRYING AT COLLECTOR FLOW RATE OF 0.45 $m^3/(min\text{-}m^2)$

TIME OF DAY	AMBIENT TEMPERATURE °C	COLLECTOR OUTLET °C	TEMPERATURE RISE °C	SOLAR RADIATION WATTS/m^2	TOTAL AVAILABLE ENERGY MEGAJ/m^2	TOTAL ENERGY COLLECTED MEGAJ/m^2	COLLECTOR EFFICIENCY %	ACCUMULATED COLLECTOR EFFICIENCY %
8,00	21,6667	25,2778	3,6107	295,820	0,1331	0,01237	,092887	,092887
8,25	21,6667	28,3333	6,6660	380,340	0,4374	0,04756	,133377	,100731
8,50	22,5000	28,3333	5,8327	412,035	0,7940	0,09036	,107727	,113809
8,75	23,8889	36,3889	12,4987	454,295	1,1838	0,15314	,209370	,129359
9,00	25,2778	41,3889	16,1095	507,120	1,6164	0,25111	,281745	,155344
9,25	25,8333	46,1111	20,2757	549,380	2,0919	0,37571	,280860	,179604
9,50	27,5000	49,7222	22,2200	591,640	2,6053	0,52123	,285807	,200065
9,75	27,5000	54,7222	27,2195	633,900	3,1568	0,69054	,326773	,218746
10,00	28,0556	55,5556	27,4972	676,160	3,7463	0,87792	,309475	,234340
10,25	27,5000	58,8889	31,3857	718,420	4,3739	1,07956	,332461	,246819
10,50	27,7778	60,5556	32,7745	739,550	5,0300	1,29928	,337252	,258307
10,75	28,3333	62,7778	34,4410	760,680	5,7051	1,52946	,344556	,268087
11,00	28,3333	64,4444	36,1075	781,810	6,3992	1,77106	,351465	,276761
11,25	29,1667	65,2778	36,1075	802,940	7,1124	2,01836	,342216	,283782
11,50	29,4444	67,5000	38,0517	824,070	7,8445	2,27232	,351396	,289670
11,75	30,0000	68,0556	38,0517	845,200	8,5957	2,53293	,342611	,294675
12,00	30,0000	72,2222	42,2180	887,460	9,3754	2,80782	,362022	,299489
12,25	30,5556	70,8333	40,2737	929,720	10,1931	3,09031	,329652	,303177
12,50	30,5556	75,0000	44,4400	950,850	11,0394	3,38042	,355671	,306215
12,75	31,1111	71,3889	40,2737	908,590	11,8761	3,67052	,337319	,309067
13,00	31,1111	74,4444	43,3290	866,330	12,6748	3,95682	,380611	,312179
13,25	31,9444	73,3333	41,3847	866,330	13,4545	4,24692	,363532	,315650
13,50	31,1111	71,1111	39,9960	845,200	14,2247	4,52561	,360117	,318151
13,75	33,0556	70,2778	37,2185	845,200	14,9854	4,79003	,345109	,319647
14,00	31,6667	65,5556	33,8855	834,635	15,7413	5,03353	,308961	,319765
14,25	31,9444	61,6667	29,7192	802,940	16,4782	5,25134	,281670	,318684
14,50	31,1111	55,8333	24,7197	750,115	17,1771	5,43777	,250785	,316571
14,75	32,2222	58,3333	26,1085	707,855	17,8332	5,61183	,280688	,314685
15,00	31,1111	59,1667	28,0527	676,160	18,4560	5,79731	,315727	,314115
15,25	31,9444	58,8889	26,9417	633,900	19,0455	5,98564	,323438	,314281
15,50	30,8333	52,7778	21,9422	570,510	19,5875	6,15304	,292687	,314131
15,75	31,3889	55,8333	24,4420	507,120	20,0724	6,31189	,366786	,314455
16,00	32,2222	49,7222	17,4982	443,730	20,5003	6,45551	,300097	,314898

TABLE XII

SOLAR COLLECTOR PERFORMANCE DURING SOLAR PEANUT DRYING
AT COLLECTOR FLOW RATE OF 0.64 $m^3/(min\text{-}m^2)$

TIME OF DAY	AMBIENT TEMPERATURE °C	COLLECTOR OUTLET °C	TEMPERATURE RISE °C	SOLAR RADIATION WATTS/m^2	TOTAL AVAILABLE ENERGY MEGAJ/m^2	TOTAL ENERGY COLLECTED MEGAJ/m^2	COLLECTOR EFFICIENCY %	ACCUMULATED COLLECTOR EFFICIENCY %
8,00	21,6667	25,5556	3,8885	295,820	0,1331	0,01950	,146515	,146515
8,25	21,6667	28,0556	6,3882	380,340	0,4374	0,07105	,187213	,162440
8,50	22,5000	28,0556	5,5550	412,035	0,7940	0,13095	,150271	,164939
8,75	23,8889	35,8333	11,9432	454,295	1,1838	0,21872	,293029	,184761
9,00	25,2778	40,2778	14,9985	507,120	1,6164	0,35586	,329658	,218910
9,25	25,8333	43,6111	17,7760	549,380	2,0919	0,51825	,360651	,247743
9,50	27,5000	46,9444	19,4425	591,640	2,6053	0,70493	,366286	,270571
9,75	27,5000	49,4444	21,9422	633,900	3,1568	0,91250	,385822	,289057
10,00	28,0556	51,9444	23,8865	676,160	3,7463	1,14237	,393758	,304929
10,25	27,5000	55,8889	26,3862	718,420	4,3739	1,39453	,409379	,318828
10,50	27,7778	56,3889	28,6082	739,550	5,0300	1,67037	,431171	,332081
10,75	28,3333	57,2222	28,8860	760,680	5,7051	1,95875	,423264	,343532
11,00	28,3333	58,6111	30,2747	781,810	6,3992	2,25548	,431624	,352462
11,25	29,1667	60,0000	30,8302	802,940	7,1124	2,56197	,427977	,360214
11,50	29,4444	61,3889	31,9412	824,070	7,8445	2,87682	,432030	,366730
11,75	30,0000	62,2222	32,2190	845,200	8,5957	3,19864	,424892	,372121
12,00	30,0000	63,6111	33,6077	887,460	9,3754	3,52881	,422101	,376591
12,25	30,5556	63,6111	33,0522	929,720	10,1931	3,86316	,396255	,378997
12,50	30,5556	67,2222	36,6630	950,850	11,0394	4,21284	,429776	,381619
12,75	31,1111	65,5556	34,4410	908,590	11,8761	4,56948	,422507	,384762
13,00	31,1111	65,5556	34,4410	866,330	12,6748	4,91498	,443117	,387774
13,25	31,9444	66,1111	34,1632	866,330	13,4545	5,25908	,439544	,390878
13,50	31,1111	62,7778	31,6635	845,200	14,2247	5,58925	,417567	,392925
13,75	33,0556	63,0556	29,9970	845,200	14,9854	5,89853	,395589	,393618
14,00	31,6667	54,4444	22,7755	834,635	15,7413	6,16322	,304157	,391532
14,25	31,9444	56,6667	24,7197	802,940	16,4782	6,40145	,343153	,388479
14,50	31,1111	49,1667	18,0537	750,115	17,1771	6,61599	,268266	,385163
14,75	32,2222	52,5000	20,2757	707,855	17,8332	6,80824	,319271	,381774
15,00	31,1111	52,7778	21,6645	676,160	18,4560	7,01861	,357129	,380289
15,25	31,9444	52,5000	20,5535	633,900	19,0455	7,23036	,361403	,379636
15,50	30,8333	47,7778	16,9427	570,510	19,5875	7,41844	,331014	,378733
15,75	31,3889	52,7778	21,3867	507,120	20,0724	7,61069	,470068	,379161
16,00	32,2222	45,2778	13,0542	443,730	20,5003	7,78344	,327914	,379674

TABLE XIII

SOLAR COLLECTOR PERFORMANCE DURING SOLAR PEANUT DRYING AT COLLECTOR FLOW RATE OF 0.75 $m^3/(min\text{-}m^2)$

TIME OF DAY	AMBIENT TEMPERATURE °C	COLLECTOR OUTLET °C	TEMPERATURE RISE °C	SOLAR RADIATION WATTS/m^2	TOTAL AVAILABLE ENERGY MEGAJ/m^2	TOTAL ENERGY COLLECTED MEGAJ/m^2	COLLECTOR EFFICIENCY %	ACCUMULATED COLLECTOR EFFICIENCY %
8,00	21,6667	24,1667	2,4997	295,820	0,1331	0,01594	,119719	,119719
8,25	21,6667	27,2222	5,5550	380,340	0,4374	0,06729	,206921	,153841
8,50	22,5000	26,6667	4,1662	412,035	0,7940	0,12927	,183255	,162811
8,75	23,8889	33,3333	9,4435	454,295	1,1838	0,21603	,294502	,182490
9,00	25,2778	37,2222	11,9432	507,120	1,6164	0,35238	,333661	,217998
9,25	25,8333	40,5556	14,7207	549,380	2,0919	0,52237	,379621	,249716
9,50	27,5000	43,6111	16,1095	591,640	2,6053	0,71893	,385760	,275945
9,75	27,5000	45,8333	18,3315	633,900	3,1568	0,93850	,409704	,297294
10,00	28,0556	47,7778	19,7202	676,160	3,7463	1,18110	,413196	,315266
10,25	27,5000	50,0000	22,4977	718,420	4,3739	1,45025	,443664	,331569
10,50	27,7778	52,2222	24,4420	739,550	5,0300	1,74951	,468233	,347815
10,75	28,3333	53,3333	24,9975	760,680	5,7051	2,06471	,465573	,361905
11,00	28,3333	54,7222	26,3862	781,810	6,3992	2,39230	,478156	,373842
11,25	29,1667	56,6667	27,4972	802,940	7,1124	2,73582	,485176	,384658
11,50	29,4444	57,2222	27,7750	824,070	7,8445	3,08821	,477511	,393677
11,75	30,0000	58,6111	28,6082	845,200	8,5957	3,44767	,479540	,401093
12,00	30,0000	60,2778	30,2747	887,460	9,3754	3,82307	,483309	,407778
12,25	30,5556	59,4444	28,8860	929,720	10,1931	4,20024	,440178	,412067
12,50	30,5556	63,3333	32,7745	950,850	11,0394	4,59335	,488334	,416088
12,75	31,1111	62,2222	31,1080	908,590	11,8761	5,00063	,485062	,421066
13,00	31,1111	61,3889	30,2747	866,330	12,6748	5,39196	,495097	,425407
13,25	31,9444	61,3889	29,4415	866,330	13,4545	5,77268	,481470	,429051
13,50	31,1111	58,8889	27,7750	845,200	14,2247	6,13745	,465573	,431464
13,75	33,0556	60,0000	26,9417	845,200	14,9854	6,48629	,451606	,432841
14,00	31,6667	52,7778	21,1090	834,635	15,7413	6,79263	,358314	,431516
14,25	31,9444	53,6111	21,6645	802,940	16,4782	7,06533	,382260	,428768
14,50	31,1111	46,3889	15,2762	750,115	17,1771	7,30084	,288524	,425033
14,75	32,2222	51,6667	19,4425	707,855	17,8332	7,52219	,389156	,421808
15,00	31,1111	51,9444	20,8312	676,160	18,4560	7,77895	,436475	,421486
15,25	31,9444	50,8333	18,8870	633,900	19,0455	8,03217	,422119	,421735
15,50	30,8333	46,1111	15,2762	570,510	19,5875	8,24997	,379356	,421185
15,75	31,3889	52,5000	21,1090	507,120	20,0724	8,48194	,589726	,422566
16,00	32,2222	44,7222	12,4987	443,730	20,4003	8,69620	,399062	,424198

TABLE XIV

SOLAR COLLECTOR PERFORMANCE DURING SOLAR PEANUT DRYING AT COLLECTOR FLOW RATE OF 1.0 $m^3/(min\text{-}m^2)$

TIME OF DAY	AMBIENT TEMPERATURE °C	COLLECTOR OUTLET °C	TEMPERATURE RISE °C	SOLAR RADIATION WATTS/m^2	TOTAL AVAILABLE ENERGY MEGAJ/m^2	TOTAL ENERGY COLLECTED MEGAJ/m^2	COLLECTOR EFFICIENCY %	ACCUMULATED COLLECTOR EFFICIENCY %
8,00	21,6667	24,7222	3,0552	295,820	0,1331	0,02452	,184190	,184190
8,25	21,6667	26,9444	5,2772	380,340	0,4374	0,09139	,247447	,208943
8,50	22,5000	26,6667	4,1662	412,035	0,7940	0,16718	,180326	,210560
8,75	23,8889	33,0556	9,1657	454,295	1,1838	0,27417	,359813	,231599
9,00	25,2778	36,3889	11,1100	507,120	1,6164	0,43689	,390706	,270276
9,25	25,8333	39,1667	13,3320	549,380	2,0919	0,63304	,432781	,302619
9,50	27,5000	41,9444	14,4430	591,640	2,6053	0,85594	,435358	,328535
9,75	27,5000	44,1667	16,6650	633,900	3,1568	1,10559	,468847	,350223
10,00	28,0556	45,8333	17,7760	676,160	3,7463	1,38199	,468847	,368889
10,25	27,5000	47,2222	19,7202	718,420	4,3739	1,68291	,489531	,384760
10,50	27,7778	49,4444	21,6645	739,550	5,0300	2,01503	,522429	,400602
10,75	28,3333	50,2778	21,9422	760,680	5,7051	2,36498	,514429	,414539
11,00	28,3333	51,3889	23,0552	781,810	6,3992	2,72608	,525868	,426003
11,25	29,1667	52,7778	23,6087	802,940	7,1124	3,10056	,524368	,435940
11,50	29,4444	53,8889	24,4420	824,070	7,8445	3,48618	,528955	,444410
11,75	30,0000	55,0000	24,9975	845,200	8,5957	3,88294	,527452	,451732
12,00	30,0000	56,6667	26,6640	887,460	9,3754	4,29754	,535825	,458386
12,25	30,5556	56,1111	25,5530	929,720	10,1931	4,71659	,490158	,462724
12,50	30,5556	58,8889	28,3305	950,850	11,0394	5,14902	,531359	,466424
12,75	31,1111	57,5000	26,3862	908,590	11,8761	5,58814	,517912	,470536
13,00	31,1111	57,2222	26,1085	866,330	12,6748	6,00942	,537458	,474122
13,25	31,9444	57,5000	25,5530	866,330	13,4545	6,42402	,526023	,477461
13,50	31,1111	55,2778	24,1642	845,200	14,2247	6,82301	,509871	,479659
13,75	33,0556	56,1111	23,0532	845,200	14,9854	7,20194	,486428	,480598
14,00	31,6667	48,8889	17,2205	834,635	15,7413	7,52515	,367956	,478051
14,25	31,9444	51,3889	19,4425	802,940	16,4782	7,81938	,431832	,474528
14,50	31,1111	45,8333	14,7207	750,115	17,1771	8,09355	,349984	,471182
14,75	32,2222	49,1667	16,9427	707,855	17,8332	8,34766	,426860	,468097
15,00	31,1111	48,0556	16,9427	676,160	18,4560	8,61960	,446869	,467035
15,25	31,9444	47,7778	15,8317	633,900	19,0455	8,88262	,445404	,466389
15,50	30,8333	43,8889	13,0542	570,510	19,5875	9,11444	,408070	,465319
15,75	31,3889	50,5556	19,1647	507,120	20,0724	9,37300	,673967	,466959
16,00	32,2222	43,3333	11,1100	443,730	20,5003	9,61597	,446521	,469064

APPENDIX B

TEMPERATURE-TIME RELATIONSHIPS FOR SOLAR PEANUT DRYING STUDIES

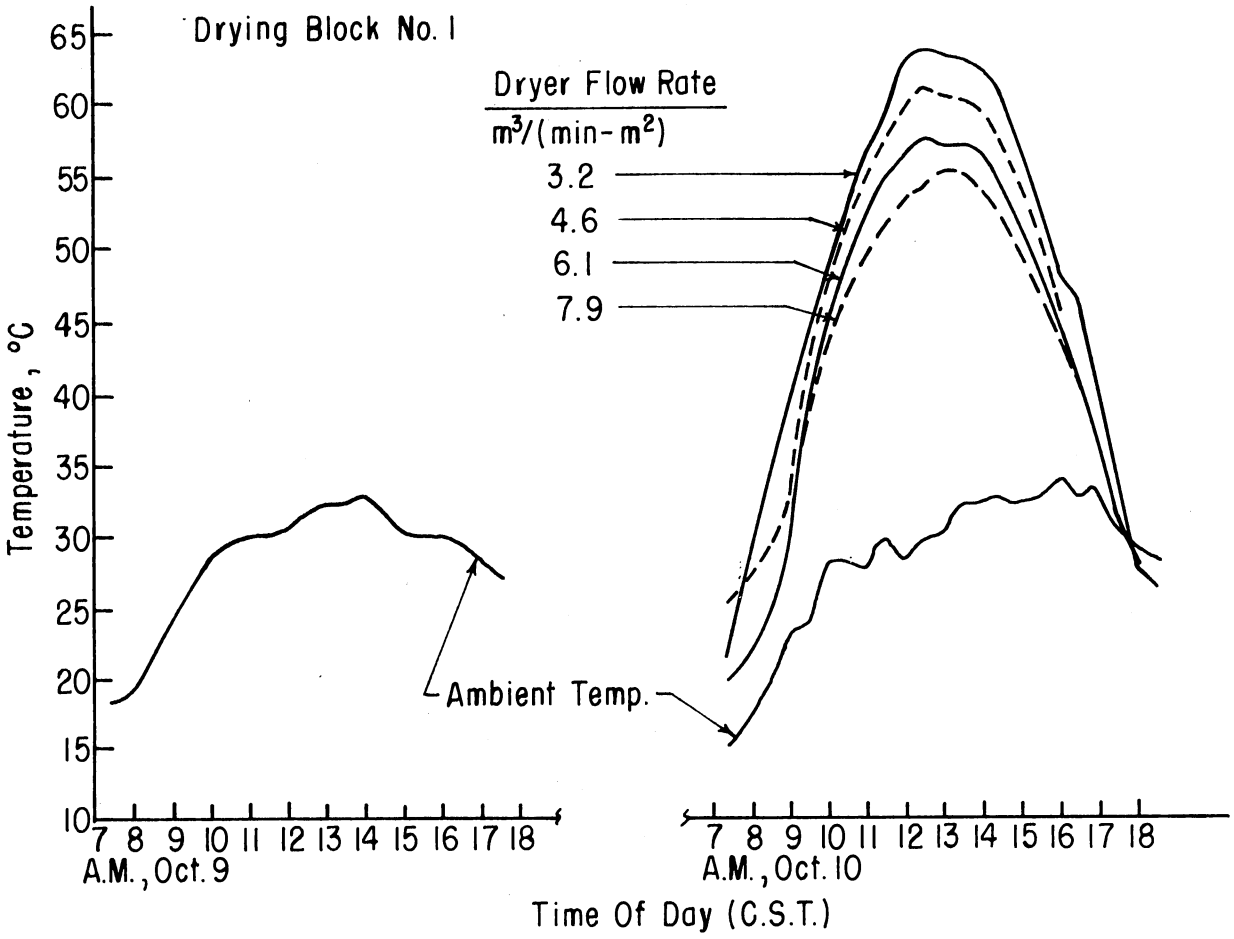

Figure 29. Dryer Inlet Temperature vs. Time of Day for October 9 and 10, 1975.

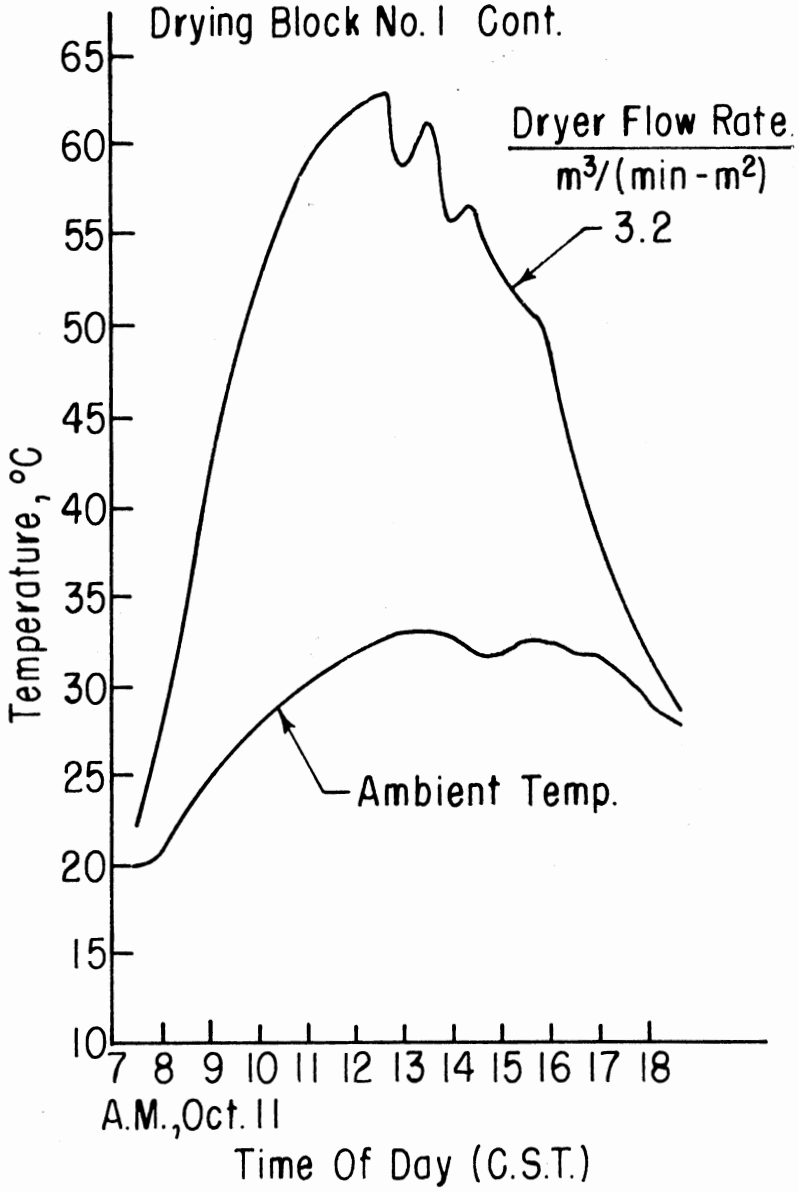

Figure 30. Dryer Inlet Temperature vs. Time of Day for October 11, 1975.

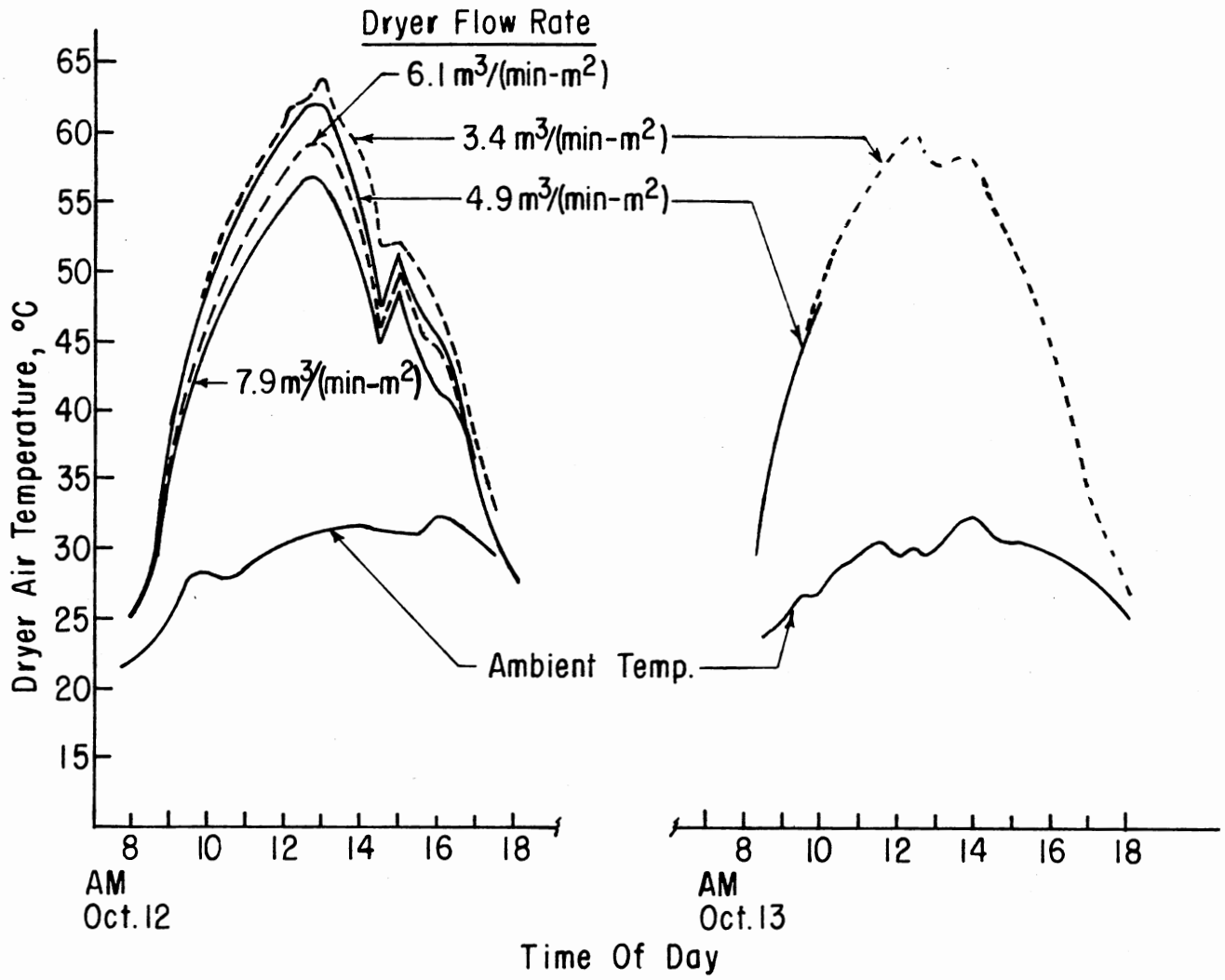

Figure 31. Dryer Inlet Temperature vs. Time of Day for October 12 and 13, 1975.

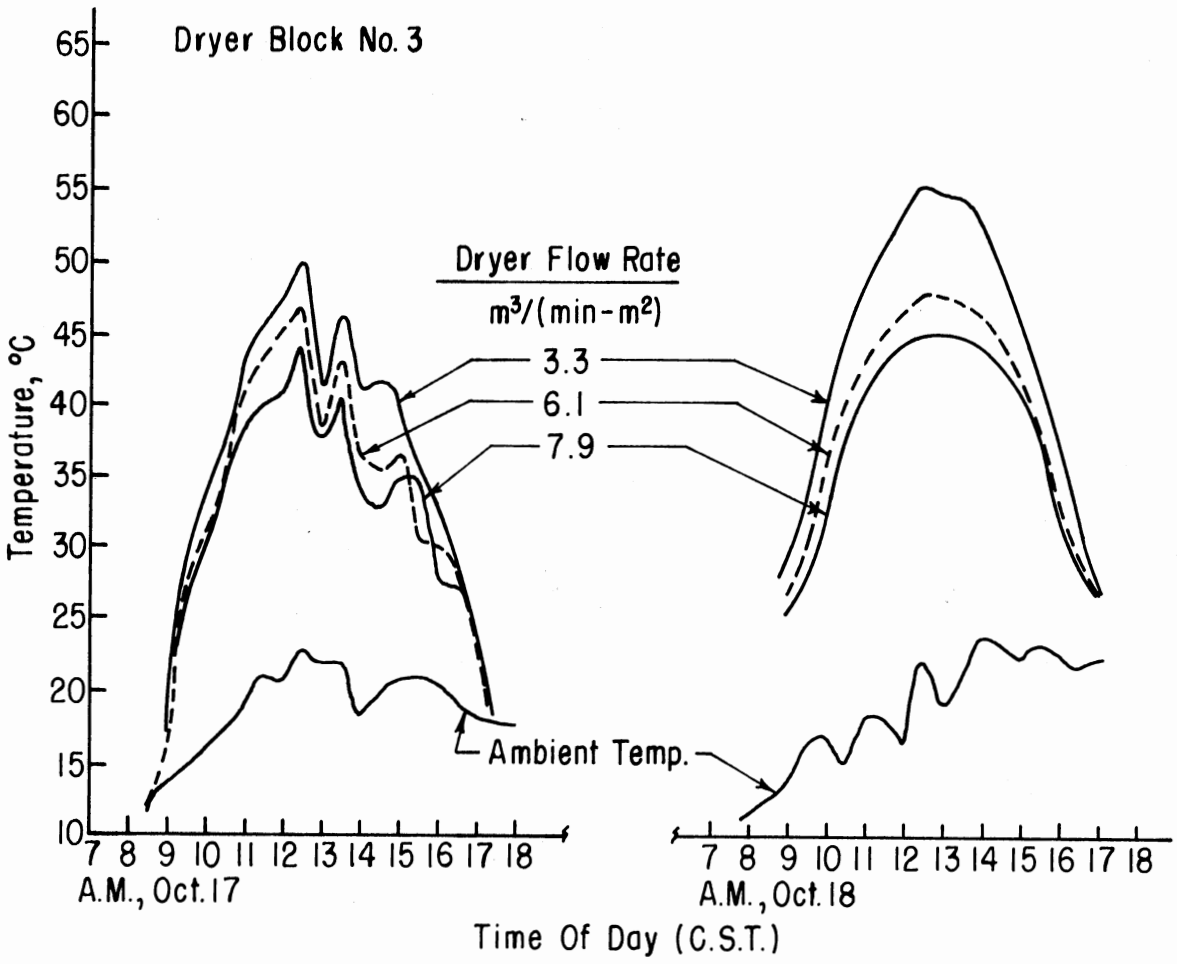

Figure 32. Dryer Inlet Temperature vs. Time of Day for October 17 and 18, 1975.

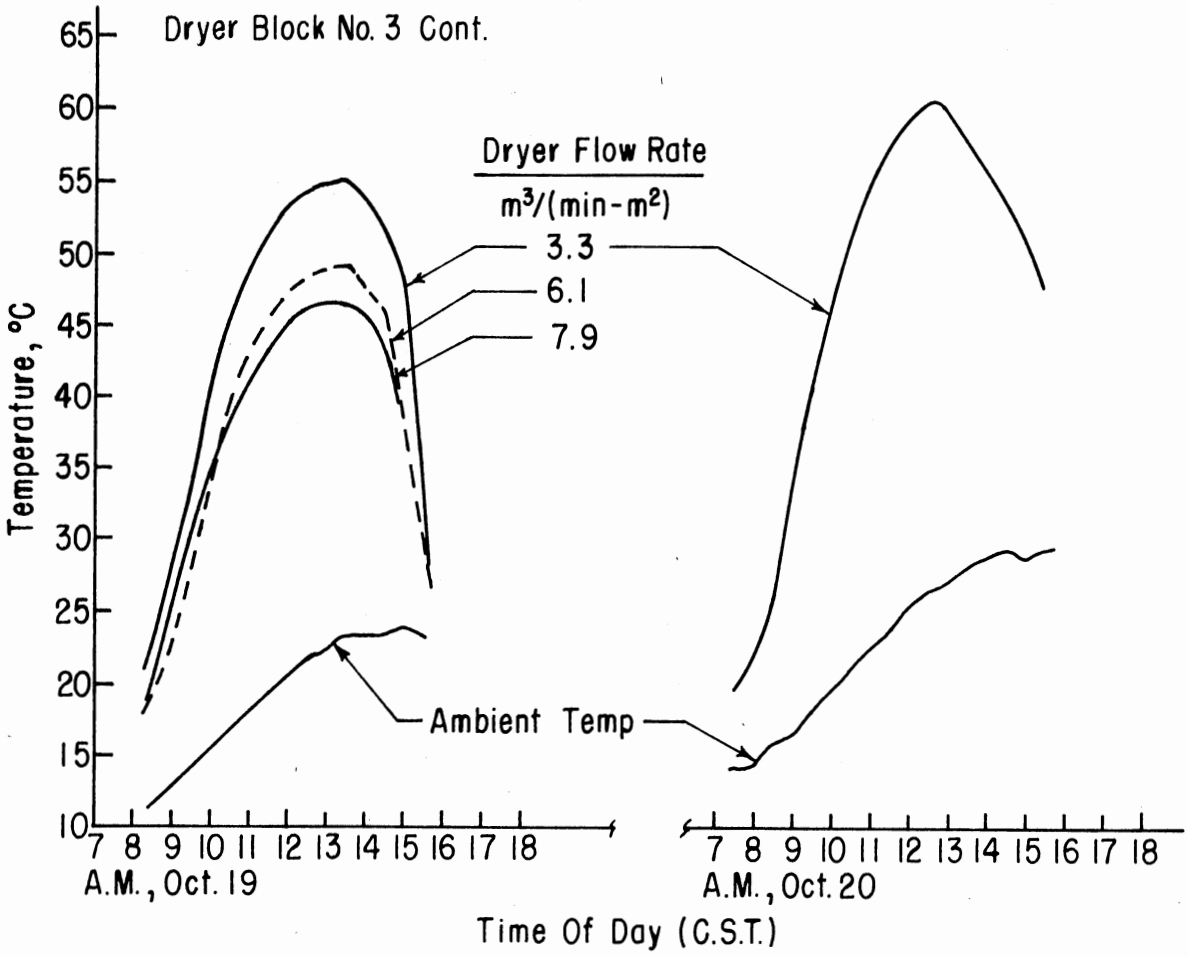

Figure 33. Dryer Inlet Temperature vs. Time of Day for October 19 and 20, 1975.

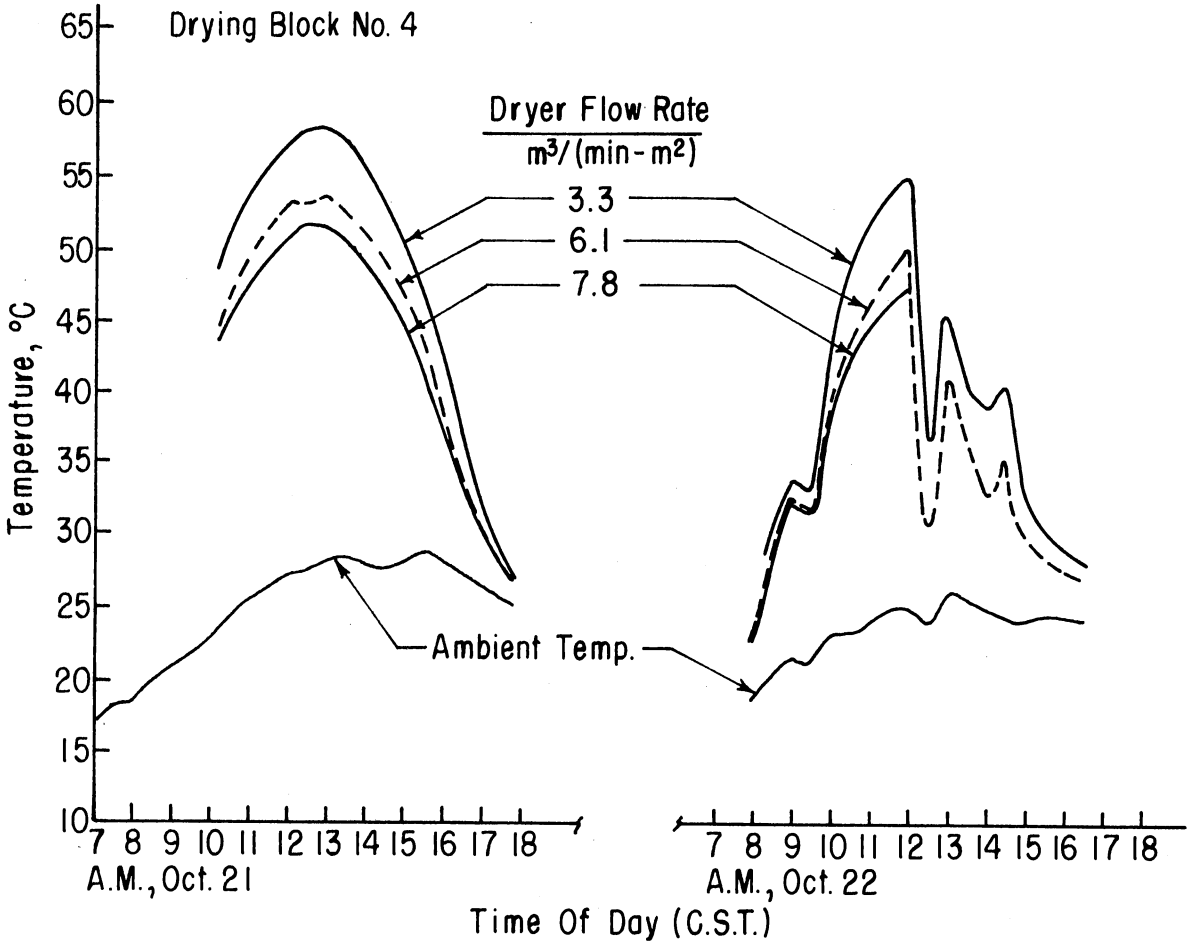

Figure 34. Dryer Inlet Temperature vs. Time of Day for October 21 and 22, 1975.

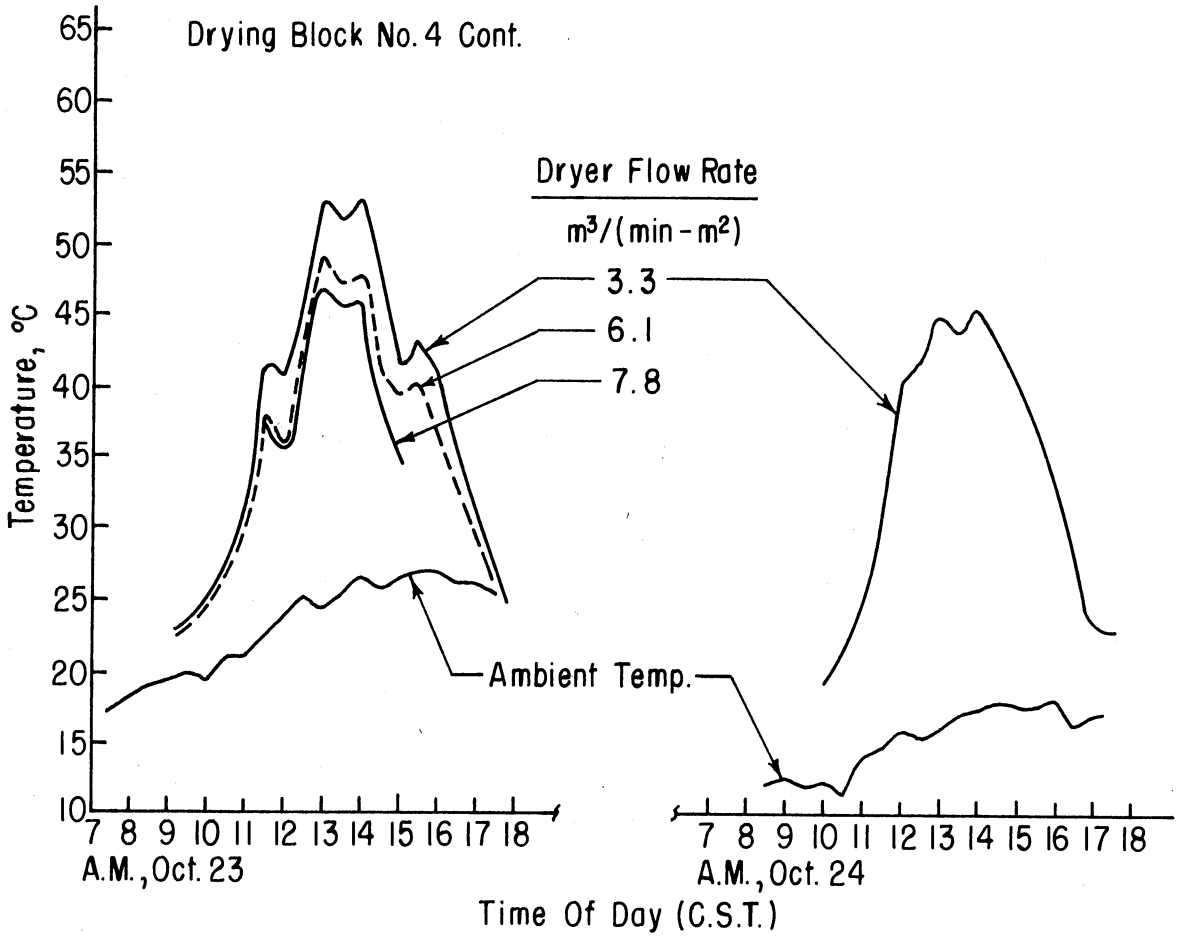

Figure 35. Dryer Inlet Temperature vs. Time of Day for October 23 and 24, 1975.

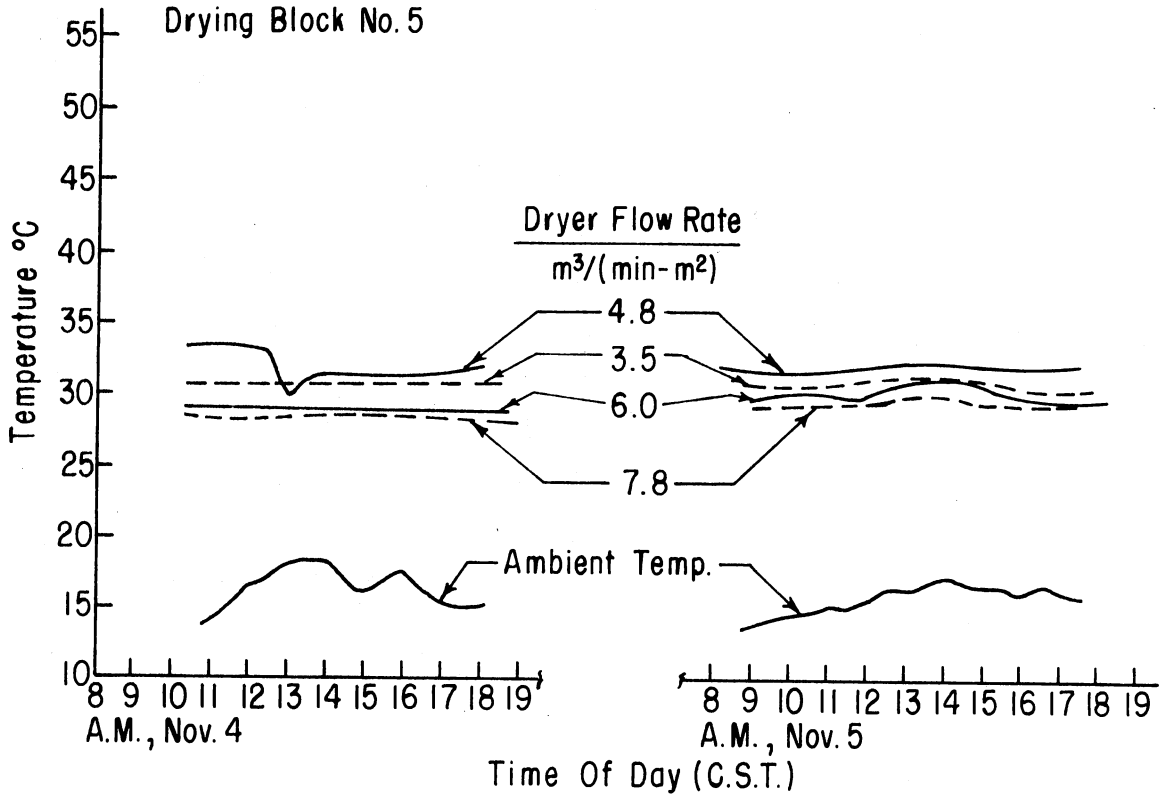

Figure 36. Dryer Inlet Temperature vs. Time of Day for November 4 and 5, 1975.

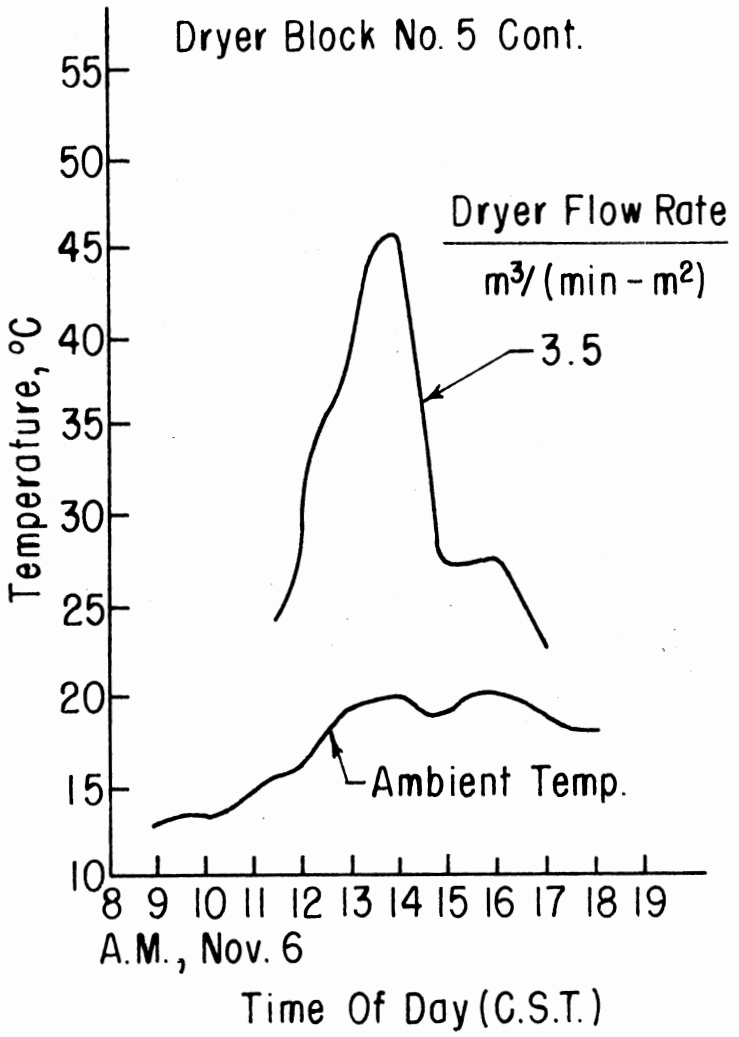

Figure 37. Dryer Inlet Temperature vs. Time of Day for November 6, 1975.

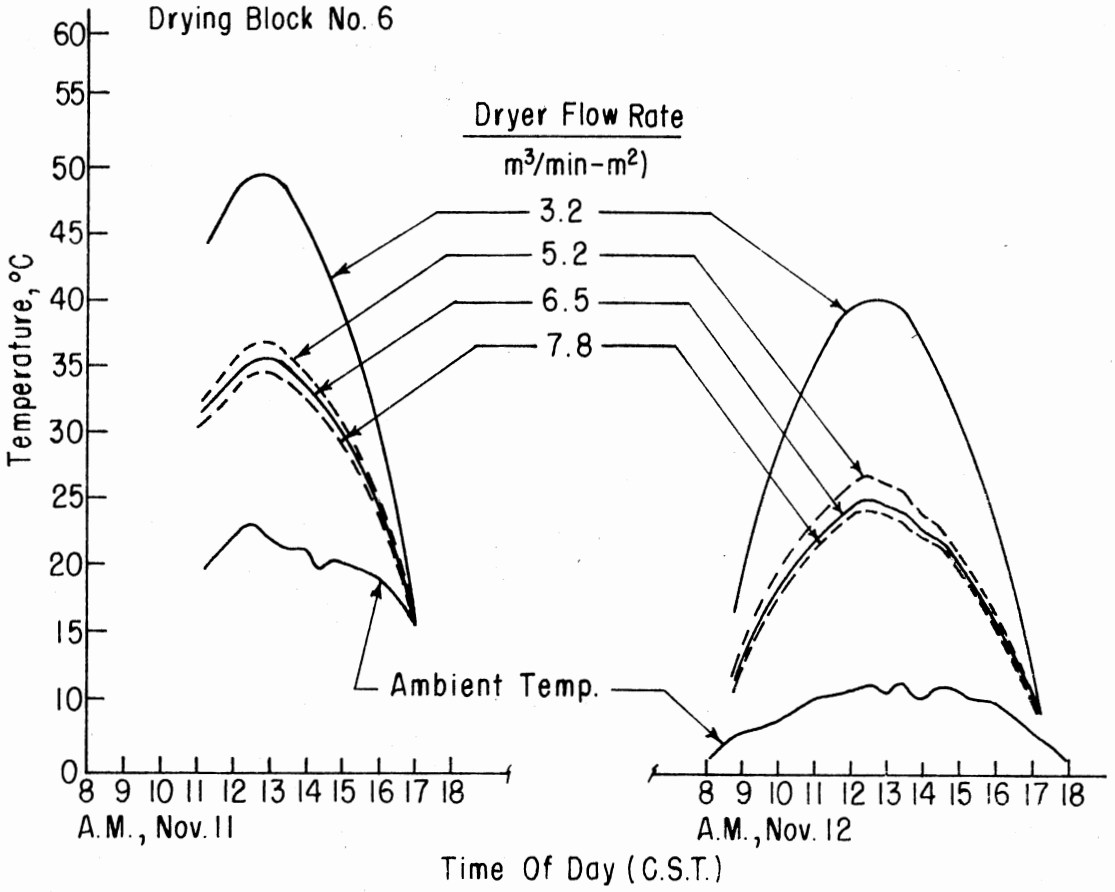

Figure 38. Dryer Inlet Temperature vs. Time of Day for November 11 and 12, 1975.

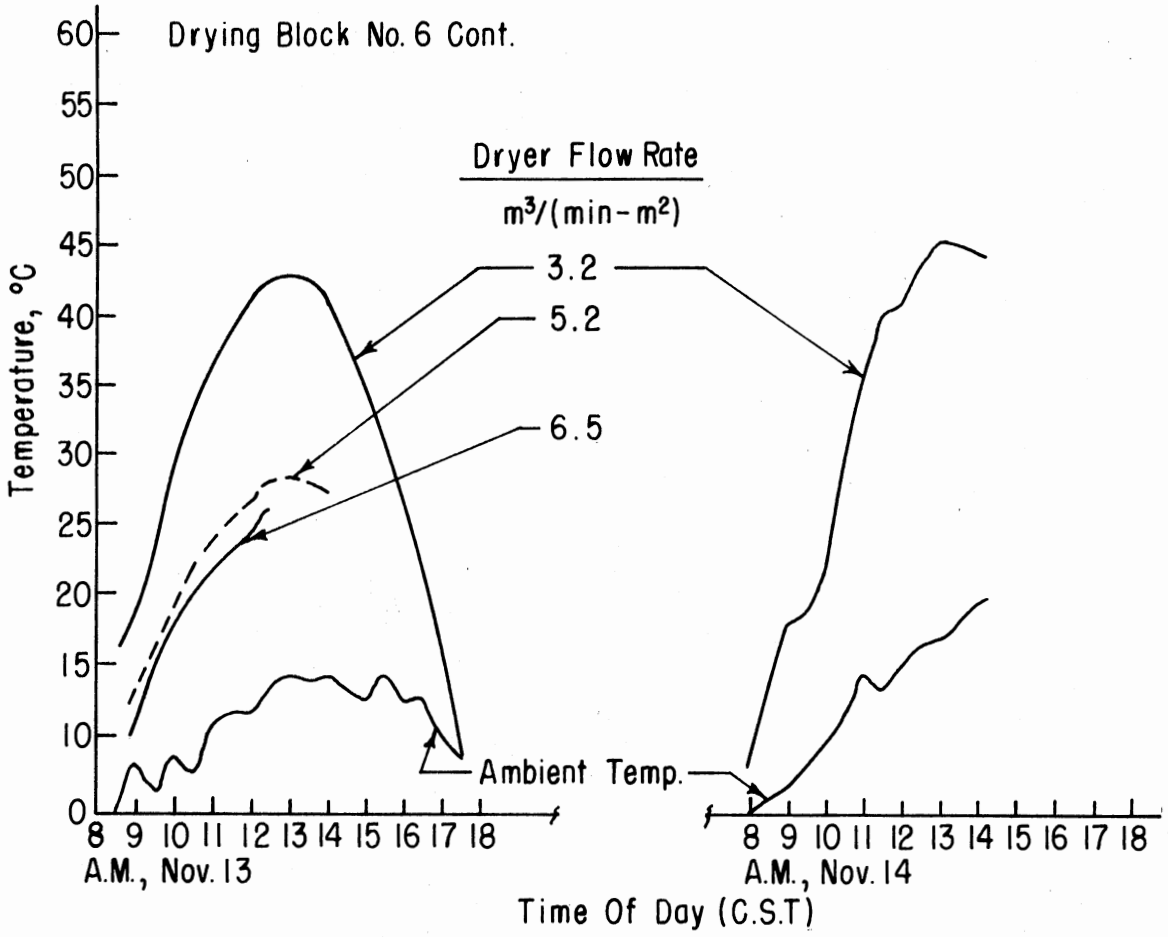

Figure 39. Dryer Inlet Temperature vs. Time of Day for November 13 and 14, 1975.

VITA

Ronnie Glen Morgan

Candidate for the Degree of

Master of Science

Thesis: DESIGN, CONSTRUCTION, AND EVALUATION OF A WEDGE-SHAPED MATRIX SOLAR COLLECTOR FOR DRYING PEANUTS

Major Field: Agricultural Engineering

Biographical:

Personal Data: Born in Waurika, Oklahoma, November 17, 1952, the son of Glen Dale and Helen Lucille; married to Sharon Sue Lemons on May 25, 1974.

Education: Graduated from Waurika High School, Waurika, Oklahoma, in 1971. Received a Bachelor of Science degree in Agricultural Engineering from Oklahoma State University in May, 1975; completed the requirements for the Master of Science degree from Oklahoma State University in December, 1976.

Professional Experience: Civil Engineering Technician for Army Corps of Engineers, Tulsa District, Tulsa, Oklahoma, May, 1974, to August, 1974. Undergraduate Research Assistant for Agricultural Engineering Department of Oklahoma State University from August, 1971, to May, 1975. Graduate Research Assistant for Agricultural Engineering Department of Oklahoma State University from June, 1975, to August, 1976.

Professional and Honorary Organization: Student member of: American Society of Agricultural Engineers; National Society of Professional Engineers; Oklahoma Society of Professional Engineers; American Peanut Research and Education Association, Inc.; Institute of Food Technologists; Sigma Xi; Tau Beta Pi; Alpha Zeta; Phi Kappa Phi; Phi Eta Sigma.